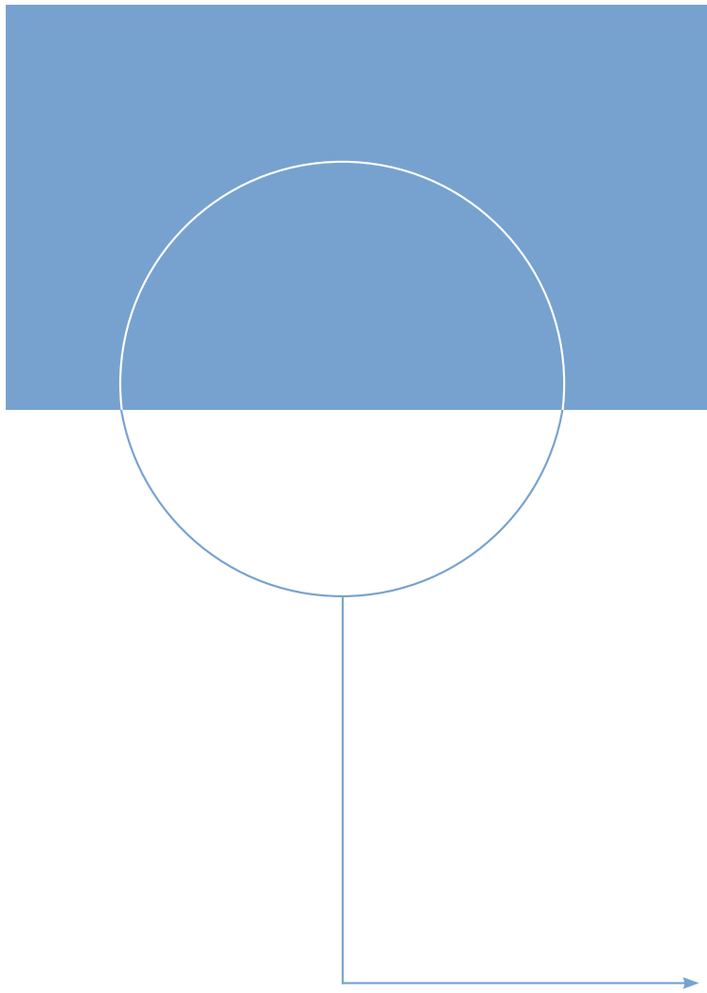

Master's thesis

2020

Brage Lysø

NTNU
Norwegian University of
Science and Technology
Faculty of Engineering
Department of Civil and Environmental Engineering

Brage Lysø

CFD Modelling of Hydrodynamics in Land-Based Aquaculture Tanks

Master's thesis in Marine Civil Engineering
Supervisor: Hans Bihs

June 2020

NTNU
Norwegian University of
Science and Technology

NTNU
Norwegian University of
Science and Technology

NTNU

Norwegian University of
Science and Technology

CFD Modelling of Hydrodynamics in Land-Based Aquaculture Tanks

Master's thesis in Marine Civil Engineering

Supervisor: Hans Bihs

Brage Lysø

Civil and Environmental Engineering
Submission date: June 2020
Supervisor: Hans Bihs
Co-supervisor: Tobias Martin

Norwegian University of Science and Technology
Department of Civil and Environmental Engineering

Preface

The present work constitutes the final 30 credits of the signatory's masters degree, thus completing the educational journey as a graduate student at the Norwegian University of Science and Technology (NTNU). The work has been conducted during the spring of 2020 under the Department of Civil and Environmental Engineering, and acts as the sole basis for assessment in the course *TBA4920 Marine Civil Engineering*.

The topic of the thesis deals with the hydrodynamics in land-based aquaculture tanks applied for rearing of Atlantic salmon, which was chosen at the initiative of the signatory. The main contribution to the existing body of knowledge (BoK) is a numerical investigation of the flow field within circular and octagonal tanks using CFD. More specifically, the velocity distributions and flow patterns occurring due to tangential inflow in a closed-containment system are examined in detail for various boundary conditions. The work is an attempt to determine the optimal tank design for rearing of Atlantic salmon.

The spring at the time of writing has been unlike any other due to the outbreak of the Covid-19 pandemic. In the middle of the semester, a state of emergency was declared across the globe, making the government shut down all forms of activity with an urge to stay at home. Except for negligible implications such as denied access to the library and office at the university, the onset of the pandemic has to a little extent impeded the work of the present study. A home office was established and consulting with the supervisors was maintained using digital communication services.

Sincere gratitude is directed towards the team at the Department of Civil and Environmental Engineering developing the numerical model applied in the study, REEF3D, under the leadership of associate professor Hans Bihs. A special thanks is extended to PhD candidate Tobias Martin for excellent guidance throughout the two final semesters, supervising the work in the project- and master thesis. Thank you also to Design Engineer at AKVA Group, Ole Jonny Nyhus for general advice regarding land-based aquaculture facility design.

Trondheim, June 2020
Brage Lysø

Abstract

Fish is an effective source of important nutrients due to large contents of high-quality protein, essential vitamins, minerals and omega-3 fatty acids, as well as a low content of saturated fat, carbohydrates and cholesterol. In addition, fish production is among the most efficient due to a low feed conversion rate (FCR), which specifies the ratio of required feed to increase the body weight by 1 kg. Consequently, fish farming is the world's fastest growing food producing industry, and it is regarded as an important sector for meeting the demands of an ever increasing world population in a sustainable way. The rapid expansion has however contributed to increased per unit GHG emissions as well as increased the demands of coastal habitats and the seabed locally, and thus further expansion must be managed in more sustainable ways using innovative technology to help reduce the environmental impact. Land-based recirculating aquaculture systems (RAS) is considered one of the most promising approaches to reduce emissions and waste products associated with industry. In addition to increased control over production conditions such as temperature, oxygen and flow conditions, RAS technology enables better handling of waste products, greatly reduced water consumption and less risk of lice outbreaks.

With increasing control over the production environment, a greater responsibility to safeguard the welfare of the produced species is required. Unlike conventional fish farming at sea, where oxygen is supplied and waste products are removed by natural convection, a healthy environment must be imposed by flow conditions generated by external energy sources. Feed and oxygen must be added, and waste products from respiration and metabolism must be removed quickly to prevent disease outbreaks and sub-optimal production conditions. The transport of inputs and outputs largely depend on the flow pattern created by a constant water exchange through the tanks. Furthermore, the geometric design of the tanks, as well as the location and orientation of inlets are expected to significantly influence the flow pattern, and thus the transport of feed and particles as well as concentrations of oxygen and toxic gases such as CO_2 and NH_3. The purpose of the present thesis was to investigate to what extent the geometric tank design, as well as placement and orientation of inlets affect the flow conditions within the production environment. Consequently, the following research questions (RQ) were formulated:

1. What are the most important hydrodynamic features of land-based aquaculture tanks?

2. How does geometry and inlet conditions influence the tank hydrodynamics?
3. How can numerical modelling by use of CFD contribute to optimization of land-based aquaculture tanks?

Mixed methods of qualitative and quantitative research were applied to answer the stated research questions. The work was structured in a sequential exploratory way, where an initial scoping literature review was conducted followed by numerical modeling using CFD. Finally, the findings from each sequence were evaluated simultaneously to achieve triangulation. The findings of the review were used as a basis to answer RQ1, as well as benchmark data for the CFD analyses. The qualitative work included validation of the numerical model REEF3D, in addition to a parameter study of various tank designs to answer RQ2. The distribution of tangential and radial velocities as well as primary- and secondary flow patterns were investigated. In conclusion, the answer to RQ3 was made based on a holistic evaluation of the results from the respective research methods.

The findings of the scoping literature review show that sufficient mixing of the inlet flow, uniform flow conditions, rapid flushing of solids and high velocities contributing to fish exercise are the most important hydrodynamic features in aquaculture tanks. Furthermore, the results of the numerical investigation show that the geometric design mainly influences primary flow velocities, while the inlet configuration have major influence on velocities and flow patterns in both the primary- and secondary currents. A prevalent and steady primary flow is especially important to avoid quiescent zones of low velocities that promote biofouling growth, in addition to fish exercise which increases the robustness and growth rates of the fish. The secondary flow is particularly important for the radial transport of particles and mixing throughout the water column. Turbulence and prominent vortices contribute to increased mixing, while sufficient radial velocities towards outlets are crucial for rapid flushing of solids.

The thesis provides a modus operandi for analysis of hydrodynamics in land-based aquaculture tanks. By applying accurate and computationally efficient numerical models, the primary- and secondary flows occurring due to tangential inflow in an enclosed environment can be studied in great detail at a relatively cheap investment costs. By quantifying the effects of improved hydrodynamics within the rearing environment, a more holistic assessment of facility design may be provided, thus guiding design engineers and contractors into making better decisions in the early phase of projects.

Sammendrag

Fisk er en effektiv kilde til viktige næringsstoffer på grunn av et rikt innhold av høyverdig protein, viktige vitaminer, mineraler og omega-3 fettsyrer, samt et lavt innhold av mettet fett, karbohydrater og kolesterol. I tillegg er fisk blant de mest effektive husdyrene å produsere grunnet lav fôrfaktor (FCR), som angir forholdet mellom mengden fôr som trengs for å øke kroppsvekten med 1 kg. Dette har gjort fiskeoppdrett til verdens raskest voksende næring innen matproduksjon, og den er ansett som en av de viktigste sektorene for fremtidig miljøvennlig matproduksjon. Den raske veksten har imidlertid ført til høyere relative klimagassutslipp og store lokale påkjenninger på havbunn og artsmangfold. Videre vekst må derfor skje på en bærekraftig måte ved bruk av innovativ teknologi som bidrar til å redusere næringens miljøpåkjenninger. Landbasert oppdrett, med særlig fokus på resirkulering av vann (RAS), er i så måte ansett som en av de mest spennende fremgangsmåtene for å redusere utslipp og avfallsprodukter tilknyttet næringen. I tillegg til økt kontroll over produksjonsforhold som temperatur, oksygen og strømningsforhold, bidrar RAS-teknologi til økt kontroll over produksjonsavfallet, betydelig redusert vannforbruk samt mindre risiko for lusepåslag.

Økt kontroll over produksjonsmiljøet medfører også et større ansvar for å ivareta fiskevelferden til arten som produseres. I motsetning til konvensjonell produksjon til sjøs, hvor oksygen tilføres og avfallsstoffer driver bort ved naturlig konveksjon, må dette skje gjennom strømningsforhold generert av eksterne energikilder. Fôr og oksygen må tilføres, samt at avfallsprodukter fra fiskens åndedrett og metabolisme må fjernes raskt for å hindre sykdomsutbrudd og sub-optimale produksjonsforhold. Måten dette blir gjort på avhenger i stor grad av strømningsmønsteret som skapes av konstant vannutskiftning i karene. Videre er det forventet at den geometriske utformingen av karene, samt plassering og orientering av inntaksrør har stor innvirkning på strømningsmønsteret, og dermed transporten av fôr og partikler i tillegg til konsentrasjonen av oksygen og giftige gasser som CO_2 og NH_3. Formålet med denne masteroppgaven var å undersøke i hvilken grad den geometriske utformingen av kar, samt innløpsplassering og orientering påvirker strømningsforholdene i produksjonsmiljøet. Følgende forskningsspørsmål (FS) ble dermed formulert:

1. Hva er de viktigste egenskapene tilknyttet strømningsmønsteret i oppdrettskar?
2. Hvordan påvirker geometri og innløpsforhold strømningsmønsteret i oppdrettskar?

3. Hvordan kan numerisk modellering ved bruk av CFD bidra til å optimere utformingen av oppdrettskar?

En kombinasjon av kvalitativ og kvantitativ forskningsmetode ble benyttet for å besvare de uttalte forskningsspørsmålene. Arbeidet hadde en sekvensiell utforskende struktur, hvor et innledende litteratursøk ble utført etterfulgt av numerisk modellering ved bruk av CFD. Til slutt ble funnene fra hver sekvens vurdert i lys av hverandre for å oppnå triangulering. Funnene fra litteratursøket ble brukt som grunnlag for å besvare FS1, samt som sammenligningsgrunnlag for det kvantitative arbeidet bestående av CFD-analyser. Arbeidet omfattet validering av den numeriske modellen REEF3D, i tillegg til et parameterstudie av forskjellige utforminger av oppdrettskar for å besvare FS2. Fordelingen av tangentielle og radielle hastigheter samt strømningsmønster i primær- og sekundærstrøm ble undersøkt. Avslutningsvis ble resultatene fra de respektive metodene vurdert helhetlig for å besvare FS3.

Resultatene fra litteraturstudiet viser at miksing av inntaksvann, jevne strømningsforhold, rask fjerning av partikler og hastigheter som bidrar til mosjon av fisken er de viktigste egenskapene som kan påvirkes av strømningsmønsteret i karene. Videre fremkommer det av den numeriske analysen at geometrisk utforming i hovedsak påvirker hastigheter i primærstrømmen, mens plassering og orientering av inntaksrør har stor innvirkning på hastigheter og strømningsmønster i både primær- og sekundærstrøm. En sterk og jevn primærstrøm er særlig viktig for å unngå dødsoner med lave hastigheter som øker sannsynligheten for begroing, samt for økt mosjon av fisken som bidrar til robusthet og gode vekstforhold. Sekundærstrømmen har særlig stor innflytelse den radielle transporten av partikler og miksing gjennom vannsøylen. Turbulens og sterke virvler bidrar til økt miksing, mens tilstrekkelige radielle hastigheter mot utløp er avgjørende for rask fjerning av partikler.

Avhandlingen presenterer et modus operandi for analyse av strømningsbildet i landbaserte oppdrettskar. Med nøyaktige og beregningseffektive numeriske modeller kan primær- og sekundærstrømmer som oppstår grunnet tangentielt vanninntak i de lukkede karene studeres i detalj til en relativt billig kostnad. Ved å kvantifisere virkningene av forbedret hydrodynamikk i oppdrettsmiljøet, kan det bli gitt en mer helhetlig vurdering av karutforming og anleggsdesign, som kan hjelpe konsulenter og entreprenører med å ta bedre beslutninger i tidligfasen av prosjekter.

Contents

List of Figures

List of Tables

List of Symbols

Symbol	Description	Unit
$L()$	Spatial discretization of the function	$[-]$
P	Pressure	Pa
$S(\phi)$	Smooth signed distance function	$[-]$
dt	Time step	s
u^*	Intermediate velocity	m/s
2ϵ	Transition zone thickness	m
C	Courant number	$[-]$
D	Diameter	m
IS_{1-3}	WENO stencil smoothness indicators	$[-]$
S_{ij}	Strain tensor	$[-]$
S_{max}	Source term contribution	$[-]$
V_0	Inlet velocity magnitude	m/s
α_{1-3}	WENO stencil weight determiner	$[-]$
ν	Kinematic viscosity	m^2/s
ν_t	Eddy viscosity	m^2/s
ω	Specific turbulent dissipation	s^{-1}
ω_{1-3}	WENO stencil weights	$[-]$
ϕ	Generic variable	$[-]$
ρ	Density	kg/m^3
$\sigma_{k,\omega}$	Closure coefficients	$[-]$
$_{i,j,k}$	Vectors along the x	$[-]$
$c_{\mu,\omega1,\omega2}$	Closure coefficients	$[-]$
d	Water depth	m
dx	Grid size	m
g	Gravitational constant (9.81)	$\frac{m}{s^2}$
k	Turbulent kinetic energy	J/kg
u	Velocity in x-direction	m/s
v	Velocity in y-direction	m/s
w	Velocity in z-direction	m/s

Abbreviations

ADV . . . . . Acoustic Doppler Velocimetry

BC . . . . . Boundary Condition

BoK . . . . . Body of Knowledge

CAD . . . . . Computer-Aided Design

CDS . . . . . Central Differences Scheme

CFD . . . . . Computational Fluid Dynamics

CG . . . . . Conjugate Gradient

D:d . . . . . Diameter-to-depth

DNS . . . . . Direct Numerical Simulation

FCR . . . . . Feed Conversion Rate

FD . . . . . Finite Differences

FE . . . . . Finite Elements

FOU . . . . . First Order Upwind

FV . . . . . Finite Volume

GE . . . . . Governing Equation

GHG . . . . . Green House Gases

HRT . . . . . Hydraulic Retention Time

LES . . . . . Large Eddy Simulation

LMS . . . . . Level Set Method

MCR . . . . . Mixed-Cell Raceways

MPI . . . . . Message Passing Interface

NS . . . . . Navier-Stokes

PDE . . . . . Partial Differential Equation

RANS . . . . . Reynolds-Averaged Navier-Stokes

RAS . . . . . Recirculating Aquaculture Systems

RQ . . . . . Research Question

TAN . . . . . Total Ammonia Nitrogen

TSS . . . . . Total Suspended Solids

TVD . . . . . Total Variance Diminishing

WENO . . . . . Weighted Essentially Non-Oscillatory

1 Introduction

The world food producing sector has to secure food and nutrition for an ever increasing world population, which is expected to reach 9.7 billion by 2050 (UN 2015). In a more crowded world, fundamental resources for food production such as land and water use become more scarce, which makes higher demands to resource utilization and efficiency in the sector. Food systems contribute to about a quarter of global anthropogenic greenhouse gas (GHG) emissions (Willett et al. 2019). Facing the climate change crisis, waste must be reduced and increased production needs to fulfill requirements to social, economical and environmental sustainability. More efficient use of energy and resources in food processing, distribution and retail is needed to reduce emissions, and changes in patterns of consumption in terms of amounts and types of food is crucial for meaningful mitigation benefits (Vermeulen et al. 2012).

Fish is an important source of high-value protein, a wide range of vitamins, minerals and polyunsaturated omega-3 fatty acids as well as being generally low in saturated fats, carbohydrates and cholesterol. This makes fish provisions effective nutrients, and fish consumption is expected to play a major role in improving global food production efficiency (Msangi et al. 2013). Compared to terrestrial animals, farmed fish is significantly more effective in terms of protein output per use of land (Poore & Nemecek 2018, Froehlich et al. 2018), as well as being associated with some of the lowest GHG emissions (Hilborn et al. 2018, Poore & Nemecek 2018). In addition, aquatic animals are more efficient than terrestrial in turning feed into meat because they spend less energy moving, staying upright and regulating body temperature due to buoyancy and ectothermic nature (Naylor et al. 2009). This results in lower feed conversion ratios (FCR), which is calculated as the ratio of feed intake to weight gain, than terrestrial animals, as well as efficient protein and calorie retention (Fry et al. 2018).

Between 1961 and today, the average annual increase in fish consumption has been twice as high as population growth, 3.2% and 1.6% respectively, which is largely due to aggressive expansion in the aquaculture industry. While capture fishery has remained relatively static since the late 1980's due to stock capacity saturation, aquaculture production has seen exceptional growth rates of 11.3%, 10.0% and 5.8% in the 1980s, 1990s and since 2000 respectively, which makes the aquaculture industry the fastest growing food production

sector in the world (FAO 2018). However, the rapid expansion has increased per unit GHG emissions of the world fisheries, estimated by Parker et al. (2018) to a 21 % increase in average emissions per tonne of produced fish between 1990 and 2011. In addition, more extensive aquaculture production poses a threat to coastal habitats, freshwater and terrestrial systems related to feed production, and further expansion must be be managed in more sustainable ways. In other words, there is an urgent need of innovative technology to create novel culture systems and alternative feed strategies that can help reduce the environmental impact of the aquaculture industry (Willett et al. 2019).

Klinger & Naylor (2012) appoints the development of Recirculating Aquaculture Systems (RAS) technology as one of the most promising strategies for reducing environmental impact and waste while simultaneously intensifying fish production. RAS facilities are designed to collect and remove organic substances, bacteria and hazardous compounds from the culture tanks so that water can be recycled back into the system (Klinger & Naylor 2012). By use of a wide variety of mechanical filters, biofilters, disinfection methods, degassers, aerators and oxygenators, RAS enables 90 - 99 % of the water to be recycled (Badiola et al. 2012). Although the technology has been utilized in European fish production for decades, starting in the Netherlands in the mid 1980's, it has not been dedicated much focus in Norwegian aquaculture until the last decade (Martins et al. 2010). However, due to high costs related to heating of inflow water, limited access to fresh water during dry periods and advantages of optimized and stable temperature conditions all year, the focus on RAS has increased (Kristensen et al. 2009). In production of Atlantic salmon, RAS technology were initially applied for breeding of smolt (Bergheim et al. 2009), but land based facilities with on-growing of post-smolt and market size salmon production using RAS have become more common in recent years (Hagspiel et al. 2018).

Furthermore, there are several industry specific incentives to boost land based production of Atlantic Salmon in Norway, where the most prominent barrier to increased production is impact of sea lice (Vollset et al. 2018). Sea lice have for several years been considered a major risk to environmentally sustainable aquaculture, and problems in controlling its occurrence has caused stagnation of the Norwegian production volume since 2012 (FAO 2005). By extending the production time on shore, shorter time is spent at sea where the fish is susceptible to lice and diseases. In addition, the traditional open cage system is restricted to a maximum stocking density of $25 kg/m^3$ while closed containment systems are allowed higher densities, making land based production more effective in terms of volume utilization (Akvakulturdriftsforskriften 2018).

1.1 Background and motivation

Welfare and growth rates are major concerns when cultivating fish in land based facilities, and ensuring conditions that optimize the breeding environment is a vital task. Tank hydrodynamics is an important aspect in this regard because it affects swimming conditions, distribution of feed, oxygen and inorganic compounds as well as particle transport and cleaning patterns in the tanks (Shahzad 2019). By providing swimming speeds that are optimal for the reared species, growth rates, disease resistance and robustness of the fish is improved (Castro et al. 2011, Ytrestøyl et al. 2013). Distribution of feed and dissolved oxygen in addition to accumulation of fish metabolites, such as carbon dioxide and ammonia, influence the water quality which affect fish welfare and behaviour (Terjesen et al. 2013, Kolarevic et al. 2014, Good et al. 2018). Particle transport is particularly important in relation to the occurrence of quiescent zones, where water velocities are low and particles tend to settle at the tank floor causing sedimentation of organic matter (Huggins et al. 2005, Gorle et al. 2018a), which in turn promotes microbial growth of harmful bacteria that may cause infections, disease and in worst case mortality (Vadstein et al. 2018). Hence, ensuring optimal water flow conditions in the rearing tanks is of high importance.

According to Lekang (2007), optimally functioning rearing tanks are designed with inlets and drains that promote self-cleaning and even distribution of water and dissolved oxygen throughout the entire unit. However, a wide variety of parameters influence the tank hydrodynamics, both physical parameters such as hydraulic retention time (HRT), inflow and outflow boundary conditions, tank geometry and piping within tank walls, as well as biological parameters such as fish biomass, stocking density and fish behaviour (Lekang 2007, Plew et al. 2015). Furthermore, turbulence and complexity increase with increasing tank size, making self-cleaning and uniform flow distribution more challenging (Shahzad 2019). Solely experimental based tank design optimization is not feasible due to large labour and time dependence. Consequently, numerical modelling by use of computational fluid dynamics (CFD) is a promising and more appropriate approach (Gorle et al. 2019). CFD is a rapidly evolving science that uses powerful computers to solve equations that describe fluid flow within a domain. The method is often ideal for parametric studies or flow investigation that otherwise would be impractical or impossible by use of experiments (Chung 2010).

Optimization and improvement through simulation based design is a rather new branch in the field of aquaculture. Although interest in developing rearing facilities with new designs

has recently increased due to current innovation in production methods such as RAS, very few hydrodynamic studies of land-based tank environments have been conducted (Gorle et al. 2019). Existing literature study relatively small tanks compared to the currently applied commercial sized land-based and sea-based systems. It is therefore necessary to better understand the hydrodynamics in larger units to safeguard fish welfare and bring new knowledge into optimization of the inlet and outlet arrangements in aquaculture tanks (Klebert et al. 2018).

1.2 Research objective

Due to the existing knowledge gap in optimal designing of aquaculture tanks, the present study aims to provide insights and increased knowledge into the field of research. By combined use of qualitative and quantitative research methods, a literature review and numerical investigation by CFD-analyses, the study examines the hydrodynamics of rearing tanks without the presence of fish. The research objective is to uncover important hydrodynamic features of the rearing tanks, investigate the hydrodynamic influence by tank geometry and inflow conditions, and discuss the significance of numerical modelling with respect to optimized tank design. Consequently, the following research questions (RQ's) were formulated:

1. What are the most important hydrodynamic features of land-based aquaculture tanks?
2. How does geometry and inlet conditions influence the tank hydrodynamics?
3. How can numerical modelling by use of CFD contribute to optimization of land-based aquaculture tanks?

By answering these RQ's, the purpose of the study is to provide a broad understanding of the subject, while simultaneously generate detailed insights in order to generalize the findings and predict the best-practice tank design. A scoping literature review is to be carried out as a preliminary activity in order to identify the scope and size of available research literature, acquire an overview of the research topic and provide benchmark data for the qualitative study. Subsequently, CFD simulations in a numerical flow tank will be conducted to study the hydrodynamic effects influenced by different input parameters. The qualitative study will consist of two parts: 1) validating the numerical model and 2) applying the validated model in a parameter study of various tank designs. RQ1 is to be answered based on qualitative findings in review of current literature, RQ2 by the quantitative results of CFD-analyses, and RQ3 as a result from triangulation of the findings in RQ1 and RQ2.

1.3 Scope and limitations

Land based aquaculture plants are complex systems taht combine several branches within biology, chemistry and engineering, which depend upon a wide variety of physical and biological variables (Davidson & Summerfelt 2004). All land based facilities require a degree of waste water treatment, with water reuse and quality requirements being particularly strict in RAS. Hence, the facilities are often large and consist of several critical components beyond the production units, e.g. mechanical filters, UV filters, CO_2 degassers and biofilters to name a few (Lekang 2007). In the present study however, the aim is directed exclusively to the rearing tanks that enclose the production volume. The boundaries of the thesis are set at the tank walls, and solely the domain within the production units will be considered. Thus, the focus will be directed towards the 'hydrodynamic features', i.e. properties that occur in the rearing environment which can be manipulated by convective transport of flow, that optimize water quality. Furthermore, optimal conditions in the tank environment are depending on the reared species and biomass size (Lekang 2007). The present study focus on cultivation of Atlantic salmon in medium sized tanks of volumes around 100 m^3.

Even the tank environment itself is too complex to be completely numerically modelled with all operational variables present. For instance, modelling of fish behaviour and particle tracking of pellets is not feasible with the magnitudes involved in an aquaculture tank. The scope of the thesis is therefore limited to tanks without the presence of fish, feed and other technical installations beyond inlets. The microbial community and appearance of chemical compounds in the environment is also excluded from the thesis. Due to limitations in the applied numerical model, several simplifications of the tank components are made. Mass inflow is not considered and inlets are not designed with nozzles, but rather assigned with a vertical velocity line which prescribes the velocity of inlet boundary cells. Furthermore, outflow conditions in the tanks could not be incorporated in the current version of the numerical model, and hence the study is limited to exclude hydrodynamic effects imposed by draining. Justification of the simplifications are further described in chapter 3.3.2.

2 Theory

The following chapter is divided into two parts. The first part deals with tank design in land-based aquaculture, including definitions and general hydrodynamic aspects, as well as tank geometries and water inlet design. Section 2.1 is the theoretical foundation obtained by the findings in the scoping literature review, which serve as the basis for the answer to RQ1. The second part comprises theoretical aspects in computational fluid dynamics (CFD), including governing equations, discretization methods, turbulence modelling and boundary conditions.

2.1 Tank design in land-based aquaculture

The aquaculture production units are unquestionably one of the most important parts of a land based aquaculture facility. Each unit encloses a volume where the fish is being bred, and the environment in the body of water dictates the living conditions of the fish. The microbial community of the rearing unit directly interacts with the fish, and may therefore have a great influence on their health status (Blancheton et al. 2013). The water within the units is exchanged to provide feed and dissolved oxygen, and remove waste products such as excess feed, faeces, CO_2 and NH_3 from the environment, to ensure that the breeding environment is of high quality (Ebeling et al. 2010). The water exchange generates a flow field which dictates how the fundamental inputs are brought to the fish, as well as affecting transport of waste out of the environment. In addition, the hydrodynamics influence the swimming conditions of the fish, which in turn affect production growth rates (Nilsen et al. 2019).

Production units may be classified into two types, depending on the flow pattern of the water in the unit (Lekang 2007): 1) Units with one-way water flow, and 2) units with circulating water flow. The former include units such as raceways and ponds, which are mainly used in extensive fish farming, and are not included in the present work. The latter include tanks in different shapes and materials, which is the subject for this thesis. The optimal choice of tank type depends on the cultivated species, e.g. flatfish require a larger diameter-to-depth ratio compared to pelagic fish, as well as the facility in which the tanks are embedded. Hatcheries and juvenile farms, smolt or post-smolt facilities all produce fish of different size, where fish of larger size naturally require larger tanks which

in turn affect the choice of tank type (Lekang 2007).

Tank geometry in addition to water inlet and outlet characteristics are the main design parameters that influence tank hydrodynamics (Oca & Masalo 2013). Various tank types may be categorized on the basis of geometry and dimension ratios. The main types used in commercial recirculating design are circular-, octagonal- and mixed cell raceway tanks (Lekang 2007, Ebeling et al. 2010), where circular and octagonal tanks are popular choices at Norwegian sites. Typical tank volumes in cultivation of post-smolt Atlantic salmon range between $500 - 1300m^3$ (Summerfelt et al. 2016), however the present thesis is aimed at lower tank volumes around $100m^3$.

The main purpose of the rearing tanks is to enclose a water body for breeding of fish. The presence of biomass blocks the flow and significantly affect the tank hydrodynamics. According to Plew et al. (2015), the mean tank velocity is reduced between 15 – 57 % respectively for average biomass stocking densities between 15.3 - 79.4 kg/m^3, and the distributions of mean velocity, turbulence and dissolved oxygen are altered. For a stocking density of 60 kg/m^3, Gorle et al. (2018a) found that mean rotational velocities were reduced by 25%, but that the secondary flow and radial velocities remained unchanged. Furthermore, the turbulent intensity, kinetic energy and dissipation rates increase in the presence of fish (Plew et al. 2015). Solids removal is also affected by fish re-suspension of settled materials, which generally lead to better cleaning in tanks with higher biomass (Timmons et al. 1998). However, the dynamics involved with fish motion and behaviour cannot be modelled numerically, and it is a separate topic that deserve extensive research to develop and incorporate into turbulence models (Gorle et al. 2019). For this reason, the present study did not consider the presence of biomass in the tanks.

2.1.1 Hydrodynamics in circular flow tanks

Flow rates through the tanks are decided by the mean hydraulic retention time (HRT), which indicate how frequently the tanks are being flushed. The HRT usually varies depending on tank size and the capacity of the water treatment facility, however a range of 20 - 200 minutes is common, where new tanks usually are operated with lower HRT's (Ebeling et al. 2010, Summerfelt et al. 2016, Nyhus 2020).

Primary and secondary flow

Aquaculture tanks are operated by injecting a water flow tangentially to the side wall at the tank outer radius. The tangential inlet give rise to two flow patterns within the tank,

i.e. primary and secondary flow, as shown in figure 2.1.1 (Lekang 2007). The impulse force from the inlet creates a rotating flow in the horizontal plane around the tank center, i.e. the primary flow. The no-slip condition between the primary flow and tank boundaries creates a secondary flow in the vertical plane of the tank, which has an inward flow component at the bottom and an outward flow component at the surface (Timmons et al. 1998).

The secondary flow drives the process known as 'hydraulic self-cleaning' of the tank, where the inlet flow is utilized to clean the tank walls and bottom by removing settleable solids that are introduced to the tank by faeces, uneaten feed and feed fines (Lekang 2007). Circular tanks are self-cleaning when the primary rotational create a secondary flow that has velocities sufficient to transport solids along the bottom towards the center drain. This effect is also known as the 'tea-cup' or 'bathtub' solids transport phenomenon, which rapidly cleans settleable solids from the tank (Davidson & Summerfelt 2004).

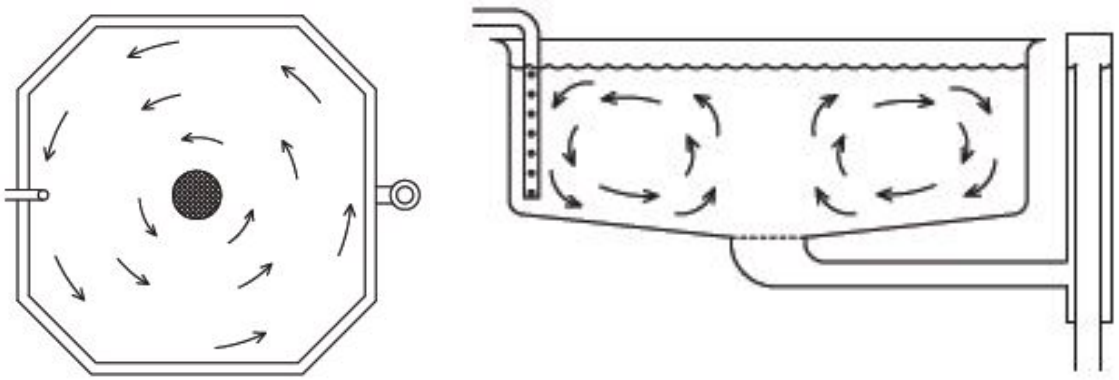

(a) Primary flow **(b)** Secondary flow

Figure 2.1.1: Tank flow patterns

Generally, two different vortices are present in circular aquaculture tanks; a 'forced vortex' and a 'free vortex' (Oca & Masalo 2013). A forced vortex is rotational and obtained when a recipient is spun or a torque force is applied to an enclosed body of water. It occurs in the tank as a response to the energy input from the inlet. In a forced vortex, angular momentum and flow velocities are increasing proportional to the tank radius. A free vortex is irrotational and occurs when the fluid is drained through the central outlet. In contrast to forced vortices, no force is applied to the water body and there is no energy consumption from an external source. Angular momentum is constant in a free vortex, and the flow velocities are largest at the center and decrease linearly with distance from the center (Oca & Masalo 2013). The occurrence of forced and free vortices give rise to different zones in the tank environment: a rotational zone due to the forced vortex in the outer tank volume, and an irrotational zone close to the central outlet (Timmons et al.

1998). The rotational zone is usually characterized by higher velocities and better mixing properties than the irrotational zone, however it is largely influenced by orifice inflow velocity, HRT and draining characteristics (Davidson & Summerfelt 2004, Oca & Masalo 2013).

Flow velocities

Tank performance is assessed by the velocities of the flow field that is generated by the inflow and outflow boundary conditions. For optimal tank conditions, the flow velocities should be evenly distributed to ensure utilization of the whole tank volume and be sufficiently high to provide good mixing of the inflow water (Timmons et al. 1998, Davidson & Summerfelt 2004, Oca & Masalo 2013) . Furthermore, there are velocities that optimizes the self-cleaning properties of the tank, as well as optimal values for fish exercise and growth rates (Lekang 2007, Castro et al. 2011). The velocity distribution in the tank usually have large radial variation, but relatively uniform distribution vertically when vertical inlets are present (Tvinnereim & Skybakmoen 1989). It is however heavily influenced by the inflow and outflow boundary conditions. In a traditional tank design, with a tangential inlet close to the tank wall and a central bottom drain, velocities have maxima near the wall and center and a minimum in the intermediate region between the inlet and drain (Oca & Masalo 2013). However, when inflow angles are changed and dual drains are present, further described in chapter 2.1.3, the flow pattern and velocity distribution changes radically (Davidson & Summerfelt 2004, Gorle et al. 2019).

The orifice velocity in the inlet pipes usually range between 1.0 - 1.5 m/s (Lekang 2007, Nyhus 2020). Ebeling et al. (2010) suggest that tank velocities near the wall may be as high as 15 - 20 % of orifice velocity if the inlets are properly designed, and experiments conducted by (Oca & Masalo 2013) indicate that outflow velocities through the center may be even higher. As a practical rule of thumb, average rotational velocity is assumed 10% of the orifice velocity in inlet pipes, with maximum velocities may reach 25-30 cm/s close to inlets and outlets in large tanks (Nyhus 2020). To ensure transport of settled solids for sufficient self-cleaning behaviour as well as removal of algae on the tank bottom and wall, Lekang (2007) recommends that velocities at the bottom are above 6-8 cm/s, which corresponds to velocities in the free water mass of approximately 12 – 15 cm/s. Timmons et al. (1998) do however suggest that rotational velocities should be in the range of 15 - 30 cm/s in order to drive settleable solids to the center drain. Furthermore, flow velocities of 1.0 – 1.5 body lengths per second are optimal for aerobic training that stimulate growth of Atlantic salmon (Castro et al. 2011).

2.1.2 Tank geometries

The most common geometries used for cultivating Atlantic salmon are circular and octagonal tanks (Summerfelt et al. 2016). Circular flow tanks are proper rearing units because they easily provide a uniform water flow, can be operated under a wide range of rotational velocities to optimize fish swimming conditions, and may be used to rapidly concentrate and remove settleable solids (Timmons et al. 1998). Circular tanks allows obtaining more stable flow patterns and higher velocities than rectangular tanks, thanks to the rotating characteristics of the flow. This results in a more homogeneous distribution of dissolved oxygen and metabolites, and facilitates the elimination of biosolids from the tank bottom (Oca & Masalo 2013). Numerical studies conducted by Papáček et al. (2018) indicate that circular tanks are most efficient in terms of power use, providing higher velocities per unit input compared to octagonal and square tanks when the inflow is injected tangentially adjacent to the tank wall.

A main important factor that is affected by the tank geometry is the flow uniformity. Corners or bends within the tank promotes the occurrence of quiescent (or dead) zones, where water velocities are low. Dead zones causes several hydrodynamic disadvantages, such as reducing the effective farming volume, reducing the amount of dissolved oxygen and promoting the accumulation of biosolids within the tank (Timmons et al. 1998, Duarte et al. 2011, Oca & Masalo 2013). Circular tanks easily avoid this phenomena, which typically appear in corners of square tanks, as shown in figure 2.1.2 (Lekang 2007). Octagonal tanks are an intermediate design between rectangular and circular tanks, where the corners are cut in order to improve the hydrodynamic features, however not completely avoiding the occurrence of dead zones which is the case for circular tanks (Gorle et al. 2018b). Regions of low velocities and poor mixing may however also occur in circular tanks, in a torus-shaped 'irrotational zone' about the central axis of the tanks (Timmons et al. 1998).

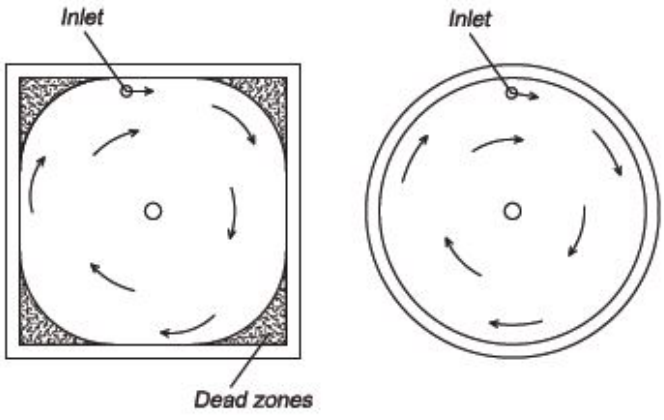

Figure 2.1.2: Dead zones where water velocities are low

Other important aspects that are affected by the tank geometry is utilization of surface area and utilization of the tank construction material (Lekang 2007). Land cost can be a significant factor when constructing a land based facility, and may affect the choice of tank (Badiola et al. 2018). Rectangular tanks are most efficient in providing the largest tank volume per land area, and they may together with octagonal tanks be installed adjacent to each other by sheared walls, which further increases the the stocking efficiency of the tanks (Gorle et al. 2018b). Circular tanks do however provide the best utilization of the construction material, due to equal pressure distribution around the circumference of the tank. In contrast, square and octagonal tanks have hydrostatic forces accumulate in the mid-span of the wall. A larger wall thickness must therefore be used in such tanks, and the effect is amplified as tank sizes increase (Lekang 2007).

Increasing the tank height in order to achieve higher volume per surface area is however paradoxical for several reasons. Higher tanks increases the operational energy demand by requiring more pumping (Badiola et al. 2018). Increased height also increases the hydrostatic pressure in the tank, causing a need for more material and thicker walls. The hydrodynamic properties of silos (D¡d) are insufficient, because it is difficult to achieve sufficient uniform water exchange and secondary flow (Lekang 2007). Ebeling et al. (2010) also point out that problems regarding fish management in silos. According to Lekang (2007) and Ebeling et al. (2010), a diameter-to-depth (D:d) ratio between 2 and 5 is recommended in tanks with a circular flow pattern. Nyhus (2020) state that a ratio of D:d = 3:1 is a general recommendation in order to provide good self-cleaning properties and avoid a powerful vortex at the tank center. Summerfelt et al. (2016) do however indicate that the industry uses tanks with slightly higher ratios, ranging from 3.6:1 to 5.5:1. In addition, tanks usually have a sloping floor of 4.0-6.5 % to reduce labor when removing dead fish (Summerfelt et al. 2016), however the slope has low significance on the cleaning properties, because gravitational effects are low compared to the hydraulic flow and impulse forces from the inlets (Lekang 2007).

2.1.3 Design of water inlets

Although the tank geometry influence the overall flow pattern, the inflow and outflow boundary conditions usually have the largest impact on the tank hydrodynamics (Davidson & Summerfelt 2004, Oca & Masalo 2013, Gorle et al. 2018b). It is possible to design the water inlet and outlet arrangements in such a way that full control over the flow conditions in the tanks can be achieved (Tvinnereim & Skybakmoen 1989). The inlet and outlet of a tank are optimized for a given flow rate, and correct design is necessary to ensure self-cleaning, even distribution of velocities and mixing of new water (Lekang

2007). Furthermore, the flow inlet and outlet structures should be engineered to reduce the labor requirements of handling fish and to obtain effective tank rotational characteristics, and solids flushing (Timmons et al. 1998).

The most basic configuration is a tangential inlet close to the tank wall and an outlet placed in the bottom center, as illustrated in figure 2.1.3a (Timmons et al. 1998). The figure shows: (A) tangential inlet placed close to the tank wall, and (C) a central outlet at the bottom. This configuration is the most efficient in providing high flow velocities within the tank, as well as achieving sufficient secondary flow to ensure good particle flushing properties (Tvinnereim & Skybakmoen 1989, Timmons et al. 1998, Davidson & Summerfelt 2004, Oca & Masalo 2013). The tank in figure 2.1.3a also shows a type of dual-drain, where large particles are flushed and separated in an external swirl separator (B), and water with low particle consentration is flushed in an elevated drain trough and external standpipe (D) that controls the water level in the tank.

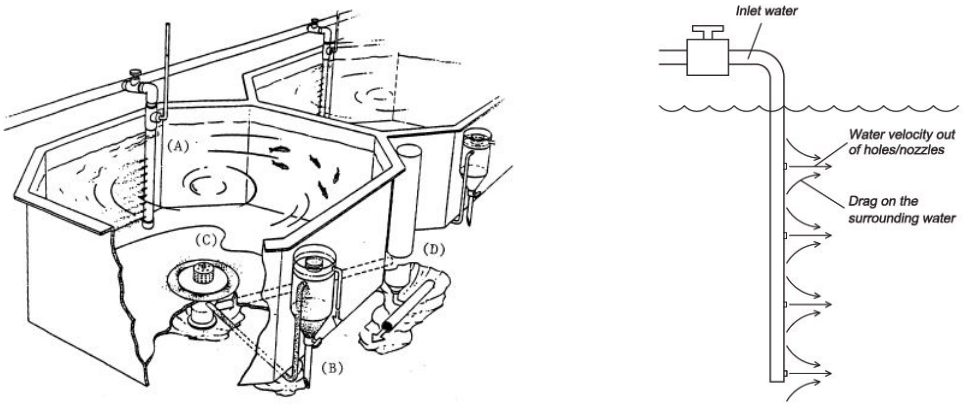

(a) Basic tank setup

(b) Impulse force from inlet

Figure 2.1.3: Water inlet and draining components

Inlet design

New, oxygen-rich water is injected trough several nozzles in inlet pipes that are installed throughout the water column. The velocity out of the nozzles exert an impulse force that causes drag on the surrounding water, which creates a flow pattern inside the tank as illustrated in figure 2.1.3b (Lekang 2007). The impulse force is the main factor affecting the average rotational velocity in circular and octagonal tanks, which is depending on the water flow, rotational velocity in the tank, as well as size and direction of the inlet velocity vector through the nozzles (Tvinnereim & Skybakmoen 1989, Oca & Masalo 2013, Gorle et al. 2018a). The overall water flow is governed by the hydraulic retenition time (HRT), while the velocity and direction of the inlet water is adjusted manually by opening, closing or rotating the nozzles (Nyhus 2020). Manual operation of the inlet valves makes it nearly

impossible to maintain definite velocities and equal inflow between multiple inlets, and usual flow rates through two pipes usually vary between 10-15 %, however the difference may be as high as 30-40 % (Gorle et al. 2019).

As shown in figure 2.1.4 (Lekang 2007), different inlet arrangements may be applied to the tank. Experiments conducted by Tvinnereim & Skybakmoen (1989) show that the vertical inlet 2.1.4a creates a flow pattern with the highest primary and secondary flow patterns, while the horizontal inlet 2.1.4b creates better mixing and a uniform flow pattern along the radial axis of the tank. A combined inlet 2.1.4c can be used as an intermediate solution to achieve higher uniformity while at the same time preserve the secondary bottom current. Due to a stable bottom current toward the outlet assuring sufficient self-cleaning properties, the vertical inlet is a popular choice (Lekang 2007). Other variants of the vertical inlet have also been tested, e.g. where nozzles on the upper part of the pipe point tangential to the wall and nozzles at the bottom point toward the outlet, resulting in an even stronger secondary flow (Gorle et al. 2019).

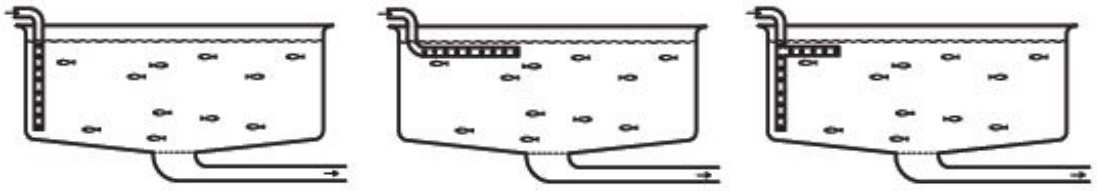

(a) Vertical inlet **(b)** Horizontal inlet **(c)** Combined inlet

Figure 2.1.4: Various inlet designs

Outlet design

Faeces, uneaten feed and feed fines settle at the tank bottom and need to be transported out of the environment before sedimentation occur. A central outlet is practically always present in aquaculture tanks, and dual-drain configurations with additional drains elevated at the tank wall are also applied (Timmons et al. 1998, Davidson & Summerfelt 2004, Oca & Masaló 2007, Oca & Masalo 2013, Gorle et al. 2018b). The drain must be designed to continuously remove the concentrated matter, periodically being able to remove dead fish that are captured in the bottom center, and to act as control of the water level in the tank (Ebeling et al. 2010). Correct design of the drain is also important regarding the water exchange rate and self-cleaning properties of the tank, to avoid that the outlet system acts as a settling basin (Lekang 2007). Due to limitations in the numerical model applied in the thesis, outlets were not included in the quantitative study of tank designs. Design of outlets is therefore not described in further detail.

2.2 Computational fluid dynamics (CFD)

Design and analysis of fluid flow engineering systems may be done using either experimentation or calculation. The former is usually done by testing of constructed models in specialized facilities, while the latter solves differential equations that describe fluid flow analytically or numerically Yunus (2010, p. 880). Numerical modelling by use of computational fluid dynamics (CFD) is a field of study that resolves the Navier-Stokes (NS) equations in order to describe a flow problem in detail within a domain. The equations are used to calculate important variables such as velocity, pressure and turbulence. Few assumptions have to be made in order to apply the NS equations, and fluid viscosity as well as rotational flow are included in the solution, making CFD a powerful tool to realistically represent the evolving hydrodynamics (Bihs et al. 2016).

CFD is usually applied as a complementary tool to experiments and theoretical fluid dynamics in design engineering, however CFD offer a number of distinct advantages (Hu 2012): 1) Results can be produced quickly at relatively low computational expense. The cost of computing is ever decreasing, which makes the application of CFD more effective. 2) Complete and detailed information of all relevant variables is generated throughout the domain of interest. 3) Changes to parameters can easily be done, thereby facilitating design optimization. Compared to experiments, CFD offers more possible variations at significantly lower cost. 4) It is possible to simulate realistic, ideal or extreme events. There is no need for small- or large-scale models to simulate realistic events, certain terms can be switched off in the numerical model to examine ideal conditions, and investigation of unwanted situations such as dam breaks or tsunamis may be done.

Numerical models do however rely on quality results from conducted experiments. In order to ensure that the numerical model is accurate and to gain trust in the simulation results, the numerical model has to be validated against experimental results. Validation is done by replicating a conducted experiment, using the identical setup in the numerical model. The experimental and numerical results are in turn compared to check whether there is correlation and if the error is within acceptable limits (Yunus 2010, p. 880). A valid numerical model provide highly accurate results that are close to the results gained from an experiment with the same setup. The concept of numerical accuracy is described in subsection 2.2.3.

Even though the importance and accuracy of numerical models using CFD has increased, the predicted results are never exact. Ferziger et al. (2020) emphasize the importance of

estimating errors in numerical modelling. Although an incorrect solution to a problem may seem reasonable, the consequence of accepting it can be severe. Furthermore, a poor solution can be of value if treated with care. Several potential error sources are involved in a numerical simulation, with the most common sources being (Ferziger et al. 2020, Hu 2012):

- *Modeling error* is the difference between the actual flow and the exact solution of the mathematical model. It can be considered negligible for laminar flows, but it may be severe when flow problems are complex and involve phenomena that cannot be described completely by current scientific theories. E.g. turbulence, atmospheric and multi phase flow modeling require dedicated schemes to be solved, which contain error sources.

- *Discretization error* is the difference between the exact solution of the governing equations and the exact solution of the discretized algebraic system of equations. It is inherent in all numerical methods, and it arise whenever a continuous system is approximated by a discrete system. The magnitude of the discretization error depends on the type and order of the applied numerical scheme, which is further discussed in subsection 2.2.4.

- *Iteration errors* is the difference between the iterative and exact solutions of the algebraic equations systems.

- *Input data error* emerges due to the fact that the fluid properties and flow geometry may be know approximately, and not in full detail.

- *Initial and boundary condition error* is associated with knowledge of the initial state of a problem. The flow boundary conditions may represent an incomplete real situation, or the initial conditions may not be known exactly.

2.2.1 The numerical model REEF3D::CFD

The numerical model applied in the present work is the CFD model in the open source hydrodynamics software REEF3D, presented by Bihs et al. (2016), which focuses on coastal, marine and hydraulic engineering flows. The model apply high-order spatial and temporal discretization schemes that produces accurate and stable results, which is done by efficient use of a large number of processors running in parallel. It solves relevant governing equations at all scales, providing optimized wave and flow modules depending on the hydrodynamic problem (Bihs 2020).

Initially presented by Bihs (2011), REEF3D was used to study local scouring in open channel flow. Since then, further development of the model has been made to make it applicable to a wide variety of hydrodynamic engineering problems, such as: wave propagation, transformation, breaking and forces (Kamath 2012, Aggarwal 2015, Chella et al. 2015, Elakel 2018), sediment transport (Afzal 2013), sea state and coastal modeling (Bihs et al. 2020, Wang et al. 2020), and sloshing (Grotle et al. 2018). Recent development also introduces the model to the field of aquaculture, as simulations of moored floating bodies (Martin et al. 2020b) and net motion in waves and current (Martin et al. 2020a) have been conducted. The present work intend to further expand into the aquaculture industry, by presenting a model that may be applied to rearing tank design, allowing optimization of land-based facilities.

2.2.2 Governing equations

The fundamental basis of CFD is a set of conservation laws that give rise to a set of coupled partial differential equations, which are the governing equations (GE's) that describe fluid flow. More specifically, conservation of mass and momentum is assumed. When a quantity is conserved, the total amount of the quantity exiting a control volume is equal to the amount entering added to the quantity produced or consumed in the control volume. In addition, the fluid is assumed incompressible, which states that the density do not change in space or time. Impressibility is a reasonable assumption for liquid flow and gases with low Mach numbers (Ferziger et al. 2020, p. 2). The assumptions of mass conservation combined with fluid incompressibility lead to the first GE, the continuity equation:

$$\frac{\partial u_i}{\partial x_i} = 0 \tag{2.2.1}$$

A Newtonian fluid is a fluid that obeys Newton's law of viscosity, which states that the effects of viscosity are important only near wall regions, so that flow in the largest part of a domain may be considered inviscid (Ferziger et al. 2020, p. 2). Conservation of momentum arises from Newton's second law, which states that the rate of change of linear momentum is directly proportional to the sum of the forces acting on the fluid. The three last GE's, the momentum equations, are derived by assuming momentum conservation and a Newtonian fluid:

$$\frac{\partial u_i}{\partial t} + u_j \frac{\partial u_i}{\partial x_j} = -\frac{1}{\rho}\frac{\partial P}{\partial x_i} + \frac{\partial}{\partial x_j}\left[\nu\left(\frac{\partial u_i}{\partial x_j} + \frac{\partial u_j}{\partial x_i}\right)\right] + g_i \tag{2.2.2}$$

The first term on the left-hand side is a temporal term that describe how the quantity changes with time. The second term, convection, represent the spatial change of the

quantity. The first term on the right-hand side accounts for the effect of pressure. The second is a shear stress term that describe the viscous forces affecting the flow, such as wall effects and turbulence. The last term accounts for gravitational forces.

2.2.3 Numerical treatment of the governing equations

The equations 2.2.1 and 2.2.2 are collectively known as the Navier-Stokes (NS) equations. They describe the flow of Newtonian fluids accurately, however they can only be solved analytically for a small number of impractical cases. Hence, the NS-equations need to be solved numerically in order to make them applicable to engineering flow problems. "Much as the accuracy of experimental data depends on the quality of the tools used, the accuracy of numerical solutions is dependent on the quality of discretizations used" (Ferziger et al. 2020, p. 25).

Discretization is done by using dedicated schemes, which approximates the GE's by a system of algebraic equations that can be solved on a computer. Several different approaches may be applied, but the most important methods include finite differences (FD), finite volume (FV) and finite element (FE). There are both advantages and disadvantages with all approaches, which make some methods more suitable to certain flow problems than others (Ferziger et al. 2020, p. 27). REEF3D uses finite differences method for discretising the NS-equations, which is further described in subsection 2.2.4.

The variables of interest, such as velocities, pressure and turbulence, are calculated at discrete locations defined by a *numerical grid*. The grid divides the flow domain into a finite number of cells, as shown in Figure 2.2.1a (Ferziger et al. 2020, p. 42), where the GE's 2.2.1 and 2.2.2 are resolved in each cell. "Even with the same method, the discretization error will be different depending on the distribution of grid points used in a scheme. In most applications, one needs to properly select a numerical method and choose a grid to control the error" (Hu 2012). The grid may be structured; simple structure of regular cells that has an organized structure of rows and columns, or unstructured; flexible grid that fit and 'wraps around' any arbitrary boundary of the domain. Structured grids are generally more computationally efficient and simplifies the implementation of high order discretization schemes, while unstructured grids are more applicable to complex geometries and more suitable to control the distribution of grid points (Ferziger et al. 2020, p. 28).

In REEF3D a staggered Cartesian grid is utilized for spatial discretization, where the grid points are structured and evenly distributed in the domain forming parallelotopes

or 'bricks'. 'Staggered' implies that the unknown variables are not located at the same grid point, e.g. velocities are calculated at the middle of cell surfaces, while pressure is located at the cell centre, as illustrated by Figure 2.2.1b (Griebel 1997, p. 27). The main advantage of using a staggered grid is that it prevents pressure oscillations that may occur in collocated grids, where all variables are located at the cell centres (Kamath 2012).

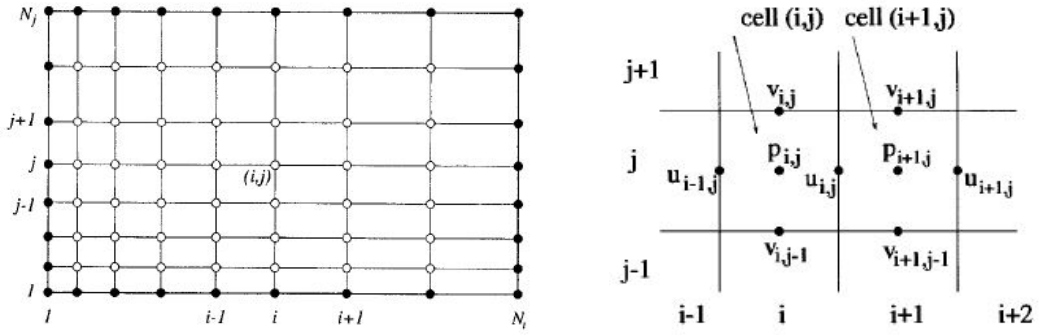

(a) 2D Cartesian grid **(b)** Staggered grid

Figure 2.2.1: Numerical grids used in FD discretization methods

Properties of numerical models

The solution methods in numerical models have certain properties that determine the applicability of their algorithm to flow problems. If the solution do not possess these properties, neither will the model. The most important properties are: *stability, consistency, convergence* and *accuracy* (Ferziger et al. 2020, p. 34).

- Numerical *stability* implies that the applied scheme does not magnify the errors that appear throughout the numerical solution process. A stable scheme produces solutions that are properly 'bounded' to upper and lower limits, e.g. physical quantities such as density and turbulent kinetic energy must always be positive. In contrast, an unstable scheme produces results with unbound errors that tend to blow out of proportions, causing an emergency stop of the iteration process if maximum values stated in the model are exceeded.

- A numerical scheme has *consistency* if the discretization become exact as the cells in the numerical grid is refined. The difference between the exact solution and the approximation is called the *truncation error*, which is obtained by applying Taylor expansion to the discrete approximation about a single point. The result is the governing differential equation in addition to the truncation error. For a consistent scheme, the truncation error tends to zero as the grid size, $dx \to 0$ or time step, $dt \to 0$.

- Likewise, the scheme *converges* if the solution of the discretized equations approaches the exact solution as $dx \rightarrow 0$ or $dt \rightarrow 0$. A scheme may be consistent without convergence, but not vice versa, and a consistent scheme is useless without convergence (Ferziger et al. 2020, p. 34). Examination of whether a scheme is converging is normally done by use of numerical experiments, i.e. grid- and time convergence tests. In such tests, simulations of the flow problem is repeated with successively refined grids and time steps to examine whether the results approaches the exact solution, which is usually done as a part of validation of the numerical model. Convergence occurs if the rate of change of the solution is reduced as the grid or time step is refined.

- The *accuracy* is a measure on how close the computed result is to the real solution, which is closely related to convergence and the consistency of the scheme. If the scheme is consistent and converging, higher accuracy of the results are obtained by improving the resolution of the grid. Since numerical solutions are only approximate solutions, there is always inherent some degree of error in the results. Improving the accuracy of the numerical results is largely about minimizing the different error sources in the model.

2.2.4 Convection discretization

The first step in evaluating 2.2.2 numerically is discretization of the convective terms. This can be done by using several different schemes, which provide different orders of accuracy and stability. On one side there is a need for high order schemes to provide accurate results and avoid numerical diffusion, which can lead to an unphysical damping of the solution (Bihs et al. 2016). On the other side, higher order schemes require higher computational power and may reduce the numerical stability. A key aspect in discretizing the convective terms is hence to balance accuracy and stability by using efficient schemes. In REEF3D, *finite differences (FD)* is applied as the discretization method. It is simple and computationally effective, and synergizes well with structured grids where the grid lines serve as local coordinates. High-order schemes are easily applied, which makes it possible to obtain high accuracy solutions. A drawback with the FD method is that it is difficult to resolve flow around complex geometries (Kamath 2012).

Discretizing partial derivatives

The FD method uses the direct definition of derivatives to discretize the governing equations :

$$\left(\frac{\partial \phi}{\partial x}\right)_{x_i} = \lim_{dx \to 0} \frac{\phi(x_i + dx - \phi(x_i))}{dx} \tag{2.2.3}$$

At each point in the numerical grid, the partial derivatives in the GE's are approximated by point values of the functions, with one unknown providing one algebraic equation. As shown in Figure 2.2.2 (Ferziger et al. 2020, p. 43), the exact derivative $\frac{\partial \phi}{\partial x}$ of the quantity $\phi(x)$ at point x_i is the tangent at that point. This derivative may however be approximated by points close to the point of interest. The approximations shown in Figure 2.2.2 are called 'forward-', 'backward-' or 'central difference' depending on whether the nearby points used in the approximation are upstream or downstream of the point of interest.

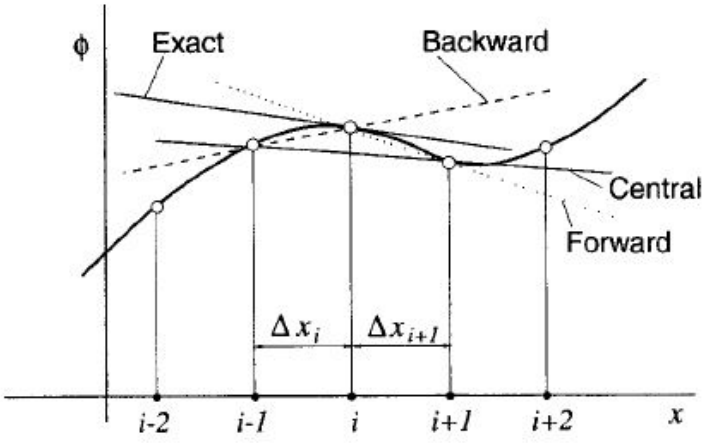

Figure 2.2.2: Definition of the derivative and its approximations

The number of points used in the approximation scheme represent a geometric sketch called a *stencil*. The stencil is related to the point of interest and gives an idea of the number of points used in the approximation, the order of the scheme, and if the scheme is explicit or implicit. If the stencil is widened, i.e. more points are used in the approximation, the order of the scheme is increased and higher accuracy is obtained. Explicit schemes only consider values from cells upstream of the point of interest, i.e. there is an explicit definition for the unknown variable. Implicit schemes utilize cells on "both sides" of the point of interest, i.e. they have stencils with more than one point at the new time step, $n + 1$ (Kamath 2012).

Any continuous differentiable function ϕ can, in the proximity of x_i, be represented by

a Taylor series, which is an infinite sum of first and higher derivatives of ϕ evaluated at x_i. Taylor expansion implies that higher order derivatives are included in the sum, which is approximated by use of Equation 2.2.4. If the distance between the points in a stencil, dx, is small, the higher order terms will be small except for situations with large gradients. Sufficient accuracy can then be obtained by only using the first derivative to approximate ϕ, i.e. truncating the Taylor series after the first term. The truncation error of the approximation then becomes the sum of the higher order derivatives that were excluded from the Taylor expansion (Ferziger et al. 2020, p. 45). The order of an approximation indicates how fast the error is reduced when the grid is refined, where higher order schemes have the error reduced faster.

Convection discretization schemes

The order of accuracy in discretization schemes is important to acquire high quality results. Higher order schemes are however more computationally demanding, so efficiency and numerical stability cannot be neglected (Bihs 2020). The following include a few schemes that may be applied for convection discretization (Ferziger et al. 2020, p. 45):

- *First Order Upwind (FOU) Scheme*
  The FOU scheme is a first order accurate, explicit scheme which evaluates the terms in the direction of the flow. Values from the grid cells upstream from the point of interest are used to approximate the unknown variables.

$$\left(\frac{\partial \phi}{\partial x}\right)_i \approx \frac{\phi_i - \phi_{i-1}}{x_i - x_{i-1}}$$

- *Central Difference Scheme (CDS)*
  The CDS is a second order scheme that uses the values from grid cells on either side of the point of interest. It is easier to implement than higher order upwind schemes because the flow direction does not have to be checked. However, the scheme is unconditionally unstable for damped differential equations with viscous terms, which provides inaccurate results (Kamath 2012).

$$\left(\frac{\partial \phi}{\partial x}\right)_i \approx \frac{\phi_{i+1} - \phi_{i-1}}{x_{i+1} - x_{i-1}}$$

- *Weighted Essentially Non-Oscillatory (WENO) Scheme*
  The Essentially Non-Oscillatory (ENO) scheme is a high order method that uses adaptive stencils for approximations (Jiang 1995). Each grid cell is assigned its own ENO-stencil, as shown in Figure 2.2.3, which are weighted according to their

'smoothness'. The WENO scheme is adaptive in the way that the stencil which provides the smoothest solution among the candidates is given the largest weight in the approximation. In this way, arbitrarily high order accuracy is achieved in smooth regions, while at the same time providing stable, non-oscillatory results in 'shock' regions. The scheme is minimum third-order accurate in areas with large gradients, while areas with smooth solutions deliver fifth-order accurate results (Bihs et al. 2016).

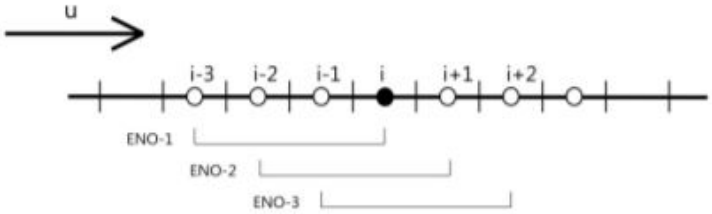

Figure 2.2.3: ENO-stencils

In x-direction, the convection term of velocity is approximated as such:

$$u_i \frac{\partial u_i}{\partial x_i} \approx \frac{1}{dx}(\tilde{u}_{i+1/2} u_{i+1/2} - \tilde{u}_{i-1/2} u_{i-1/2}) \tag{2.2.4}$$

where $\tilde{u}$ is the convection velocity, which is obtained at the cell faces, $i+1/2$, through simple averaging. $u_{i+1/2}$ is reconstructed through the WENO procedure:

$$ENO^{\pm}_{i+1/2} = \omega_1^{\pm} ENO^{1\pm}_{i+1/2} + \omega_2^{\pm} ENO^{2\pm}_{i+1/2} + \omega_3^{\pm} ENO^{3\pm}_{i+1/2} \tag{2.2.5}$$

ENO^1, ENO^2 and ENO^3 represent the three possible ENO stencils, while $\pm$ indicates upwind direction. For positive i-direction, the ENO stencils become:

$$\begin{aligned} ENO^{1\pm}_{i+1/2} &= \frac{1}{3}u_{i-2} - \frac{7}{6}u_{i-1} + \frac{11}{6}u_i \\ ENO^{2\pm}_{i+1/2} &= -\frac{1}{6}u_{i-1} + \frac{5}{6}u_i + \frac{1}{3}u_{i+1} \\ ENO^{3\pm}_{i+1/2} &= \frac{1}{3}u_i + \frac{5}{6}u_{i+1} - \frac{1}{6}u_{i+2} \end{aligned} \tag{2.2.6}$$

$\omega_1^{\pm}$, $\omega_2^{\pm}$ and $\omega_3^{\pm}$ in Equation 2.2.5 represent the non-linear weights, which are given by:

$$\omega_1^{\pm} = \frac{\alpha_1^{\pm}}{\alpha_1^{\pm} + \alpha_2^{\pm} + \alpha_3^{\pm}}, \quad \omega_2^{\pm} = \frac{\alpha_2^{\pm}}{\alpha_1^{\pm} + \alpha_2^{\pm} + \alpha_3^{\pm}}, \quad \omega_3^{\pm} = \frac{\alpha_3^{\pm}}{\alpha_1^{\pm} + \alpha_2^{\pm} + \alpha_3^{\pm}} \tag{2.2.7}$$

and

$$\alpha_1^{\pm} = \frac{1}{10}\frac{1}{(\tilde{\epsilon} + IS_1^{\pm})^2}, \quad \alpha_2^{\pm} = \frac{6}{10}\frac{1}{(\tilde{\epsilon} + IS_2^{\pm})^2}, \quad \alpha_3^{\pm} = \frac{3}{10}\frac{1}{(\tilde{\epsilon} + IS_3^{\pm})^2} \tag{2.2.8}$$

where IS represent the smoothness indicators, and $\tilde{\epsilon} = 10^{-}6$ is a regularization factor that avoids divizion by zero. A large smoothness indicator indicates a non-smooth solution in the particular ENO stencil, and consequently the weight of this stencil will be small.

$$\begin{aligned} IS_1^{\pm} &= \frac{13}{12}(q_1 - 2q_2 + q_3)^2 + \frac{1}{4}(q_1 - 4q_2 + 3q_3)^2, \\ IS_2^{\pm} &= \frac{13}{12}(q_2 - 2q_3 + q_4)^2 + \frac{1}{4}(q_2 - q_4)^2, \\ IS_3^{\pm} &= \frac{13}{12}(q_3 - 2q_4 + q_5)^2 + \frac{1}{4}(3q_3 - 4q_4 + q_5)^2 \end{aligned} \tag{2.2.9}$$

where

$$\begin{aligned} q_1 = \frac{u_{i-2} - u_{i-3}}{dx}, \quad q_2 = \frac{u_{i-1} - u_{i-2}}{dx}, \quad q_3 = \frac{u_i - u_{i-1}}{dx}, \\ q_4 = \frac{u_{i+1} - u_i}{dx}, \quad q_5 = \frac{u_{i+2} - u_{i+1}}{dx} \end{aligned} \tag{2.2.10}$$

2.2.5 Time discretization

In addition to spatial discretization in three dimensions, the time advancement of unsteady flows have to be considered. Time is discretized in a step-by-step manner by choice of a time step, dt. Complex and transient flow problems require accurate and stable time treatment methods, such as the Adam-Bashforth scheme or the Total Variance Diminishing (TVD) Runge-Kutta scheme, which are included in REEF3D (Kamath 2012). These are all explicit methods which are easily applied, providing accuracy from 2^{nd} to 4^{th} order. The schemes are used for temporal discretization of velocities and all scalar values except for equations of the RANS turbulence models, where implicit schemes are recommended due to large source terms (Bihs 2020).

The Total Variation Diminishing (TVD) scheme was developed by Harten et al. (1987). A TVD scheme produces a solution where the number of unrealistic oscillations, i.e. total variation, around the real solution decreases as the time-step procedure advances. It avoids local extremes or 'wiggles' and preserves the monotonicity of the solution (Kamath 2012). This is done by reducing the order of approximation in the proximity of discontinuities, which results in very smooth solutions of shocks (Gottlieb & Shu 1998). Runge-Kutta methods uses several points within a single dt in the approximation, and

obtain higher accuracy when more steps are used (Ferziger et al. 2020, p. 163).

- 3^{rd} *Order TVD Runge-Kutta Scheme (RK3)*
  The RK3 scheme applied in REEF3D consists of three Euler steps:

$$\begin{aligned} \phi^{(1)} &= \phi^n + dtL(\phi^n) \\ \phi^{(2)} &= \frac{3}{4}\phi^n + \frac{1}{4}\phi^{(1)} + \frac{1}{4}dtL(\phi^{(1)}) \\ \phi^{n+1} &= \frac{1}{3}\phi^n + \frac{2}{3}\phi^{(2)} + \frac{2}{3}dtL(\phi^{(2)}) \end{aligned} \tag{2.2.11}$$

When equation (2.2.11) is used for time treatment of the momentum equation (2.2.2), continuity has to be fulfilled for the velocities in each Euler-step. Consequently, the correct pressure is required for velocity correction in order to make the solution divergence free, i.e. make sure that the fluid is incompressible (Bihs 2020). As a result, the pressure term in the momentum equation has to be solved. As presented in chapter 2.2.6, this is done by solving a Poisson equation, which is quite computationally demanding. To save a significant amount of time, the 'fractional step' version of RK3 may be used. This approach uses pressure from the previous dt to correct the velocities after the two first Euler steps in Equation 2.2.11. Only after the last Euler step, the pressure for the current dt is calculated (Bihs 2020).

Adaptive time stepping

To produce a stable and accurate numerical solution, it is important that the simulated fluid does not advance further than the grid size, dx, in one time step, dt (Kamath 2012). In the initial state of the simulation, when the approximation is far away from the final solution and the flow is changing rapidly, a small dt is needed for the discretization to be accurate. As the flow approaches steady state however, dt may be relatively large and still produce an accurate solution (Ferziger et al. 2020, p. 237). To increase the computational efficiency, adaptive time stepping can be applied to control and adjust the time step depending on the rate of change in the flow. For implicit time stepping schemes, the Courant criterion (Courant et al. 1967) is used to restrict dt depending on the Courant number, C:

$$\frac{u * dt}{dx} \leq C \tag{2.2.12}$$

All the time advancement schemes applied in REEF3D are however explicit, which implies that the Courant criterion cannot be implemented. To handle adaptive time stepping in explicit methods, a condition called the CFL-criterion is applied, as proposed by Courant, Friedrichs and Levy (Courant et al. 1967). Through the CFL condition, the next time

step at n+1 is influenced by maximum velocities, the viscosity, volume- and surface forces in the current time step:

$$dt \leq 2 \left(\left(\frac{|u|_{max}}{dx} + D \right) + \sqrt{\left(\frac{|u|_{max}}{dx} + D \right)^2 + \frac{4|S_{max}|}{dx}} \right)^{-1} \tag{2.2.13}$$

with a maximum contribution from the diffusion term, D:

$$D = max(\nu + \nu_t) \cdot \left(\frac{2}{(dx)^2} + \frac{2}{(dy)^2} + \frac{2}{(dz)^2} \right) \tag{2.2.14}$$

2.2.6 Pressure-velocity coupling

The pressure term in the RANS-equations causes some complications in arriving at a solution, as an independent equation for pressure is absent. Pressure is included as a source term, whose gradient contributes to each of the three momentum equations (2.2.2). Velocity is clearly defined in these equations, which leaves the continuity equation (2.2.1) to determine the pressure. However, this equation does not contain a pressure term, which makes a direct approach to determine this term unavailable (Ferziger et al. 2020, p. 193). The solution to this problem is to combine the equations (2.2.1) and (2.2.2), which results in a pressure-velocity coupling relation. The presence of non-linear terms in these equations makes arriving at an analytical solution challenging, because it would involve application of implicit methods that are lengthy and computationally expensive. Hence, use of iterative schemes is more appropriate (Kamath 2012).

An appropriate method to solve for pressure is Chorins projection method (Chorin 1968). Here, the momentum equation (2.2.2) is first solved for an intermediate velocity field, u_i^*, that excludes the pressure gradient:

$$\frac{\partial(u^* - u_i^*)}{\partial t} + u_j^n \frac{\partial u_i^n}{\partial x_j} = \frac{\partial}{\partial x_j} \left[\nu(\phi^n) \left(\frac{\partial u_i^n}{\partial x_j} + \frac{\partial u_j^n}{\partial x_i} \right) \right] + g_i \tag{2.2.15}$$

At this stage, u_i^* is not divergence free and does not satisfy the continuity equation (2.2.1) (Bihs 2020). The projection step is conducted next, where pressure is included to calculate velocity at the next time step, n+1:

$$\frac{\partial(u_i^{n+1} - u_i^*)}{\partial t} + \frac{1}{\rho(\phi^n)} \frac{\partial P^{n+1}}{\partial x_i} = 0 \tag{2.2.16}$$

P^{n+1} has to be known in order to solve equation (2.2.16), and it is obtained by applying a divergence operator to the equation. To fulfill the continuity equation (2.2.1), a divergence

free velocity field is provided by setting the divergence of $u_i^{n+1} = 0$. The result is the Poisson pressure equation:

$$\frac{\partial}{\partial x_i}\left(\frac{1}{\rho(\phi^n)}\frac{\partial P}{\partial x_i}\right) = -\frac{1}{dt}\frac{\partial u_i^*}{\partial x_i} \tag{2.2.17}$$

The acquired pressure value is further used in equation (2.2.16) to determine the divergence free velocity at the new time step, n+1, and consequently the RANS-equations can be solved.

Pressure solver

Direct solution of the Poisson pressure equation (2.2.17), such as Gauss elimination, is too computationally demanding to be feasible (Kamath 2012). Hence, an iterative method for solving non-linear equations is applied. In iterative methods an initial solution is guessed, before the equation is used to systematically improve it. Non-linear iterative solvers are divided into two categories: 'Newton-like' and 'global' methods (Ferziger et al. 2020, p. 128). *Newton-like* methods solve equations through linearization, by using the two first terms of the Taylor series about an estimated initial value of the solution. Such methods achieve convergence quickly if the initial estimate of the solution is accurate, but risk to not converge at all if the initial estimation is far from the exact solution. *Global* methods solve equations by turning them into minimization problems, where the solvers are searching for minimum values of the functions. This process is carried out iteratively until the solution converges, which is very time consuming. If an exact solution exist, global methods will always converge, but in at a much slower rate compared to Newton-like methods (Kamath 2012).

Since global solvers are guaranteed to converge, they are an appropriate tool to start with when solving systems of non-linear equations. The original system is converted into a minimization problem, which is then solved by use of various methods. The oldest and best known method for seeking the minimum of a function is 'steepest descent' (Ferziger et al. 2020, p. 129). Here, the minimum value of a function is found by following an arbitrary starting point's path of orthogonal gradients down the contour map of the function, as illustrated in figure 2.2.4a (Shewchuk et al. 1994). The convergence rate of this method is however very slow, which has led to several improved methods. One of such is the 'Conjugate Gradient method (CG)', which is the most prominent iterative method for solving sparse systems of linear equations (Shewchuk et al. 1994). It can also be applied to solve non-linear equation systems, as illustrated in figure 2.2.4b. The CG method increases efficiency by minimizing the function with respect to several directions

simultaneously while searching in one direction. It is valid when the all the gradient vectors are conjugate, i.e. orthogonal, and may be extended to as many directions as needed (Ferziger et al. 2020, p. 130).

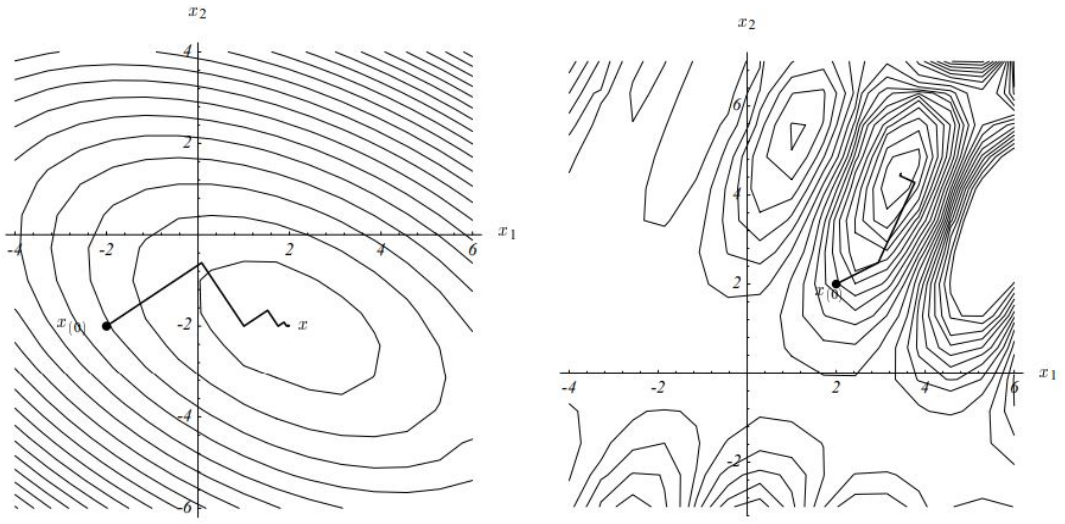

(a) Steepest descent

(b) Non-linear Conjugate Gradients

Figure 2.2.4: Minimization problem solvers

A drawback with the CG method is that it can only be applied to symmetric equation systems, which generally is not adequate to represent fluid dynamic problems (Kamath 2012). This issue can be solved by use of the Biconjugate Gradient (BiCG) method, which converts non-symmetric systems into symmetric systems by use of the transpose matrix. It is a robust method that can be applied in a wide variety of problems, but it require almost twice the computational power to obtain the same convergence rate as the CG method (Ferziger et al. 2020, p. 133). REEF3D applies the Biconjugate Gradient Stabilized (BiCGSTAB) method, which is an improved version of BiCG that is more accurate and converges faster (Van der Vorst 1992). In addition, the method is 'preconditioned' by use of Jacobi Scaling, which imply that the original problem is replaced by a faster converging problem with the same solution (Kamath 2012). Figure 2.2.4 shows a couple of global methods to solve equation systems that are turned into minimization problems (Shewchuk et al. 1994).

2.2.7 Turbulence modelling

Turbulence is encountered in most flows considered in engineering problems, and it may arise when the flow interact with structures or when velocities are relatively high. Turbulent flows are chaotic with rapid fluctuations in all three spatial directions, which creates a high degree of vorticity. The swirling of the fluid in such vortices are called 'eddies', whose size, strength and occurrence vary on a broad range of length and time scales. Turbulence

affects the flow by increased mixing, changing the viscous behavior of the fluid and influencing the experienced force on structures within the fluid (Ferziger et al. 2020, p. 347).

The most accurate approach to account for turbulence in numerical modelling is by 'direct numerical simulation (DNS)', in which the Navier-Stokes equations are resolved for all scales of eddies. This approach is however incredibly computationally demanding, and is not feasible for engineering problems (Bihs 2020). Instead, separate turbulent models may be applied in order to account for turbulent effects in the flow, without directly resolving all scales of eddies. A set of equations are obtained by decomposing the governing equations (2.2.1) and (2.2.2) into a mean and a fluctuating part, i.e. Reynolds decomposition. These equations do not form closed sets and have to be approximated, which is done by turbulence models. When the mean component is achieved by averaging the equations over finite volumes in space, a 'large eddy simulation (LES)' is obtained. LES accurately resolves the flow for most scales of motion, while approximating only the smallest eddies using a turbulence model.

If the mean part acquired by Reynolds decomposition is averaged over time, the Reynolds-averaged Navier-Stokes (RANS) equations are obtained. Turbulence models can be applied to the RANS equations instead of resolving any scale of eddies, and thus reduce the computational demand considerably (Ferziger et al. 2020, p. 349). This is done by Boussinesq approximation, which acknowledges the fact that turbulence increases the viscous behaviour of the fluid. Consequently, the eddy viscosity, ν_t, is introduced. In the presented work, the $k-\omega$ turbulence model (Wilcox et al. 1998), which uses two additional transport equations to account for turbulent effects, is applied to the RANS equations. The quantities transported in this model is turbulent kinetic energy, k, and specific turbulent dissipation, ω. The former determines the energy within the turbulence, while the latter determines the scale of turbulence in the simulation (Kamath 2012). By including the Reynolds stress term in the NS-equations (2.2.2), the RANS equation is obtained:

$$\frac{\partial u_i}{\partial t} + u_j \frac{\partial u_i}{\partial x_j} = -\frac{1}{\rho}\frac{\partial P}{\partial x_i} + \frac{\partial}{\partial x_j}\left[\nu\left(\frac{\partial u_i}{\partial x_j} + \frac{\partial u_j}{\partial x_i}\right) - \overline{u_i u_j}\right] + g_i \tag{2.2.18}$$

The introduction of the extra stress terms, $\overline{u_i u_j}$, results in a non-linearity due to the presence of more unknowns than equations. These stress terms are replaced by the Boussinesq approximation in order to solve the RANS equations:

$$-\overline{u_i u_j} = \nu_t\left(\frac{\partial u_j}{\partial x_i} + \frac{\partial u_i}{\partial x_j}\right) - \frac{2}{3}k\delta_{ij} \tag{2.2.19}$$

where the eddy viscosity, ν_t is given by:

$$\nu_t = c_\mu \frac{k}{\omega} \tag{2.2.20}$$

The transport equations for k and ω are defined by:

$$\frac{\partial k}{\partial t} + u_j \frac{\partial k}{\partial x_j} = \frac{\partial}{\partial x_j}\left[\left(\nu + \frac{\nu_t}{\sigma_k}\right)\frac{\partial k}{\partial x_j}\right] + 2\nu_t|S|^2 - k\omega \tag{2.2.21}$$

$$\frac{\partial \omega}{\partial t} + u_j \frac{\partial \omega}{\partial x_j} = \frac{\partial}{\partial x_j}\left[\left(\nu + \frac{\nu_t}{\sigma_\omega}\right)\frac{\partial \omega}{\partial x_j}\right] + 2c_\mu c_{\omega 1}|S|^2 - c_{\omega 2}\omega^2 \tag{2.2.22}$$

with closure coefficients: $c_\mu = 0.09$, $c_{\omega 1} = 5/9$, $c_{\omega 2} = 5/6$ and $\sigma_\omega = \sigma_k = 2$. $|S|^2$ is constituted of the mean rate of the strain tensor:

$$S_{ij} = \frac{1}{2}\left(\frac{\partial u_j}{\partial x_i} + \frac{\partial u_i}{\partial x_j}\right) \tag{2.2.23}$$

Surface roughness is accounted for by Schlichting's rough wall law (Schlichting & Gersten 2016) at solid boundaries:

$$u^+ = \frac{1}{\kappa} ln\left(\frac{30d}{k_s}\right) \tag{2.2.24}$$

where u^+ is dimensionless wall velocity, $\kappa = 0.4$, d is water depth and k_s is equivalent sand roughness. Near the wall, turbulent production is assumed equal to the dissipation of k (Wilcox et al. 1998). The wall function for specific turbulent dissipation, ω, for a bed cell with the distance Δy_p from the wall to the cell center then become:

$$\omega_{wall} = -\frac{c_\mu^{3/4} k_w^{1/2} U_w^+}{\Delta y_p} \tag{2.2.25}$$

Turbulent kinetic energy, k, at the wall is treated by integrating the source terms of equation (2.2.21) over the wall cell:

$$\int (P_k - \epsilon_{wall})\rho = \left[\frac{\tau_w u_w}{\Delta y_p} - \frac{\rho c_\mu^{3/4} k_w^{3/2} u_w^+}{\Delta y_p}\right] \tag{2.2.26}$$

The rough wall law is further used to determine u^+ and the wall shear stress, τ_w. Equation (2.2.26) is discretized as source terms in the transport equation for k (2.2.21).

2.2.8 Free surface modelling

In fluid dynamics problems where multi-phase flows occur, the boundary of interaction, i.e. the interface, has to be resolved if its effects has importance for the numerical solution

and engineering design. In the present study, two phase flow interaction between water and air occur at the free surface. Several approaches may be applied to resolve multi phase flow interaction, such as the marker and cell approach, volume of fluids method or the level set method. In the numerical model REEF3D, the latter is used to model the free surface, in which a signed distance function called the level set function, $\phi(\vec{x}, t)$, is applied. It has the property of $\phi(\vec{x}, t) = 0$ at the free surface, and away from the free surface it takes the value at the closest distance from the interface, where the sign of the function denotes which fluid governs the point. The main advantage with this approach is that it is smooth across the interface, which makes it avoid instabilities because it is differentiable at $\phi(\vec{x}, t) = 0$ (Kamath 2012). The level set function is defined as:

$$\phi(\vec{x}, t) = \begin{cases} > 0 & \textit{if } \vec{x} \textit{ is in phase 1, water} \\ = 0 & \textit{if } \vec{x} \textit{ is at the interface} \\ < 0 & \textit{if } \vec{x} \textit{ is in phase 2, air} \end{cases}$$

The convection of the level set function dictates the movement of the free surface, determined by:

$$\frac{\partial \phi}{\partial t} + \vec{u} \nabla \phi = 0 \tag{2.2.27}$$

In incompressible fluids, the material derivative of density and viscosity is zero. Due to the large difference in density across the interface between water and air, a numerical instability occur if the material derivative is discretized directly (Kamath 2012). Consequently, a transition zone proportional to the grid size with thickness 2 ϵ is defined, where the interface region is smoothed by use of a Heavyside function $H(\phi)$:

$$\begin{aligned} \rho(\phi) &= \rho_1 H(\phi) + \rho_2 (1 - H(\phi)) \\ \nu(\phi) &= \nu_1 H(\phi) + \nu_2 (1 - H(\phi)) \end{aligned} \tag{2.2.28}$$

where,

$$H(\phi) = \begin{cases} 0 & \textit{if } \phi < -\epsilon \\ \frac{1}{2}(1 + \frac{\phi}{\epsilon} + \frac{1}{\pi} sin(\frac{\pi \phi}{\epsilon})) & \textit{if } |\phi| \leq \epsilon \\ 1 & \textit{if } \phi > \epsilon \end{cases}$$

Re-initialization

The main challenge of applying the LSM is that the signed distance property of ϕ is not maintained as the interface change, and thus not indicate the shortest distance to the free surface. As a fix, the function has to be re-initialized at certain intervals, e.g. after every iteration. The position of the interface should not be changed in this process (Kamath

2012). In the present study, the partial differential equation (PDE) approach is applied for re-initialization (Sussman et al. 1994):

$$\frac{\partial \phi}{\partial \tau} + S(\phi)\left(\left|\frac{\partial \phi}{\partial x_j}\right| - 1\right) = 0 \tag{2.2.29}$$

where S(ϕ) is the smooth signed function:

$$S(\phi) = \frac{\phi}{\sqrt{\phi^2 + |\frac{\partial \phi}{\partial x_j}|^2 (dx)^2}} \tag{2.2.30}$$

The signed distance property is restored by solving equation 2.2.29 until steady state. Equation 2.2.30 assigns the value of zero at the interface.

2.2.9 Boundary conditions

The fluid behaviour close to the boundaries in the numerical flow tank, where viscous effects become important, is largely dependent on the features set by the boundary conditions (BC's). The presence of a wall boundary influence turbulent flow in two main ways: 1) damping the components normal to the wall, making the flow anisotropic, and 2) increasing the production of turbulence through the shearing mechanisms in the flow (Bredberg 2000). The wall give rise to a boundary layer, where velocities change from the free stream value to the no-slip condition at the wall. The largest gradients are usually found near the wall region, where shear stresses have significant influence (Schlichting & Gersten 2016, p.29). Because flow friction is computed using gradients of dependent variables, it is crucial to accurately capture the near-wall variation (Bredberg 2000).

Values of all variables have to be initialized in order to start the iterative solution procedure, which is done by the use of BC's. The values may be set constant over the whole boundary (Dirichlet BC), given as a gradient in a particular direction, usually normal to the boundary (Neumann BC), or a linear combination of the two approaches (Ferziger et al. 2020, p. 56). The BC's need to be applied at every time step, and they can be constant or vary in time. The following BC features may be implemented in REEF3D (Griebel 1997, p. 30):

- *No-slip BC*: imposed at a wall. The fluid is at rest at the boundary causing the velocities to vanish. Horizontal boundaries contain no u-values and vertical boundaries contain no v-values, thus enforcing the zero boundary value. Alternatively, in the case of a moving boundary, the velocities are set equal to a Dirichlet wall velocity.

- *Free-slip BC*: applied at a symmetry plane, which reduces the size of the required computational domain. No fluid penetrates the boundary, but no friction losses are present. The velocity component normal to the boundary should vanish along with the normal derivative of the velocity component tangent to the boundary.
- *Inflow BC*: velocities are explicitly given at the boundary, either by a Dirichlet or a Neumann condition. In REEF3D, the inflow is given as a discharge normal to the boundary.
- *Outflow BC*: the normal derivatives of both velocity components are set to zero, which imply that the flow do not change in the direction normal to the boundary. This can be done by setting velocities at the boundary equal to the velocities of the neighbouring cells inside the numerical domain.
- *Periodic BC*: may be used for cases which are periodic in a certain direction, to reduce the computations by restricting them to one period interval.

Wall functions

The standard method to capture the near-wall flow variations is through the integration method, which means applying a very refined numerical grid close to boundaries. Since approximations of variables are linear by use of finite differences, accurate resolving usually require significant refinement of the grid near boundaries where gradients are high (Ferziger et al. 2020, p. 410). Instead of resolving the flow near the boundaries however, *wall functions* may be applied to account for the viscous behavior in these regions. Wall functions are empirical, non-linear functions that are fitted to the observed behavior close to the wall, which can improve numerical stability. They can be used to bridge the region between the wall and where the fluid turbulence is fully developed without resolving the flow, which reduces the amount of grid cells needed and thus the computational demand significantly (Bredberg 2000).

Complex boundaries

The presence of complex geometries within the fluid domain require special consideration, as they may affect the realization of the discretization methods applied in the model. The properties of the solution close to complex boundaries depend on the choice of grid and arrangement og variables on the grid (Ferziger et al. 2020, p. 275). The utilization of a Cartesian grid provides advantages due to its ability to easily implement highly accurate and stable finite difference discretization schemes. However, the rigid rectangular nature of the meshes in a Cartesian grid provide low flexibility when considering fluid interaction

with complex geometries and irregular boundaries. In contrast to unstructured grids, a Cartesian grid cannot 'wrap around' the geometry in order to optimize the cell structure, which may cause problems regarding the accuracy in regions where boundaries are complex (Ferziger et al. 2020, p. 28).

To solve these challenges, the Ghost Cell Immersed Boundary Method (GCIBM), proposed by Tseng & Ferziger (2003), is implemented in the presented work. Here, the BC between fluid and solid are implicitly incorporated in the GE's. Cells adjacent to boundaries are identified in the code by advance. In this way, boundaries can be simulated without making any changes to the grid. Ghost cells are fictional extensions of the grid cells around the boundary, where solutions from the fluid are extrapolated into the solid region as shown in figure 2.2.5 (Kamath 2012). To further improve the GCIBM, the extension of the solutions across the boundary is done in the discretization direction instead of orthogonal to the boundary. In addition, the ghost cells contains several values, where the returned value is depending on the direction of which it is called upon (Berthelsen & Faltinsen 2008).

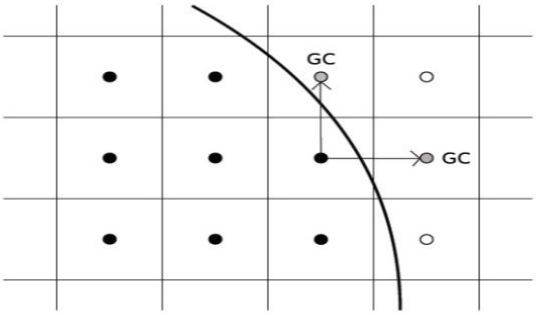

Figure 2.2.5: Ghost cell immersed boundary

2.2.10 Parallelization

The computational efficiency of CFD computations is largely dependent on the strategy for parallel processing of the numerical model. Parallelization is the technique where large problems are divided into smaller parts and simultaneously solved on a large number of processors (Griebel 1997, p. 109). In REEF3D, parallelization is achieved by using the Message Passing Interface (MPI) protocol, which decomposes the domain and explicitly assign the parts to different processors. To make the simulation progress, boundary values have to be communicated between the parts. This is done by copying the cell values at the boundaries of each part and storing them in the ghost cells associated to the neighbouring part. Three ghost cells are required due to the use of the 5th order WENO scheme for convection discretization and turbulence modelling (Bihs et al. 2016).

3 Methodology

The following chapter includes a description of how the knowledge and underlying data presented in the study was acquired. To achieve satisfactory verification of the study, a significant description of the methodology with a high level of detail is endeavored. First, essential theoretical definitions and concepts used in scientific research as well as the methods and approach applied in the study are presented. Second, the qualitative research conducted in the thesis, the literature review, is elaborated. At last a presentation of the quantitative research method is given, including a description of the applied numerical model and tanks. The chapter consequently clarifies the research methods applied in the thesis, as well as explaining why and how they were used.

3.1 Research methods

The approaches to collecting and analyzing data and acquire new knowledge is categorized in two ways; *quantitative* and *qualitative* research. To assess and measure quality of the findings in such research, various concepts and criteria are applied. In quantitative research, the terms *validity* and *reliability* are commonly used, while other parameters are often necessary to evaluate qualitative research (Yilmaz 2013). Mixing of quantitative and qualitative methods may also occur within the same research study, and the overlap of the different methods can happen in several ways (Bryman 2006).

Quantitative and qualitative research

Quantitative research is application of empirical methods and measurable parameters to examine a phenomena and test hypothetical generalizations, with emphasize on measurements and analysis of causal relationships between the variables (Golafshani 2003). It can be described as "research that explains phenomena according to numerical data which are analysed by means of mathematically based methods, especially statistics" (Yilmaz 2013).

Qualitative research is widely described as any kind of research that generate results which is not produced by means of quantification or statistical processes. Unlike quantitative research that focuses on prediction and generalization from the results, the goal of qualitative research is illumination, understanding and extrapolation to similar situations (Golafshani 2003). Yilmaz (2013) define qualitative research as an interpretive approach

to study people and phenomena in natural settings, in order to reveal their experiences of the world in descriptive terms. Qualitative methods are built on experiences and interpretations of others, and include diverse forms of systematic reviews, analysis and processing of data provided by written texts, observations or conversation (Skolbekken et al. 2010).

Validity and reliability

Validity and reliability of measurements are key indicators of quality in quantitative research, and a way to establish confidence in the results of a study (Kimberlin & Winterstein 2008). Validity indicates whether the means of measurement are accurate and an whether the intended purpose is measured (Golafshani 2003). It dictates to what degree valid conclusions can be drawn from the results of a study. Validity may be divided into external and internal, where external validity determines that results from a limited study can be generalized and applied to a larger domain, while internal validity denotes that the findings of a study are unbiased (Dahlum 2018).

Reliability is often used in the context of consistency or stability of measurements, and indicates whether the results in a study would be replicable if a study with identical setup was repeated at a later time. Error sources are always inherent in measurements when studies are repeated. Biased errors produce results that either higher or lower than the benchmark data, while random errors generate results that are both higher and lower than the data of comparison (Svartdal 2018). Kirk et al. (1986) suggest that quantitative reliability is categorized in three ways: (1) the ability of a repeated measurement to remain unchanged, (2) the stability of temporal change in a measurement, and (3) the similarity of measurements conducted in a time period (pp. 41-42). An illustration of validity and reliability is shown in Figure 3.1.1 (Souza et al. 2017).

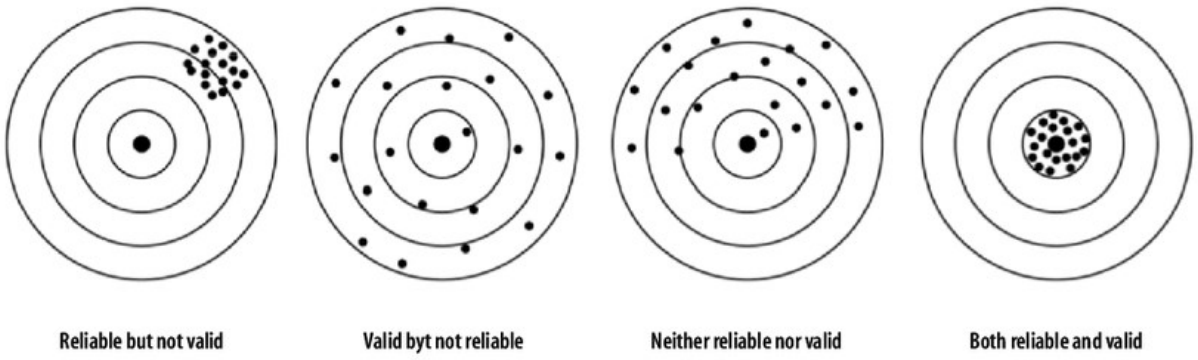

Figure 3.1.1: Validity and reliability of measurements

Quality in qualitative research

Validity and reliability is widely considered inadequate in qualitative research, as it does not provide a complete framework for the qualitative methodology where credibility and transferability are important aspects (Golafshani 2003). The qualitative interpretation of validity and reliability is not universally established but instead vary with subjective opinions of researchers (Creswell & Miller 2000). According to Stenbacka (2001), validity in qualitative research is equivalent with gaining understanding of another persons reality based on a specified problem area. In addition, she argues that reliability has no relevance in qualitative research and should not be applied as a quality criterion. Instead, concepts such as *rigor* or *trustworthiness* have been used to differentiate 'good' from 'bad' research, and establish trust in the findings of qualitative studies (Golafshani 2003, Thomas & Magilvy 2011). (Seale 1999, p. 266) states: "trustworthiness of a research report lies at the heart of issues conventionally discussed as validity and reliability". Also, a thorough description of the research process is a quality sign in qualitative methods (Stenbacka 2001).

Lincoln & Guba (1985) introduced the terms *credibility*, *transferability*, *dependability* and *confirmability* as substitutes to validity and reliability in qualitative research, which are commonly acknowledged as a 'gold standard' to assess quality in qualitative studies (Yilmaz 2013). Credibility assesses the authors and place of publishing of a study. The authors experience within the research field, institutional affiliation and impact factor of the journal affect a study's credibility. Transferability denotes whether the findings of a study is transferable to other similar settings, which require a thorough description of the context and involved parties. Dependability relates to the transparency of the research methods applied in a study, whether the methodology is well described and if the presented data is up to date. Confirmability, or objectivity, depends on the presentation of the data in a study, whether it conforms or breaks with other research within the field and whether its purpose is to inform or persuade. Table 3.1.1, adapted from Yilmaz (2013), shows quality assessment terminologies that are equivalent to validity and reliability, but more applicable to qualitative research.

Table 3.1.1: Quality in research studies: Quantitative vs. qualitative terms.

Aspect	Quantitative terms	Qualitative terms
Truth value	Internal validity	Credibility
Applicability	External validity	Transferability
Consistency	Reliability	Dependability
Neutrality	Objectivity	Confirmability

Mixed methods

Mixed methods research is a design that combines quantitative and qualitative research methods in the same research inquiry. Such an approach may provide richer insights into the phenomena of study, that cannot be fully understood using solely quantitative or qualitative methods (Venkatesh et al. 2013). By implementing both qualitative and quantitative methods, possible biases are controlled and valid propositions can be established, thus improving the validity and reliability of the research (Golafshani 2003). The mix of methods can either be conducted *concurrently*, independent of each other, or *sequentially*, findings from one approach inform the other. In concurrent procedures, the data collection from quantitative and qualitative methods happens at the same time, while in sequential approaches the data is gathered in phases (Venkatesh et al. 2013). Furthermore, Creswell & Creswell (2017) suggest that sequential mixing can be either *explanatory*, use of qualitative findings to elaborate the results of quantitative studies, or *exploratory*, collecting of quantitative data to test and explain qualitative findings. Concurrent mixing may be done by use of *triangulation* or *embedding*. With triangulation, the researcher merges data from quantitative and qualitative research concurrently, and then compares the two databases to determine if there is convergence, differences, or some combination (Creswell & Creswell 2017). Triangulation develops better insights into a phenomenon and enables deeper understanding of the problem (Venkatesh et al. 2013). In embedded mixing, findings from either the quantitative or qualitative study are used to support the other, which is regarded the primary study (Creswell & Creswell 2017).

3.1.1 Choice of methods

The thesis applied various methods in order to answer the research questions (RQ's) stated in chapter 1.2. As recommended by Bryman (2006), the method regarded as the most appropriate to distinctively answer each RQ was chosen. The purpose of the different research questions and the methods applied to answer them are shown in Table 3.1.2. RQ1 was formulated to get an overview of the existing body of knowledge (BoK), and identify critical aspects in land-based aquaculture tank design. A holistic answer to RQ1 required broad scoping and data collection from a large number of sources. Qualitative method is especially applicable to gain understanding of a certain topic, due to high efficiency in material gathering (Golafshani 2003). A scoping literature review was regarded as the most appropriate approach to establish a solid theoretical base for the study. By answering RQ2 the thesis would be able to explain how essential tank parameters affect the water flow within the tanks. Parameters that are expected to have the greatest influence on the hydrodynamics were identified through the literature review conducted to answer RQ1.

Since there is limited information on the subject available in literature (Gorle et al. 2019), and a need to quantify the hydrodynamic characteristics by use of appropriate measures (Shahzad 2019), a qualitative methodology was regarded most suitable to answer RQ2, more specifically numerical modelling by use of CFD. Findings from the literature review were used as reference data in the numerical investigation, thus an embedded mix of methods occurred. RQ3 was formulated to compare the findings from the previous RQ's, to examine whether convergence, differences or some combination occurs. The concurrent triangulation method was applied to combine the richness in qualitative research with insights and precision from quantitative research.

Table 3.1.2: Methods applied to answer the study research questions (RQ's)

RQ	Purpose	Method
RQ1	Seeking understanding and overview	**Qualitative:** Literature review
RQ2	Seeking explanation and insight	**Mixed:** Embedded
RQ3	Seeking prediction and generalization	**Mixed:** Triangulation

3.1.2 Approach

The overall design of the thesis was structured in the way that Creswell & Creswell (2017) calls sequential exploratory, where qualitative method is applied in advance of the quantitative research. In this case, a scoping literature review was conducted first to answer RQ1, followed by numerical simulations by use of CFD in order to answer RQ2. Embedded mixing was applied in the second part of the work, where essential parameters identified by the literature review were tested though a parameter study in the numerical investigation. Finally, the results from both the literature review and the CFD-simulations were compared through triangulation and used as a basis for discussion. Tank designs were acquired, important parameters identified and benchmark data used for validation of the numerical model was obtained. The findings were then incorporated into the numerical model before CFD-simulations were performed. Consequently, an interpretation of the entire study were provided by answering RQ3.

3.2 Literature review

The preliminary qualitative research was performed in the form of a scoping literature review. Conducting a literature reviews is an excellent strategy to: 1) understand the existing body of knowledge (BoK), 2) provide a solid theoretical foundation for the thesis, 3) fit the research into the existing BoK, 4) justify the study by contributing to new

research, and 5) provide a framework for valid research methods, approaches, goals and research questions (Levy & Ellis 2006). The purpose of the literature review was to identify the most important features that influence tank hydrodynamics, commercially applied land-based tank designs and experiments measuring tank flow velocities. The latter was important for use as reference data in the numerical model validation, while tank designs such as geometries and inlet pipes were replicated in a CAD-model. Literature identified in the search that was used as basis for the answers to the research questions is shown in detail in appendix B.

The approach of the literature review was based on the recommendations of NTNU University Library (NTNU 2018), and included search in databases, the bibliography of acknowledged authors, as well as forward and backward references search of high quality articles (snowballing). The quality of the research identified by the literature review was evaluated on the basis of the principals introduced by Lincoln & Guba (1985): credibility, confirmability, dependability and transferability, which was described in section 3.1. In addition, acquisition of peer-reviewed articles was emphasized to further ensure a seal of approval. Peer-reviewing is an essential process that allows published work to be used with increased confidence, because it implies that a publication has been assessed by experts within the research field (Levy & Ellis 2006).

To assess the credibility of acquired literature, responsible authors as well as the impact factor of the article itself and the journal in which it was published was evaluated using various measures. Article citations indicated the first seal of approval, while institutional affiliation and h-index of the author further affected the credibility. H-index measures both the productivity and impact of a scientist, and it is equal to the h number of articles that has been cited at least h number of times. "InCites Journal Citation Reports" provided by Clarivate Analytics was used to assess relevant journals. This tool provides rankings and impact factors of thousands of science and engineering journals which allows for comparison within the same research category (Clarivate 2018).

3.2.1 Keywords search in databases

Search in databases functioned as an efficient guide to thesis relevant articles across assorted journals. By using dedicated keywords and phrases in combination with truncation, symbols such as "?" and "*", and boolean operators such as "AND", "OR" or "NOT", searches could be customized as wide or narrow depending on the degree of specialization desired. Several databases were applied in the search in order to obtain a wide scope of available research and to minimize the possibility of missing relevant articles. Utilized

databases included: Oria, Scopus (Sco) and Web of Science (WoS), which covered most journals that were relevant for the study. Google Scholar was also initially used for keyword searches, but overwhelming amounts of hits made the database inexpedient. Scholar was however used for snowballing, described in subsection 3.2.2.

- **Oria** is a search database provided by NTNU University Library, which contains the aggregate accessible resources of the library including books, articles, journals, master- and PhD theses. Initial searches usually provide a large number of results, but the sorting mechanisms allows thorough filtration based on peer-reviewed, material type, topic, publish year etc. and enabled a transparent search string. Access to a large selection of theses made the database especially useful (NTNU 2018).

- **Scopus** is the largest abstract and citation database of peer reviewed articles, owned by Elsevier. The database provide fewer and more specified results and was suitable for acquiring topic dedicated literature. All publications were peer reviewed, and easily available information regarding citations, author- and journal indexes made it easy to assess credibility (Elsevier 2020).

- **Web of Science** is like Scopus a publisher-independent global citation database, however maintained by Clarivate Analytics. The search engine may select several databases based on the topic of interest, and the core collection database is claimed to be uniquely selective and index consistent. Consequently, more specialized results of high quality were obtained. A comprehensive index citation network made it particularly easy to assess journals (Clarivate 2020).

3.2.2 Snowballing

In order to increase the probability of catching all valid and relevant publications, it was necessary to go beyond keyword searches with an additional approach to the literature review. Hence, the concept of snowballing was applied. Snowballing refers to using the reference list of a paper or the citations to the paper to identify additional papers (Wohlin 2014). Webster & Watson (2002) presented the terms 'backward' and 'forward' searching in literature. Backward searching implies reviewing the citations of a high quality article, while forward searching implies reviewing the citing articles of said article, determining if any of the identified publications should be included in the review. Backward snowballing included search in article references, author bibliography and application of previously used keywords in further searches. Similarly, forward snowballing was conducted by examining citing articles and following publications by responsible authors.

In addition to the databases mentioned in subsection 3.2.1, Google Scholar was an appropriate search engine for snowballing of publications and authors. Google Scholar is simple and user-friendly with a wide catchment area, which makes it suitable for quick searches of authors and articles. In addition to quality indicators such as total citations and h-index, Scholar has embedded an i10-index which shows an authors amount of publications with at least 10 citations. The "cited by" feature is another handy tool that shows all citing articles of a publication in the order of total citations, that made it particularly useful for forward snowballing (Scholar 2020).

3.2.3 Search strategy

Subject specific keywords were applied to specify the database searches. However, initial searches with too general phrases resulted in excessively many hits, and needed limiting. Thus the searches were refined based on subject area, document type, year of publishing, author name or in specific journals. Due to large amounts of data emerging from the literature review, it was necessary to establish a consequent reading strategy to efficiently review and assess the identified publications. The strategy included skimming of the results by reading the text in three steps, following the order: 1) title and keywords, 2) abstract, and 3) bibliography. The literature was evaluated after each step to decide if it was relevant for the thesis or not. Irrelevant articles were discarded, while remaining articles were read in its entirety. The literature was read with a sharp eye for potential keywords that could be further utilized in database searches. A selection of keywords, filters and hits from the database searches are presented in table 3.2.1.

Table 3.2.1: Database search matrix

Keywords	Filter	Oria	Sco	WoS
aquaculture AND hydrodynamic*	Articles	7 988	459	392
+ NOT net NOT cage	Articles	4 902	323	253
+ AND tank	Articles	714	48	32
tank AND hydrodynamics	Aquaculture	204	102	27
	+ Engineering	58	47	17
"tank hydrodynamic*"	All	257	39	23
	Aquaculture	48	4	6
"tank design" AND aquaculture	All	316	40	16
	Engineering	76	3	5
cfd AND aquaculture	All	591	84	44
	Engineering	224	57	29

3.3 CFD modelling in a numerical flow tank

A quantitative study was deemed necessary in order to properly answer RQ2. The flow field within several aquaculture tanks were thus studied using the CFD model in the open-source software REEF3D. The work consisted of three main parts: 1) establishing a computational framework, 2) validating the numerical model, and 3) conducing a parameter study of several tank designs. The computational framework included pre-processing of the numerical domain, solution of the governing equations within the domain, and post-processing of the results. Validation was done by comparing the numerical solutions to experimental results, which were obtained through the literature review. Finally, using the validated model with sufficient accuracy, a parameter study was conducted to investigate the influence from various tank parameters on the tank hydrodynamics.

3.3.1 Computatational framework

Numerical modelling of the tank hydrodynamics requires extraction of a fluid body from the tank's geometry, domain discretization, a solution process for the turbulence model, as well as visualization and analysis of the results (Gorle et al. 2018b). Constant testing and adjustments to the model in search for design improvements invoked the need for integrating a consistent computational framework in the study. The framework consisted of various techniques and tools for manipulation of the numerical tank and evaluation of the flow field within it.

Pre-processing

The numerical model had to be pre-processed before any simulations could be executed. Preliminary activities were carried out in three steps: 1) development of solid boundaries using CAD software, 2) meshing, and 3) scripting of control files.

The rearing tank walls and pipes were modelled as solids in the numerical tank, where FreeCAD was used to create geometries and generate an assembly model. It is an open-source 3D CAD model with a user-friendly interface that makes for efficient development of simple geometries such as aquaculture tanks. Circular tanks were produced by making a cut of a square and a cylinder. The size of the square was identical to the dimensions of the numerical tank, while the cylinder diameter matched the internal distance of the rearing tank of study. Walls of the octagonal tanks were created in a similar way, by cutting two square solids of different sizes, where half the difference in square length was equivalent to the wall thickness. The corners of the smallest square were chamfered in

advance to replicate the octagonal shape of the tank.

As described in 2.2.3, CFD analysis require decomposition of the flow domain into a number of control volumes to create a numerical grid. Unstructured meshes are better suited for complex geometries, but more computationally demanding than structured meshes (Gorle et al. 2019). Consequently, the numerical grid generation process, called 'meshing', consisted of a hybrid solution as shown in figure 3.3.1: (a) unstructured meshing on the solid surface, and (b) a structured mesh within the core of the tank. The mesh design tool in FreeCAD was applied to generate the surface mesh, while DIVEMesh (Bihs et al. 2020) was used for core mesh generation. In FreeCAD, the meshing program called 'netgen' was used, where the fineness of the mesh was decided by a scale ranging from 'very coarse' to 'very fine'. The meshed solid was then exported in ASCII STL-format to the directory of where the REEF3D executable was present. Uniform grid sizes in all three dimensions were applied in the core mesh.

All information regarding the numerical model were scripted into two separate control files that could be read by DIVEMesh and REEF3D respectively, which were prepared according to user manuals provided by Bihs (2020). Example files are shown in appendix A. The DIVEMesh control file contained information regarding boundary conditions types, tank dimensions, grid refinement and solids. The tank walls were imported from the CAD-generated stl-file, while inlet pipes were specified directly in the control file. Direct specification of the pipes made for better control of the pipe placement as well as easing the process of making changes to the solid. The REEF3D control file specified the boundary conditions in more detail, discretization methods, free surface capture, initialization, printer options and turbulence modelling.

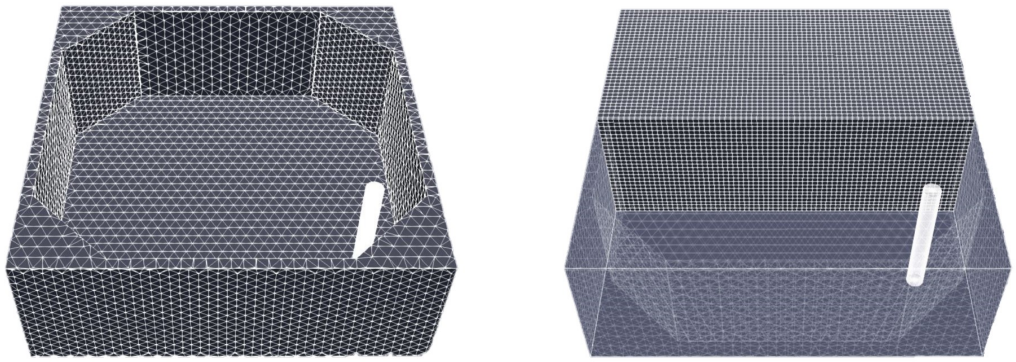

(a) Unstructured surface mesh

(b) Structured core mesh

Figure 3.3.1: The numerical grid

Solution process

Once the solids were created and adequately meshed, and the control files thoroughly scripted, the solution process could be initiated. Five files were required to be present in the simulation directory for the solution process to be a success: the two control scripts, executables for DIVEMesh and REEF3D and the ASCII stl-file representing the rearing tank. First, DIVEMesh was ran to generate the numerical grid, which created a number of grid files within the simulation directory. The number of created grid files depended on the amount of processors that were utilized for parallel computations in the simulation. Meshing did however require low computational demand and the mesh could be generated in a matter of seconds using a single processor. Nevertheless, the number of parallel processors had to be consistent in both control files in order to successfully run REEF3D.

The main simulation was initiated subsequently. After the grid files representing the numerical mesh were created, the solution of the governing equations were initialized. Several different tank designs were tested including wide variety of grid sizes and time steps, with cell numbers ranging from around 0.1 to 10 million. Consequently, the computational demand was highly variable, and the number of processors running in parallel were adapted based on the overall number of cells, time step size and the estimated simulation time upon steady state. Generally, simulations with a total cell number below 100 000 were run on an ASUS laptop with four Intel i7-7500U cores and 8 GB RAM. More demanding simulations were performed using the Linux cluster supercomputer 'Fram', hosted at the Arctic University of Norway (UiT). It hosts 32 256 cores, with a total memory of 78 TiB. When using the cluster to perform simulations, two additional batch scripts had to be included in the directory, specifying the needed resources as well as commands to perform the calculations.

Due to large demand from a lot of users, the cluster applied a workload manager. The queue pending time of submitted simulations would vary depending on the cluster's activity level by other users, as well as the required nodes and simulation wall time requested by the applied batch scripts. Shorter jobs requiring less nodes were prioritized by the queue manager, and hence reducing the queue pending time of the simulation. Thus, excess factors increasing the computational demand, e.g. space outside the tanks, unnecessarily thick walls, long-duration simulations and too short time steps had to be minimised. Ensuring the computational efficiency of the grid, as well as qualified estimations of required wall time were essential in order to complete a large amount of simulations.

Post-processing

When a simulation had been completed successfully, the directory contained information in the range of 1 – 100 GB. Useful information were stored into two separate folders, a point probe folder containing a time series of all velocity measurements, and one folder containing VTU-files which could be represented by a visualization toolkit. The directories were downloaded to the local computer for further processing. Paraview was used to visualize the results and Matlab was used to plot graphs. All variables that were plotted as points show values obtained at steady state, e.g. velocities were assumed to have reached steady state when $\frac{\delta u}{\delta t} < 0.005$. A data set of the points of reference from (Gorle et al. 2018b) were digitized using WebPlotDigitizer, and then plotted into Matlab to act as benchmark values for validation of the numerical model. In Paraview, stl-files of the tanks, vtk-files of the grid and pvtu-files containing the hydrodynamic information were imported to visualize the results. The pvtu-files were contoured by vorticity as well as clipped and sliced by velocity, vorticity, kinematic viscosity and omega to illustrate the hydrodynamic conditions within the tanks.

3.3.2 Numerical model validation

Due to the simplifications made when creating the tank geometries and boundary conditions, the accuracy of the numerical model needs to be assessed to gain trust in the results obtained from the simulations. Experimental validation is therefore pivotal in order to obtain a reliable CFD solution (Gorle et al. 2018b). Validation of CFD results includes the analysis of discretization and modelling errors, and a numerical model may be assumed validated when it produces results within appropriate convergence criteria, so that iteration errors can be excluded (Ferziger et al. 2020, p. 466). The accuracy of computational results is subject to several factors, e.g. the order of discretization, truncation error, boundary conditions uncertainty. In addition to physical dimension errors when modelling the tanks, uncertainties associated with the boundary conditions, fluid properties and measurement procedures influence the simulation output. Therefore, a meaningful validation of the CFD model requires a quantitative evaluation of errors to estimate a level of confidence (Gorle et al. 2019).

The numerical model was validated against experimental measurements presented in Gorle et al. (2018b). Because the velocity distribution within aquaculture tanks influence the flow regime and fish welfare, the velocity magnitude at certain points in the tank was compared between the CFD model and experiments. Grid convergence, time step and free surface modelling studies were carried out, and various turbulence models, convection

discretization and time discretization methods were tested in order to find the optimal numerical model set up for the parameter study. Due to incomplete development of the numerical model, several simplifications had to be made compared to the benchmark experiments. The simplifications incorporated in the CFD-model and reasons why they were made are summarized in table 3.3.1.

Table 3.3.1: Simplifications in the numerical model

Simplification	**Reason**
Simplified inflow	In REEF3D, the finite difference method on a structured grid is applied as discretization approach, which is known to be restricted to simple geometries. The inlet is in this respect regarded as a complex geometry due to the inflow through many nozzles. The applied grid cannot be locally refined around each nozzle, and thus the complex flow field in this area may not be resolved in detail. Instead, the inlet was modelled as a cylindrical solid where the inflow was imposed by a vertical velocity line, in which the theoretical inflow velocity and direction was prescribed. I.e. there was no mass inflow into the tank, but rather an impulse force was applied to the enclosed volume that was predefined at a set level.
Eccentric inlet	Initially the vertical velocity line was defined on the boundary of the cylindrical solid representing the inlet. However, this resulted in incomplete initialization of the velocities in cells near the boundary. Consequently, the line source had to be placed at a distance away from the solid boundary in order to achieve complete initialization. As a result, the inflow tended to scatter around in all directions close to the line source.
No outflow	a mass outflow boundary condition at arbitrary surfaces was not incorporated in REEF3D during the time frame of the present study. As a result, the hydrodynamic effects of the drains could not be accounted for in the simulations.
Flat bottom	The tank described in Gorle et al. (2018b) held a conical base with 10 °decline to promote particle transport towards the center drain. The gravitational effect from an inclining base is however low compared to that imposed by the secondary flow on the particles (Lekang 2007). Hence, to simplify the preliminary process, the numerical tanks were designed with a flat bottom.

Tank description

The benchmark case in (Gorle et al. 2018b) involved an octagonal tank which applied a single inlet and drain system existing of a central drain and one wall drain as shown in figure 3.3.2a. A) shows the ϕ320 mm inlet pipe, while B) and C) illustrate the central and wall drain respectively. The tank volume was approximately $100m^3$, with an inner diameter of 6.75 m and a water depth of 2.36 m. It was operated at a mean HRT of 40 min, which corresponds to an inlet flow rate, Q, of 2500 L/min. The flow was injected through 30 circular nozzles pointing at corer D), each of ϕ31 mm, resulting in an inlet velocity of 1.85 m/s. The nozzles were pointed toward corner D), giving the inlet flow a direction of 200°. The dual drain was split between the center and wall at a 45:55 ratio, with the majority outflow through the wall drain. The tank held a conical base with 10°decline towards the center drain. The computational model was simplified by assuming a stress-free boundary at the water surface (Gorle et al. 2018b).

A simplified tank was reproduced using FreeCAD and exported as an ASCII stl-file as shown in figure 3.3.2b. The bottom was designed flat in order to minimize the number of active cells and reduce the computational demand. Due to limitations in the numerical model, the outlets were not modelled. The tank wall and bottom were set to 200 mm, thus making the dimensions of the tank 7.15 x 7.15 x 2.56 m as base design when a stress-free water surface was assumed. This assumption was modelled by the symmetry plane boundary condition. The no-slip wall condition was applied at all other boundaries. The tank height was then increased to 2.8 m, and a water level at 2.56 m was set. The inlet was modelled as a cylindrical solid containing a vertical velocity line with a prescribed velocity. The inflow velocity of 1.85 m/s across the vertical line was calculated from dividing the inlet flow rate by the total area of the inlet nozzles, and the direction of 200°using figure 3.3.2a and Pythagoras theorem.

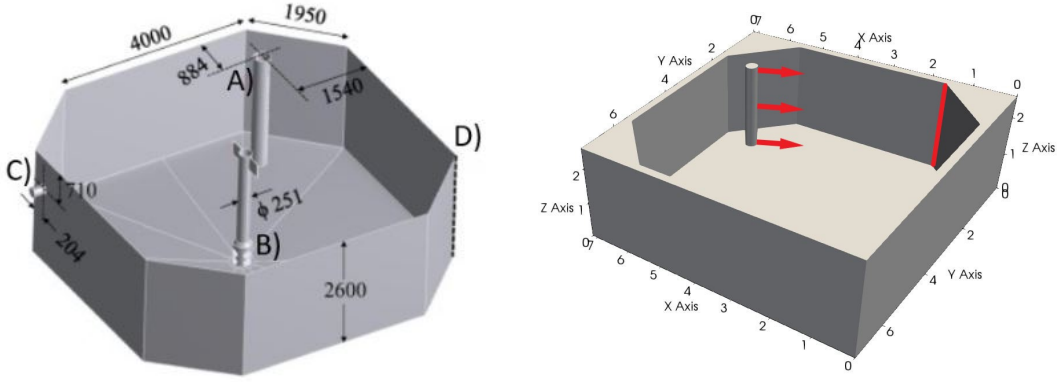

(a) Tank presented in (Gorle et al. 2018b)

(b) Reproduced tank

Figure 3.3.2: Tank used for validation

Point probe measurements

The numerical model was validated by comparing the velocity magnitude at certain point locations in the tank. Experimental measurements had been conducted at a total of 36 locations across a y-plane 0.1 m from the center axis, i.e. at y = 3.475 m. The point probes were placed across three vertical locations; 15, 36 and 58 % of the water column height, i.e. z = 0.554, 1.050, 1.569 m, each containing 12 point probes c/c 0.5 m, as shown in figure 3.3.3a (Gorle et al. 2018b). Due to the absence of outlets in the numerical model, the radial plane was divided into two areas of evaluation as illustrated by figure 3.3.3b: i) the wall area defined between the wall boundaries and a radial distance of 1.9 m towards the center, and ii) the central area between the tank center and an outward radial distance of 1.5 m. In the wall area, the flow velocities are expected to be influenced primarily by the rotational vortex forced by the inlet impulse, while the free vortex caused by the bathtub effect from a central drain is expected to be dominant in the central area (Oca & Masalo 2013). Since a central drain is present in the experiments used as benchmark data, while it is missing in the numerical model, discrepancies between the solutions are expected to be larger in the central area. Hence, half of the velocity probes were present in the wall- and central area respectively. The point probe set up resulted in 36 separate time series recording u, v, w, P, k, ω and ν_t. Probe 2 and 11 were applied in time series analyses of steady state. The velocity magnitude was calculated using Pythagoras theorem in three dimensions, i.e. by the formula:

$$V_{magnitude} = \sqrt{u^2 + v^2 + w^2} \tag{3.3.1}$$

The experimental measurements used as benchmark data in the validation were done using the Doppler shift principle and Acoustic Doppler Velocimetry (ADV), mounted vertically downwards into the tank at each location. It works such that a pulse is sent out at the center of the probe head, which is reflected by suspended solids and air in the water column. The reflected acoustic signals from the sample volume are captured by three receivers placed evenly with an azimuthal distance of 120 °, 10 cm below the transmitter. The velocity difference between the scattered particles and the probe is experienced as a Doppler shift in the reflections. A processing module on the instrument monitors radial velocities, which are turned into Cartesian coordinates. Signal processing computations are then performed in an analogue electronic system on a computer at a maximum frequency of 64 Hz, which deliver the velocity components and signal properties in three dimensions (Gorle et al. 2018b).

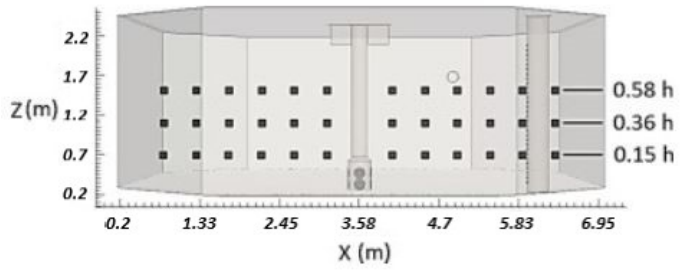

(a) Tank presented in (Gorle et al. 2018b)

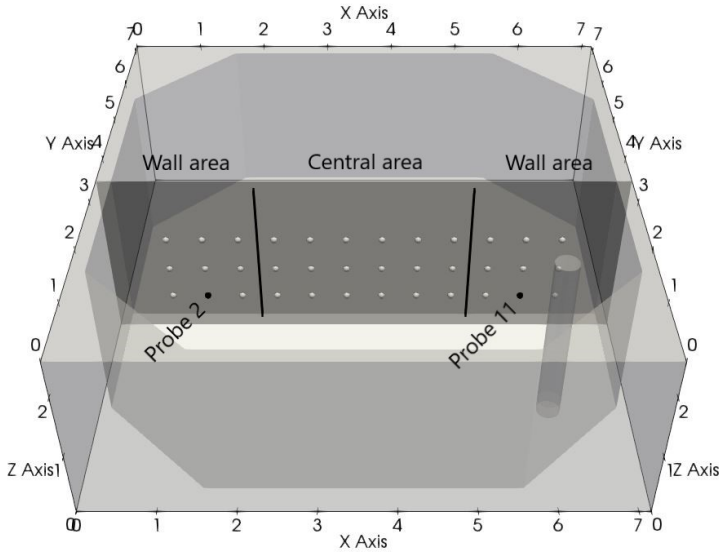

(b) Reproduced tank

Figure 3.3.3: Discrete locations of the tank velocity measurements

3.3.3 Parameter study

In order to investigate the influence of tank geometry and inlet conditions and answer RQ2, a parameter study of various tank designs was carried out using the setup of the validated numerical model. A total of 15 different cases were tested, including 6 different geometric setups and 9 different inlet conditions. The geometric study involved octagonal and circular tanks with varying diameter-to-depth (D:d) ratios and a constant inlet configuration, while the inflow study included a constant tank geometry with various placements of inlets and nozzle angles. To ensure that the tanks were minimize errors associated with the initial conditions, the tank dimensions were kept in scale with the tank used for validation of the model. A wetted diameter of 8 m was therefore chosen is all cases. Flow velocities were measured across the middle plane of the tanks, and velocity distributions in both the tangential and radial direction as well as streamline patterns were analysed and compared between the tank setups. In all cases, an inlet velocity of 1.5 m/s was prescribed close to the inlet pipes.

Geometries

The tank design study of geometric parameters was conducted by varying the tank depth of tanks with a constant diameter of 8 m. The geometric configurations consisted of octagonal and circular tanks with tank depths of 2.0, 2.5 and 3.0 m, i.e. diameter-to-depth ratios, D:d = 4.0:1, 3.2:1 and 2.7:1, as shown in figures 3.3.4 and 3.3.5. The tanks had a single inlet with D = 0.4 m placed symmetric about the y-axis at a center distance of 0.875 m from the nearest wall. An inflow of 1.5 m/s parallel to the x-axis, inflow angle $\phi = 0°$, was prescribed close to the inlet boundary. The octagonal tanks shown in figure 3.3.4a had internal wall lengths of 4.5 m, with a chamfered hypotenuse of 2.5 m at the corners. A thickness of 0.2 m at the walls and bottom was chosen to enclose the tanks with a solid boundary with the no-slip condition.

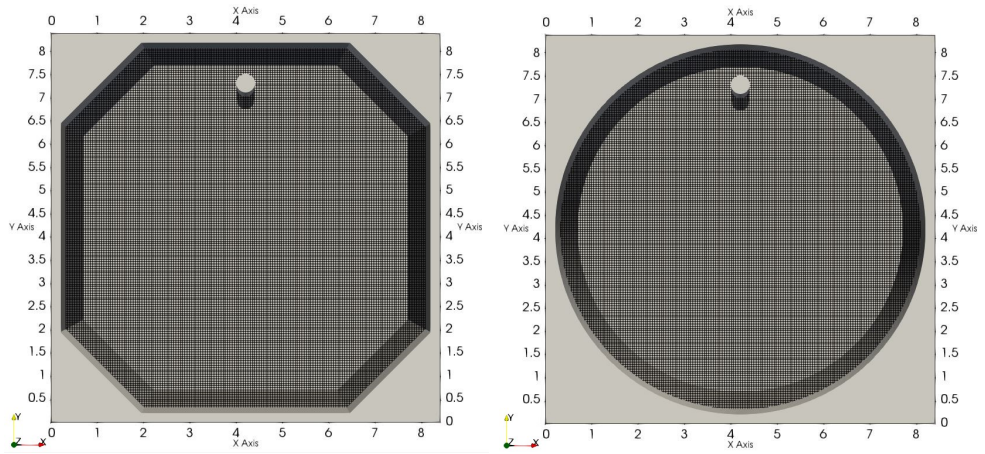

(a) Octagonal tank **(b)** Circular tank

Figure 3.3.4: Tank cross sections

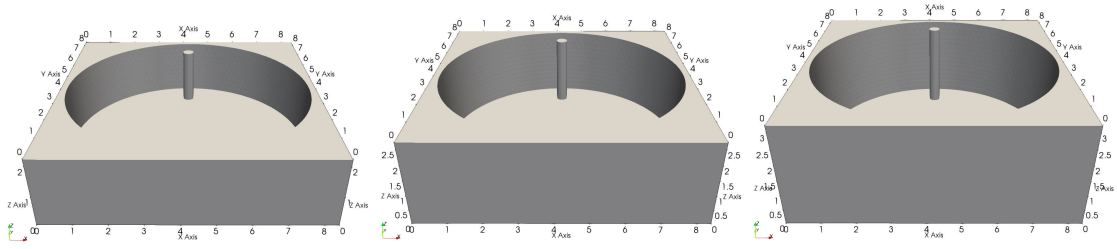

(a) D:d = 4.0:1 **(b)** D:d = 3.2:1 **(c)** D:d = 2.7:1

Figure 3.3.5: Tank depths

Inlet conditions

The inlet condition study included three different configurations: a single inlet placed close to a side wall symmetric about the y-axis, double inlets symmetric about the x-axis and single inlet close to the tank corner. Each inlet configuration were evaluated with

respect to three inflow angles ϕ, respectively with the inflow pointing parallel to the x-axis, a slight outward angle towards the tank wall, and a slight inward angle towards the tank center, as shown in figures 3.3.6 to 3.3.8. The octagonal tank shown in figure 3.3.4a with diameter D = 8 m and depth d = 2.5 m was used. All cases applied inlets with D = 0.4 m placed at a center distance of 0.875 m from the nearest side wall. The tanks in figure 3.3.6a and 3.3.6b had inlets symmetric about the y-axis, while the corner inlet in figure 3.3.6c was placed 2.25 m from the left-side wall.

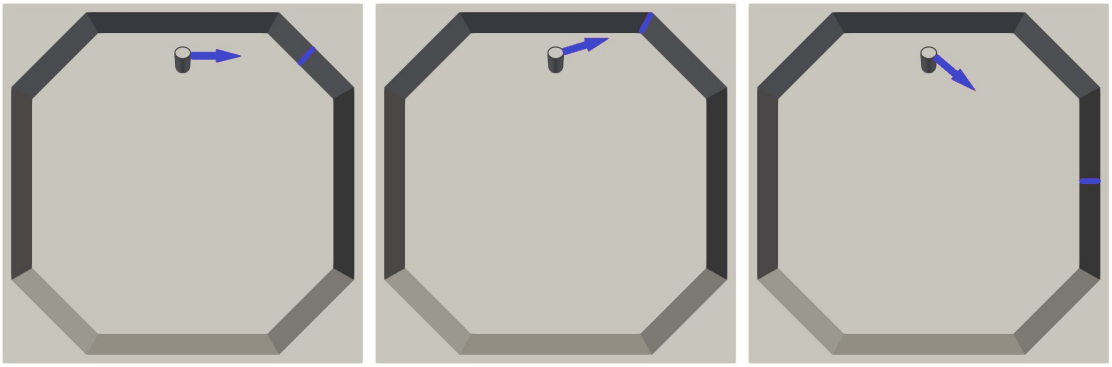

(a) $\phi = 0°$ **(b)** $\phi = 23.6°$ **(c)** $\phi = 320.2°$

Figure 3.3.6: Single inlet symmetric about the y-axis

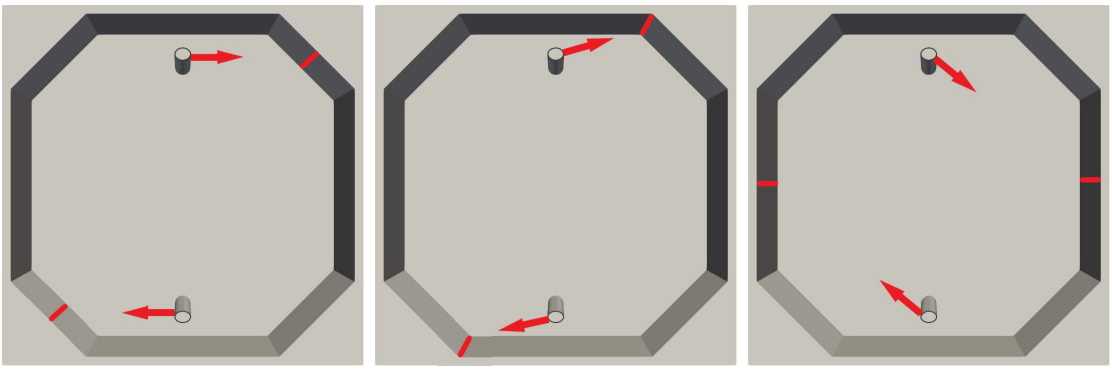

(a) $\phi = 0°$ **(b)** $\phi = 23.6°$ **(c)** $\phi = 320.2°$

Figure 3.3.7: Double inlets symmetric about the x-axis

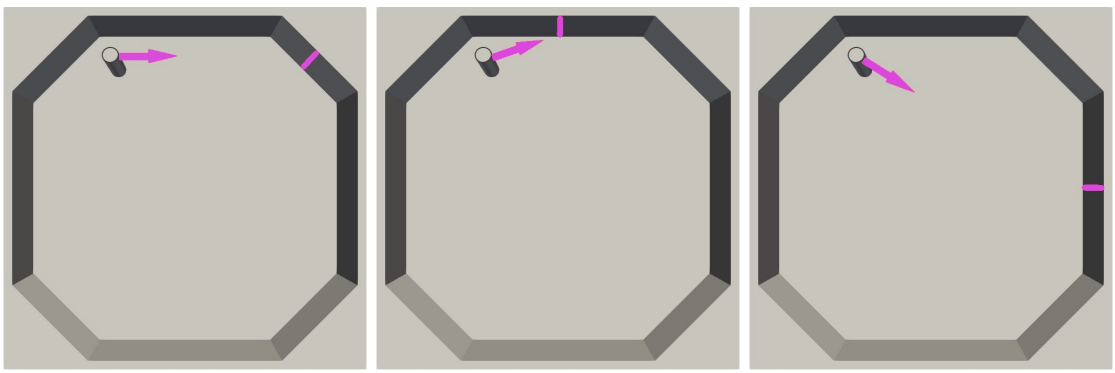

(a) $\phi = 0°$ **(b)** $\phi = 30.0°$ **(c)** $\phi = 330.4°$

Figure 3.3.8: Single corner inlet

Velocity measurements

The tank hydrodynamics was measured by the occurring flow velocities and streamline patterns of the various cases. Velocity measurement probes were placed at two depths, d = 0.25 and 1.5 m, across the center x-z-plane. A total of 30 probes, 15 at each depth, spaced with an interval of 0.5 m were applied, as shown in figure 3.3.9. The velocity v-component corresponded to the tangential velocity, while the u-component corresponded to the radial velocity. The components were plotted to analyse the primary and secondary flow respectively. All cases were run with a simulation time of 300 seconds to achieve steady state values. Time series measured close to the side walls, at probe 3 and 13, were plotted to evaluate whether the solutions had reached steady state.

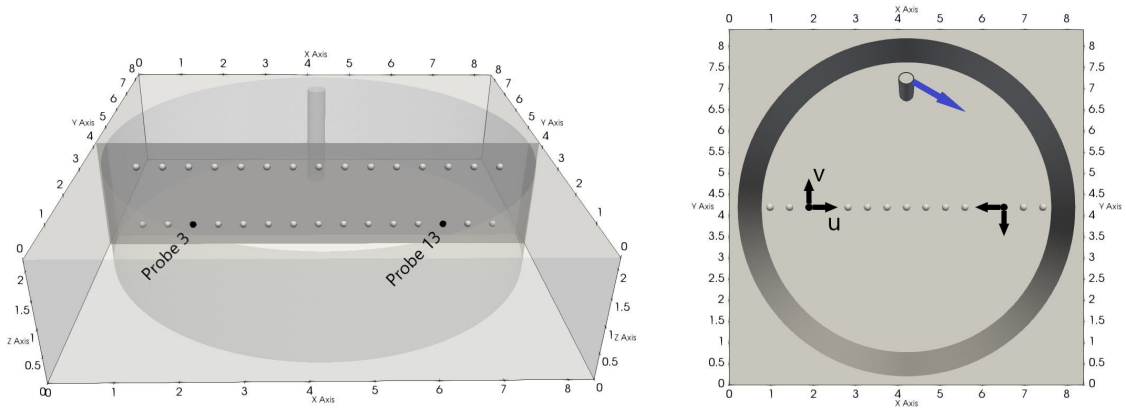

(a) Locations across the central x-z-plane

(b) Velocity components

Figure 3.3.9: Velocity measurement probes

4 Results and discussion

The following chapter is divided into three parts. First, the findings from the numerical model validation are presented. Second, the results obtained from the parameter study of various tank designs are presented. Finally, the most important findings from the literature review are presented and discussed in light of the quantitative results to achieve triangulation. Discussion of the results is done consecutively in the respective sections at where the results are presented.

4.1 Validation of the numerical model

Numerical model validation is a necessary activity that has to be conducted preliminary to the parameter study, in order to identify the variables that has significant influence on the simulation results. In the present work, the location of the vertical line in which the inlet velocity was prescribed, the refinement of the grid within the domain, the time step and choice of turbulence model were most influential in the accuracy of the numerical solution. Sensitivity studies of each variable are presented respectively in the following sub-chapters. In total, 47 simulations were run prior to the parameter study, testing the efficiency and stability as well as validating the accuracy of the model. The total number of cells within the domain, grid size dx, time step dt or CFL-number, and the resulting simulation time were recorded in order to estimate the required computational demand for the cases in the parameter study.

All of the results were compared to experimental measurements presented in Gorle et al. (2018b). The literature did not include detailed values from the experiments, but rather they were presented as graphs in figures. In order use the plots as benchmark data in the present study, the figures were first digitized into discrete values by the use of a digitizing software. This process included manual plotting of points in a manually defined coordinate system. Consequently, an extra input data error was introduced, which implies that the benchmark values are not exact. Compared to the relative change in accuracy of converging results however, this error is regarded negligible.

The base case in Gorle et al. (2018b) included dual drains where 45 % of the flow was drained trough a central outlet and the rest through a side wall outlet. The impulse

forced by the inflow water is expected to have major influence on the velocities in the area between the tank walls and some radial distance towards the center, while a free 'bathtub vortex' would be the primary source of increased velocities near the tank center (Timmons et al. 1998, Davidson & Summerfelt 2004, Lekang 2007, Oca & Masalo 2013). Since the numerical model applied in the present study only incorporates inflow effects and excludes outflow, the velocities and flow pattern outside the center area is the main focus of the validation.

4.1.1 Placement of the prescribed velocity source

As described in table 3.3.1, the inflow hydrodynamics was simplified by defining a in which the inlet velocity was prescribed vertically through the whole water column. The placement of this velocity line had a significant influence on the velocity distribution within in the tank, both on the convergence rate until steady state and the accuracy of the final solution. In order to fully initialize the velocity of the inlet cells, the velocity line could not be placed directly at the inlet boundary, but instead there had to be a certain eccentricity between the boundary and the location of prescribed velocity.

Figure 4.1.1 illustrates the difference between a velocity line defined at the inlet boundary versus a velocity line defined 6 cells away from the boundary. Note that the velocity magnitude scale in figure 4.1.1b is twice as large as that of figure 4.1.1a. Figure 4.1.1c and 4.1.1d displays the velocity distribution close to the inlet boundary in the same scale of magnitude, respectively for a velocity line prescribed at the boundary and 6 cells off the boundary. The figures clearly show the occurrence of numerical diffusion in the way that the inlet flow is 'scattered' in all directions, and not solely in the specified direction. Increased 'smearing' in the form of higher velocities around the inlet can be observed, which indicate that the velocities are prone to a significant distribution of diffusion with the use of an eccentric velocity inlet.

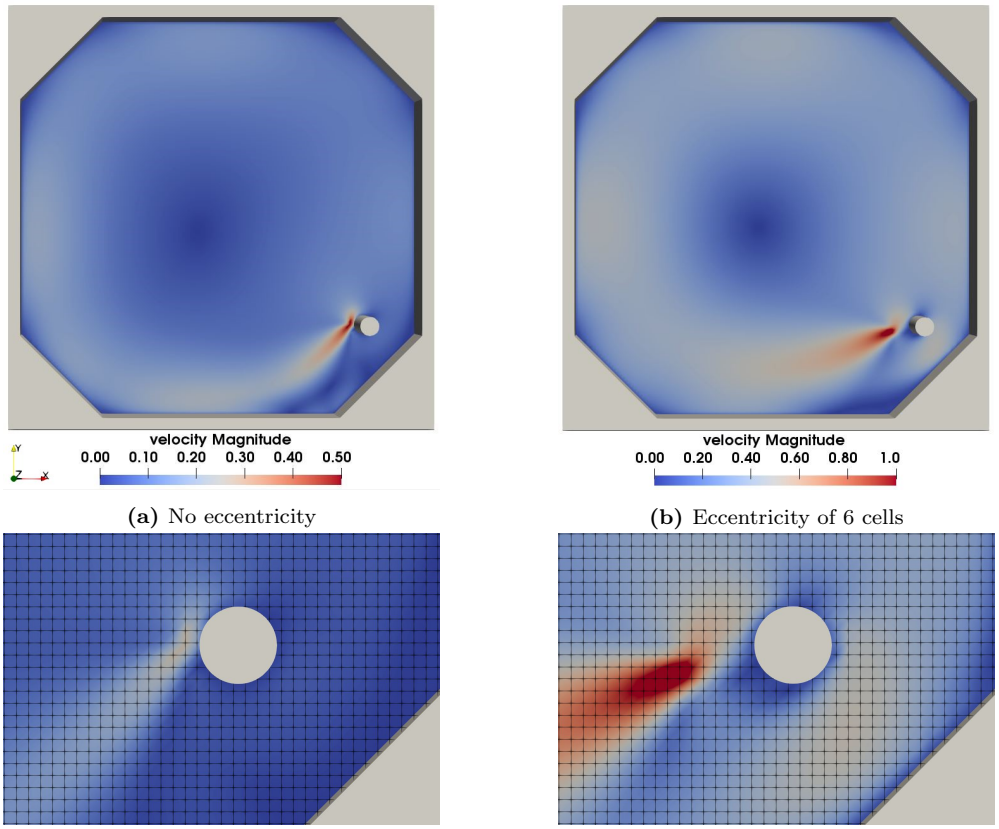

(a) No eccentricity

(b) Eccentricity of 6 cells

(c) Flow field around the inlet with the velocity defined at the boundary

(d) Flow field around the inlet with the velocity defined at a distance of 6 cells from the boundary

Figure 4.1.1: Location of the vertical line with prescribed inlet velocities

Figure 4.1.2 shows the time series of v where the inlet velocity is defined at various distances away from the solid inlet. The plotted time series were measured at probe 2 and 11, displayed in figure 3.3.3, close to the side wall and bottom of the tank. Grid size $dx = 0.05m$ and time step $dt = 0.02s$ was applied, i.e. the absolute distance between the inlet boundary and vertical velocity line is 0.05 m / cell in the direction of the flow. A positive v-value indicate flow in the y-direction. The dashed line represent the exact solution measured in experiments, which was 0.245 m/s.

In the cases of an eccentrically placed velocity line, the solution changes rapidly in the first 80 s of the simulation at probe 2. The rate of change is steadily reduced until steady state at around 150 s in the cases with largest eccentricity. For the cases where the inlet velocity is prescribed closer to the solid boundary, a temporarily steady state is observed at around 80 s. The derivative do however increase as the simulation progresses in time, which indicate that the solution is not yet at steady state. The duration of the temporarily steady plateau is larger for the cases with lower eccentricity, and thus the time before until the final steady state is increased. A velocity gradient increase can be seen at the end of the simulation when the velocity line is defined at the boundary, which may indicate that

the constant velocity observed at around 150 s is a temporarily plateau and not a final steady state. All cases except for when the velocity is prescribed at the inlet boundary can be regarded steady state after a simulation time of 200 s. The measurements at probe 11 displays a similar pattern, where steady state is reached at around 180 s. Overall, the solution seems to converge faster with an increasing distance between the inlet velocity line and the solid boundary.

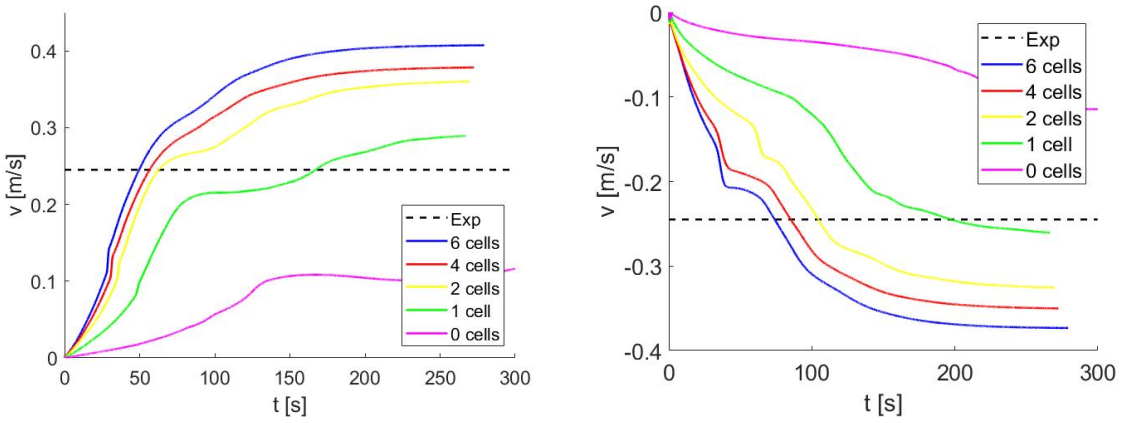

(a) Probe 2 **(b)** Probe 11

Figure 4.1.2: Time series of various inlet eccentricities at velocity probes near the tank wall

A simple way to check whether the simulations were fully initialized was to record the maximum velocity observed in the tank. Table 4.1.1 summarize the maximum velocity magnitudes, calculated using equation 3.3.1, recorded at the end of the simulations. The desired maximum velocity should be close to the value defined at the vertical line, which was 1.85 m/s for all cases. It is indicated from table 4.1.1 that an eccentricity of one cell provide the most preferable solution. It can also be seen that the maximum velocity within the tank converges toward a value of approximately 2.0 m/s, which is 8 % higher than the prescribed velocity, as the distance between the solid and velocity line in increased.

Table 4.1.1: Maximum recorded velocity in cases with various eccentric inlets

Cell eccentricity	0	1	2	4	6
$V_{mag,max}$ **[m/s]**	0.90	1.92	2.20	2.04	2.01

Figure 4.1.3 shows the velocity magnitude across the diameter of the tank. The relative change between the graphs is reduced as the eccentricity between the velocity line and inlet boundary is increased, which indicates convergence toward a significantly over estimated solution in the areas near the wall. The probable explanation is that the diffusion observed in figure 4.1.1 increases and gets distributed throughout the tank as the source of velocity is placed eccentric to the solid inlet. The diffusive effect gets amplified as the distance

between the boundary and the vertical velocity line is increased. When the velocity source is located closer to the inlet, diffusion in the wrong direction is reduced and convection in the specified direction increases. I.e. a trade-off between increased diffusion and boundary condition initialization has to be made. The velocity source needs to be defined a distance away from the boundary in order to sufficiently initialize the boundary conditions, while at the same time it should not be placed too far away from the boundary in order to force convective flow in the desired direction, as well as avoiding distributed numerical diffusion. Thus, defining the prescribed vertical velocity line one cell eccentric to the solid boundary seems to be sufficient to initialize the boundary cells, while at the same time minimizing numerical diffusion.

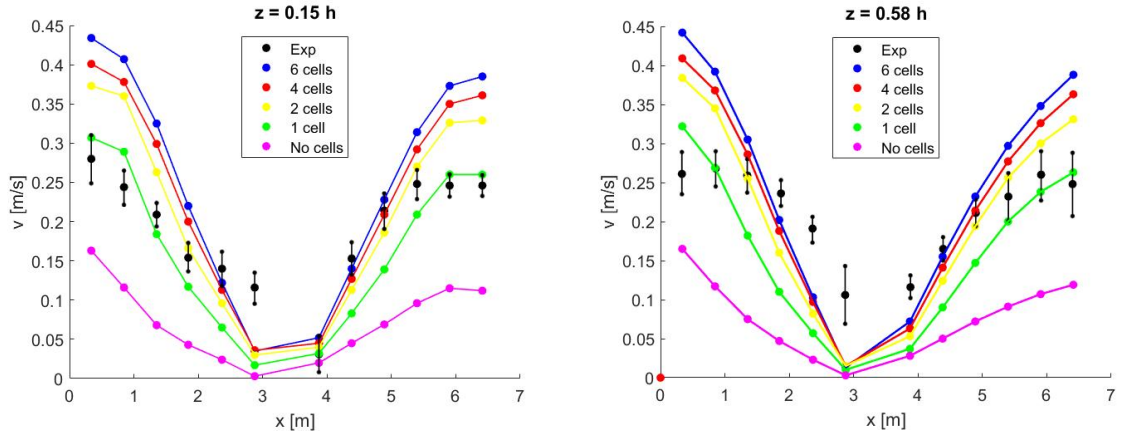

(a) At a water height of 0.35 m

(b) At a water height of 1.37 m

Figure 4.1.3: Velocity profile for various eccentric inlets across a radial plane 0.1 m from the tank center

4.1.2 Grid size sensitivity

A parameter that has great influence on the simulation results is the refinement of the numerical grid that constitutes the flow domain. A smaller grid size (dx) implies more cells within the tank, and the grid should be sufficiently refined in order to ensure satisfactory accuracy of the solution. However, large 3D meshes with very refined grid sizes require substantial computational power to achieve convergence of the solution, as a halving in grid size cause an 8-fold increase in the total number of cells in a structured Cartesian 3D domain. Thus, a trade-off between solution accuracy and computational demand has to be made, making it necessary to define an optimal grid size for the present flow.

The total volume of the tank was 130.9 m^3. A Cartesian mesh was applied where the grid size was equally refined in all three directions, i.e. $dx = dy = dz$. Thus, the total number of cells in a tank with grid size dx = 0.10 m was 130 900, while it increased to 130 900 000 using a grid size of dx = 0.01 m. The latter would not be a feasible option to use

in a parameter study, hence grid sizes of dx = 0.10 - 0.025 m were tested in the present sensitivity study.

No form of local refinement of the grid was applied in the present study. Grid stretching could be implemented in the model as a measure to reduce the computational demand of the simulations. Local refinement in areas where high velocities and turbulent flow are expected to occur, e.g. near the inlet source, could be a feasible option to reduce the total amount of cells while simultaneously preserve the accuracy in critical areas. Furthermore, since the velocity profiles looks similar at all depths investigated, the grid size in the z-direction could be coarser, or possibly stretched with refinement towards the tank bottom.

Figure 4.1.4 shows time series of the velocity magnitude at probes 1.125 m from the tank wall, plotted for different grid sizes. The dashed line represents the experimental value of ± 0.245 m/s presented in Gorle et al. (2018b). The velocities converge faster to its final solution for coarser grid sizes. For the coarsest grids, dx = 0.10 and 0.075 m, steady state is reached after around 150 s, while a mesh of dx = 0.05 m takes about 225 s to reach steady state due to the increased duration of a temporarily steady plateau at around 80 s. The simulation for dx = 0.05 m was cancelled at 267 s because the wall time specified in the batch script was inadequate. The time series do however indicate that the final solution is at steady state, hence a wall time of 267 s was deemed sufficient. The most refined grid size could advantageously have been run with a duration longer than 300 s, however the velocity measurements at probe 11 show a low rate of change for the last 30 s, which implies that steady state may be assumed.

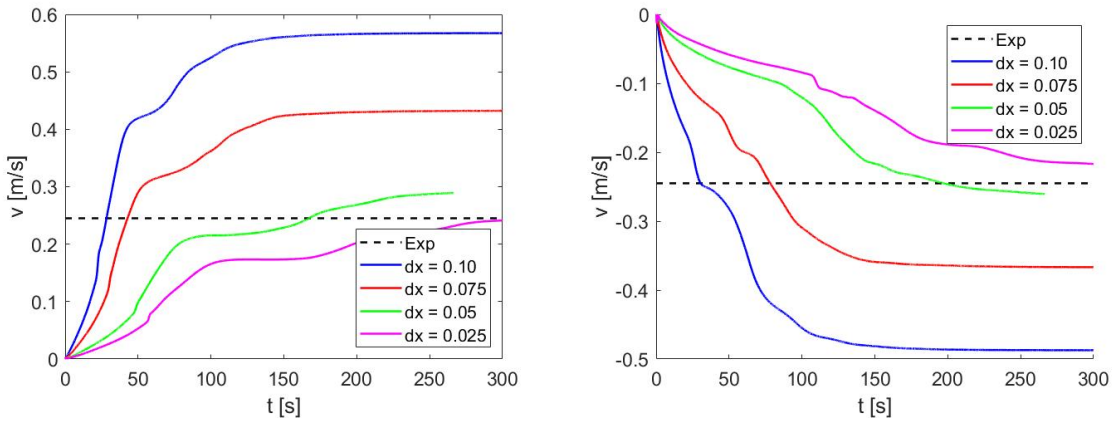

(a) Probe 2 **(b)** Probe 11

Figure 4.1.4: Time series for various grid sizes at velocity probes near the tank wall

The inlet velocity source was placed one cell eccentric to the solid inlet boundary, the ab-

solute distance would therefore vary depending on the investigated grid size. A stress-free surface boundary and a constant time step dt = 0.02 s was used in all cases. The spatial velocity distribution for different grid sizes (dx) across a plane near the tank center is shown in figure 4.1.5. The results were plotted at two water depths; close to the tank bottom and around the middle of the water column, displayed by figure 4.1.5a and 4.1.5b respectively. Each grid size is illustrated with various colors. Expected experimental values are displayed as black dots including the standard deviation.

In the near-wall region, for low and high x-values, the change in velocity is reduced as the the grid is refined, which indicates convergence of the results. The refined grid converges toward a solution that slightly underestimates the velocities compared to the experimental data. Considering probes in the wall area (see figure 3.3.3b), the converged solution are within- or close to the uncertainty limits of the expected results at both tank depths. The discrepancy between the numerical and experimental solution increases towards the tank center due to the exclusion of a central outflow in the numerical model. If the central region $x \in [1.8 - 5]$ is excluded, the maximum discrepancies of dx = 0.025 m is 31 % at probe 10 and 38 % at probe 3, at water depths 0.15 h and 0.58 h respectively. For dx = 0.05 m the maximum discrepancies in the wall region are reduced to 18 % and 30 % for the respective water depths. I.e. the numerical to experimental discrepancy increases at higher water depths, which indicates that the free vortex caused by the draining bathtub effect have larger influence on velocities at higher water depths.

Since the inlet velocity source was placed one cell eccentric to the solid boundary, the distance differed between the grid sizes of evaluation. I.e. the eccentricity was 0.10 m for dx = 0.10 m and 0.025 m for dx = 0.025 m. As discussed in section 4.1.1, the distance between the velocity source and solid had a significant impact on the solution. Indeed it can be implied by the findings in figure 4.1.5 that the coarser grid sizes are influenced by higher distribution of numerical diffusion, which lead to higher velocities in the tank periphery. The two fines grid sizes show similar velocity distribution patterns across the tank, however dx = 0.05 m display slightly higher velocities near the tank wall, which is probably due to increased diffusion as a consequence of larger eccentricity of the inlet source. Overall, the numerical results shows best compliance with experiments using a grid size of dx = 0.05 m.

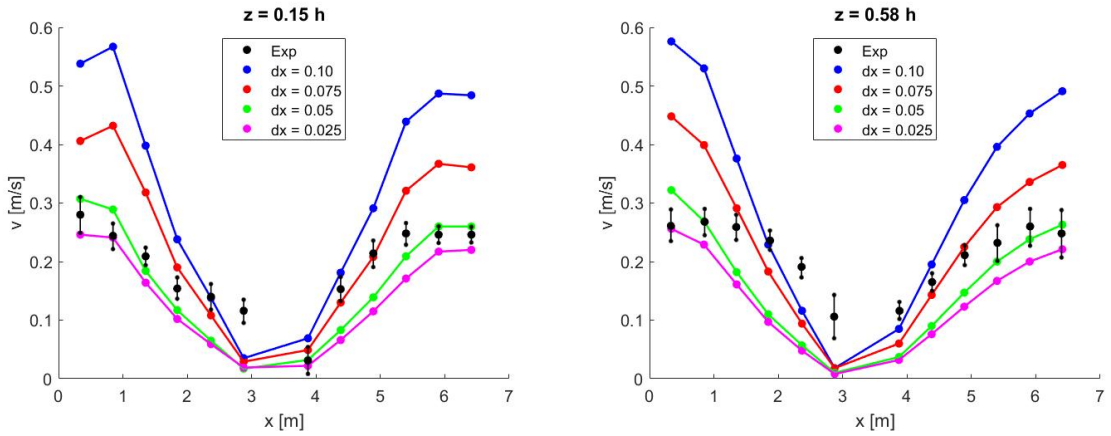

(a) At a water height of 0.35 m

(b) At a water height of 1.37 m

Figure 4.1.5: Velocity profile for various grid sizes across a radial plane 0.1 m from the tank center

4.1.3 Time step sensitivity

The length of the time step, dt, is another parameter influencing the accuracy and stability of the numerical solutions. Based on the findings in section 4.1.2, a grid size of dx = 0.05 m was applied in the time step sensitivity study. Initial tests were run using adaptive time stepping based on the CFL-criterion. However, adaptive time stepping tended to produce unstable results for refined grid sizes, and thus a sensitivity study applying a constant time step was conducted. Reasonable time steps were estimated using equation 2.2.12 with a Courant number in the range of $C \in [0.2, 1.0]$ and a maximum velocity of 2.0 m/s. Consequently the time steps $dt \in [0.005, 0.025]$ were investigated. Time series of the velocity magnitude in the near wall regions are shown in figure 4.1.6. A similar pattern can be seen for all cases, however the solution converges faster toward steady state when the time step is reduced. After 220 s, steady state is reached for all time steps.

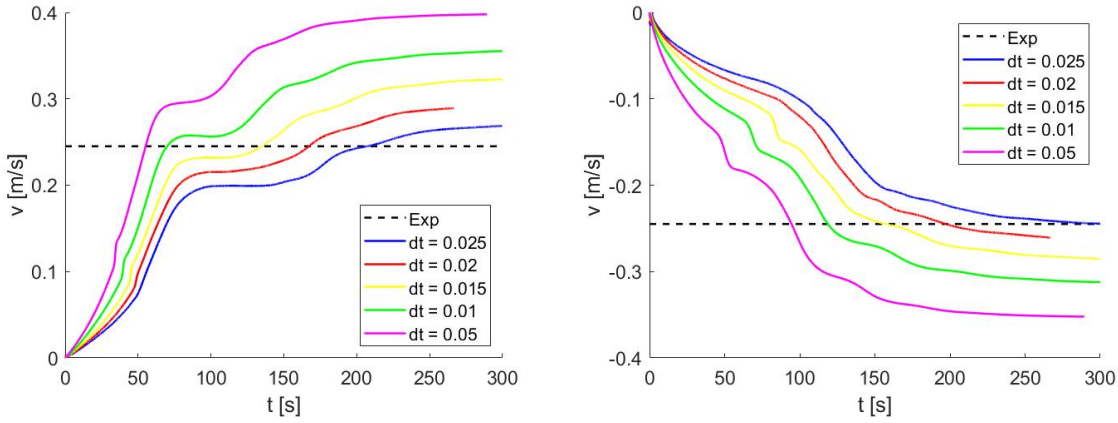

(a) Probe 2

(b) Probe 11

Figure 4.1.6: Time series for various time steps at velocity probes near the tank wall

The spatial distribution of the velocity magnitude is shown in figure 4.1.7. For a converg-

ing solution, the relative change in velocities are expected to decrease as the time step decreases. Signs of convergence can be seen for the three largest time steps, where the velocities approaches a solution that is over estimated in the widest areas of the tank. As the time step is further reduced however, the results diverge and become erroneous for dt = 0.01 and 0.005 s. A possible explanation is that the truncation error that arises in the boundary cells, gets amplified when the amount of iterations per cell increases. Since numerical diffusion arise from the prescribed inlet velocity source, its magnitude might increase as the time step is reduced and hence the number of iterations per cell is increased. The solution gets smeared directly towards the center of the tank, where the velocity measurement probes are located, instead of being transported as convection in a tangential direction as specified at the inlet source.

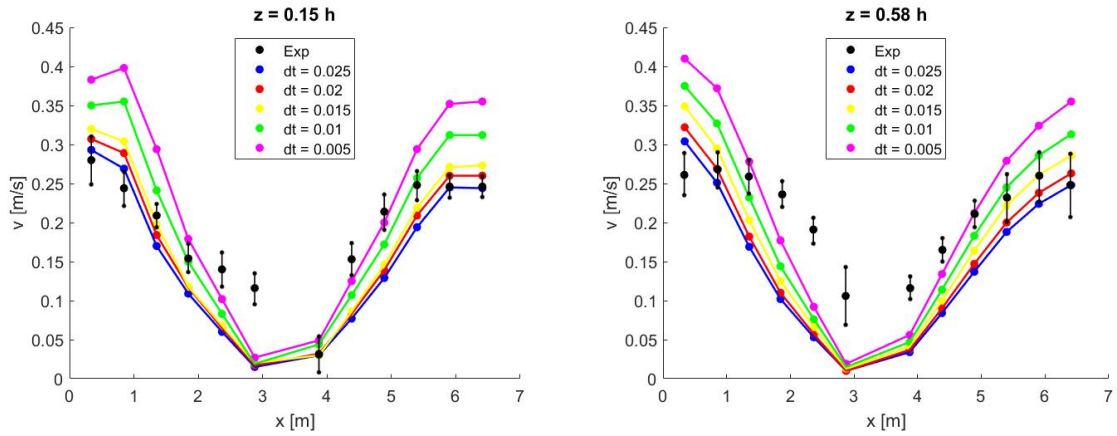

(a) At a water height of 0.35 m

(b) At a water height of 1.37 m

Figure 4.1.7: Velocity profile for various time steps across a radial plane 0.1 m from the tank center

4.1.4 Free surface and turbulence modelling

In all of the sensitivity studies presented above, a stress-free boundary at the water surface has been assumed to simplify the model and reduce the computational demand. Furthermore, the $k-\omega$ turbulence model has been applied in all cases. To investigate the influence of the surface assumption and choice of turbulence model, separate simulations were run for comparison using the $k-\epsilon$ turbulence model as well as the level set method for free surface modelling. Time series of the velocity magnitude at probe 2 and 11 are shown in figure 4.1.8. The $k-\epsilon$ model seems to provide a solution that is slightly more unstable compared to the $k-\omega$ model. The acquired time series using the $k-\omega$ model is similar regardless of the assumption made at the surface. The solution converges toward steady state at the same rate whether the free surface is resolved or assumed stress-free. A steady flow state is indicated at a simulation of approximately 230 s.

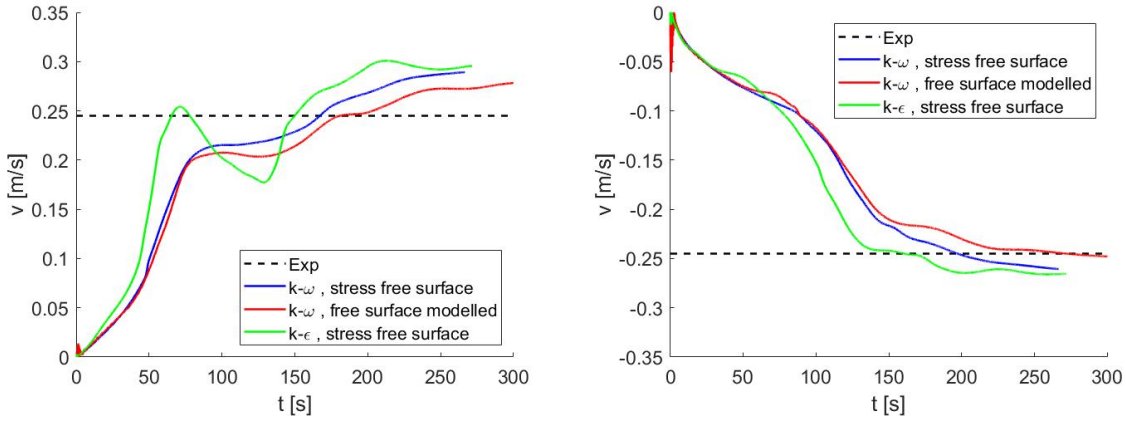

(a) Probe 2 **(b)** Probe 11

Figure 4.1.8: Time series of various turbulence models and free surface condition at velocity probes near the tank wall

The velocity distribution across the tank is shown in figure 4.1.9. The impact of the choice of turbulence model is low, as both the $k-\omega$ and $k-\epsilon$ model display a similar velocity profile. A slightly less over estimated solution is observed in the near-wall area in favour of the $k-\omega$ model. Further improvement is seen when the free surface is modelled opposed to the stress-free surface boundary assumption. At probe 2 and 11 near the tank bottom, the discrepancies to the experimental result are reduced from 18 to 14 % and 6 % to 0 % respectively. Improved results can also be seen towards the tank center when the free surface is resolved, in the form of increased velocities. In contrast to the assumption of a stress-free boundary, where the velocities approach zero almost linearly towards the center, the resolved surface result in a velocity profile that increasingly mimic the experimental velocity profile.

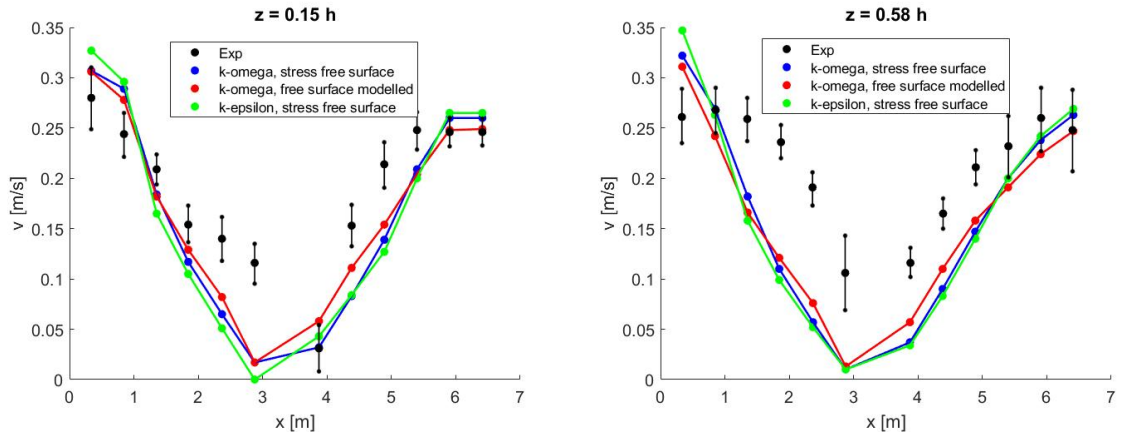

(a) At a water height of 0.35 m **(b)** At a water height of 1.37 m

Figure 4.1.9: Velocity profile for two turbulence models across a radial plane 0.1 m from the tank center

4.1.5 Concluding remarks

The most important findings from the validation of the numerical model are summarized by the following key points:

- The choice of grid size and placement of the inlet velocity source had the greatest influence on the accuracy of the numerical solution.
- The results improved as the grid was refined, and convergence towards a solution that slightly under estimated the velocities was observed. The time step sensitivity study indicated convergence for $C \geq 0.6$, however the solution diverged for lower Courant numbers, probably due to diffusion from the inlet boundary cells.
- The inlet source was placed at x = 5.86 with inflow in the negative x-direction. A velocity difference of approximately 18 % between probe 1 and probe 12 shows the occurrence of an asymmetry in the flow pattern, which indicates that the flow undergoes a gradual momentum diffusion due to wall friction.
- The simplified inflow, using a prescribed vertical velocity line through the water column, suffers from significant amount of numerical diffusion, where the amount of occurring velocity smearing depends on the distance between the inlet solid boundary and the velocity source location. The diffusive nature of the inlet is clearly observed by 3D simulations when analyzing the flow field near the inlet. It is further implied by sensitivity studies of inlet source placement and time step convergence.
- Due to the exclusion of a central outlet, large discrepancies between the numerical and experimental velocities are seen in the central area of the tank. The numerical solution is greatly underestimated compared to the benchmark data within the half-radius area from the center.
- According to the experimental measurements, the spatial distribution of the velocity magnitude is greatly affected by the water depth. A more uniform distribution and higher velocities are observed towards the tank center at higher water depths. However, standard deviations were also larger compared to measurements near the tank bottom, which indicates higher uncertainty in the results. The numerical estimation was not influenced to the same degree by the water depth, as the spatial velocity profiles across the tank were quite similar at all the evaluated water depths. This lead to higher discrepancies between the experimental and numerical solution towards the free surface, which might imply that the bathtub effect caused by a free vortex from the central drain is more prominent, and cause higher velocities with increasing water depth.

- After 250 seconds, the velocities measured at point probes close to the wall displayed low variation for all cases in the sensitivity study. Steady state flow may therefore be assumed at this run-time, hence simulations of similar flow problems in tanks with the same size scale should be run with a duration of at least 250 s.

Model applied in parameter study

Based on the results from the validating sensitivity analyses, appropriate decisions regarding the numerical model were made. The settings further applied in the parameter study of tank designs are summarized in table 4.1.2. The chosen settings showed a good balance between accuracy and computational demand, by converging towards steady state within a wall time of two hours and providing a solution within acceptable discrepancy limits. In the wall area defined in figure 3.3.3b, the maximum discrepancies between the experimental and numerical results were 18.4 %, 18.1 % and 29.7 % at the respective water heights, z = 0.35, 0.85 and 1.37 m. Furthermore, 50 % of the numerical measurements were within the standard deviation of the experimental results at these vertical locations.

Table 4.1.2: Numerical model applied in parameter study

Inlet eccentricity	0.05 m
Grid size, dx	0.05 m
Time step, dt	0.02 s
Simulation time	300 s
Turbulence model	$k - \omega$
Free surface modelling	No

4.2 Parameter study

The purpose of the parameter study was to investigate how and to what extent the tank hydrodynamics was influenced by two factors; i) the geometric properties of the tank, and ii) the inflow conditions of the tank. The study of geometric properties included two popular tank shapes, the circular and octagonal, which were investigated for three different diameter-to-depth, D:d-ratios: 2.7:1, 3.2:1 and 4.0:1, where the internal tank diameter was kept constant at 8 meters and tank depth varied accordingly. The inflow condition study included three different inlet placements, where each inlet configuration were tested for three inflow angles, as shown in figures 3.3.6 - 3.3.8. The cases were assessed and compared based on velocity measurements across the central x-z-plane at y = 4.2 m, as shown in figure 3.3.9.

The occurring primary- and secondary flow, described in section 2.1.1, for the various tank designs were evaluated separately in each subsection. A stable primary flow with high velocities is especially important in order to achieve optimal swimming conditions for the fish and prevent bio-fouling on the tank boundaries (Timmons et al. 1998, Lekang 2007) . Furthermore, the strength of vortices occurring due to secondary flow is one of the most important factors influencing mixing and transport of solid particles (Gorle et al. 2018b). Achieving secondary flow with adequately high velocities toward drains is therefore important to avoid sedimentation and secure homogeneous water quality in the tanks. The primary flow was assessed by tangential velocities represented by the v-component of the measurements, while the secondary flow was evaluated by radial velocities represented by the u-component.

A total of 15 cases were simulated in the parameter study. The choices made in the numerical model, described above, lead to a domain requiring a feasible amount of computational power. Applying the model settings described in table 4.1.2 using four nodes on the supercomputer 'Fram', with a total number of cores corresponding to 128, the required simulation time ranged between 2 - 4 hours for each case investigated in the parameter study. The simulation time could be reduced by increasing the number of active cores, however an increase in cores running in parallel caused increased domain decomposition and MPI usage, resulting in larger information files. Large VTU-files made post-processing of the results inconvenient, as significantly more lag in Paraview was experienced, as well as download time and Matlab import time increased. Thus, the size of the VTU-files were attempted reduced to a minimum by applying as few cores as possible. Applying 4 nodes for the simulations were deemed appropriate, as it kept the amount of generated information manageable. In addition, the associated wall time and queue pending time upon execution were feasible to complete the required amount of simulations in time.

4.2.1 Effect of tank geometry

The geometric parameter study was performed using tanks with dimensions described in section 3.3.3 by figures 3.3.4 and 3.3.5. The velocity prescribed at the inlet was 1.5 m/s with an inflow direction parallel to the x-axis, $\phi = 0°$. The computational domain increased for tanks with lower D:d-ratios and greater water depths, thus increasing the demand for computational power. The total number of cells amounted to 1.24, 1.52 and 1.81 million respectively for tanks with D:d-ratio 4.0:1, 3.2:1 and 2.7:1, resulting in required wall times of 2.4, 3.2 and 3.8 hours to complete simulations of 300 s.

Primary flow

The primary flow within tanks with diameter-to-depth ratio 2.7:1 is illustrated in figure 4.2.1. The observed streamline pattern appeared similar regardless of tank depth, thus only the results for D:d = 2.7:1 are displayed. The flow is contoured by streamlines acquired after simulations of 300 s, and colored by velocity magnitude to highlight regions where high and low velocities occur. Keeping in mind that an inflow velocity of 1.5 m/s was prescribed, the velocity scale relative to inflow becomes roughly 0 - 25 % from dark blue to dark red. Higher velocities are observed near the inlet. The velocity difference between the inlet stream and the current primary flow in the tank creates local shear zones, which in turn generate turbulence. The swirling motion of streamlines near the inlet indicates turbulent flow and increased mixing in the region, and the turbulent effect seems to be larger in the octagonal tanks compared to the circular ones.

By considering the colour grading within the tanks, it can be seen that the velocities in tanks with circular geometry decrease gradually as the flow propagate further downstream. A slightly different distribution is seen in the octagonal tank. The velocities decrease in regions close to the chamfered corners, however accelerating flow is observed as the flow is transported along the straight walls. Generally, higher velocities can be seen close to the walls in the octagonal tanks, whereas the circular tanks experience increased wall friction that reduce the near wall velocities. Hence, maximum velocities occur at some offset distance from the wall further downstream in circular tanks.

The dark blue coloring near the corners of the octagonal tank in figure 4.2.1a indicates that velocities are low, which means that quiescent zones prone to fouling and low degree of mixing are likely to occur in these regions. Even at corners close to the inflow, the presence of zones with low velocities are prominent, which implies that the occurrence of dead zones are hard to counter in octagonal tanks. Similarly, low velocities occurring in the near wall region at the left-hand side in figure 4.2.1b imply that increased fouling is expected further downstream of the inflow in circular tanks. However, the gradual velocity decrease seen near the wall at the right-hand side indicate that quiescent zones may be avoided, e.g. by placing another inlet close to the wall opposite to the present inlet. In both designs, a dead zone occur in the central area, however higher velocities are expected when a center drain is present (Gorle et al. 2019).

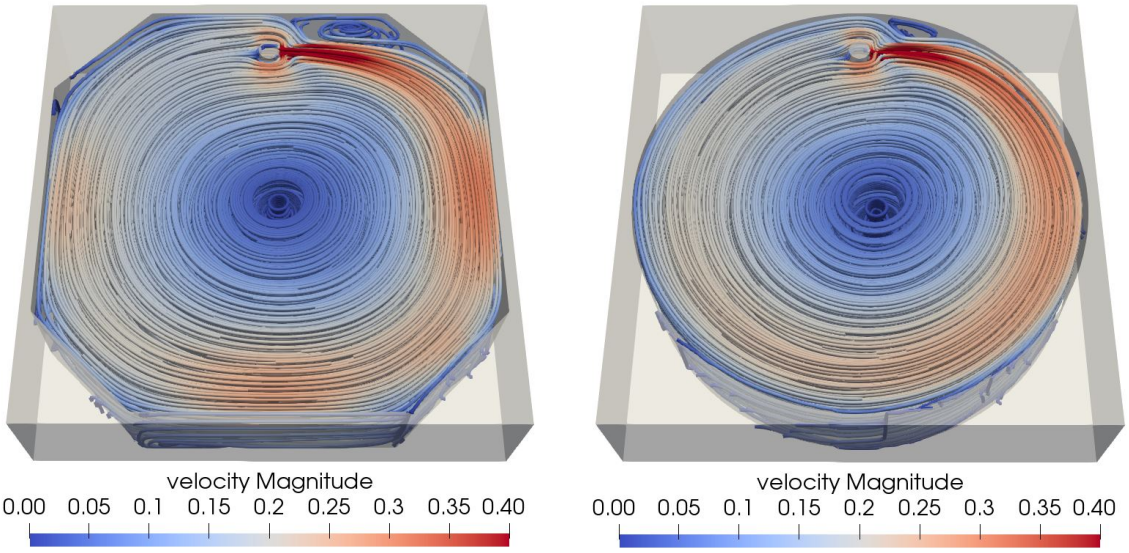

(a) Octagonal tank **(b)** Circular tank

Figure 4.2.1: Streamline pattern of tanks with D:d = 2.7:1

Figure 4.2.2 shows time series of the velocity magnitude measured at probes 3 and 13. The probes were located 1.5 m from the tank wall in the x-z-plane crossing the center of the tanks, as shown in figure 3.3.9. The velocities are dimensionless and plotted as percentage of the inflow velocity, $V_0 = 1.5$ m/s. The results in figure 4.2.2b indicates that velocities converge to steady state after approximately 230 s in the tank side to which the inlet is directed, while at the side furthest downstream the inlet steady state is reached some 30 s later as shown in figure 4.2.2a. It can also be observed that the velocities converge toward nearly the same values regardless of the tank depth, however larger variances throughout the time series are seen for larger D:d-ratios, i.e. smaller water depths.

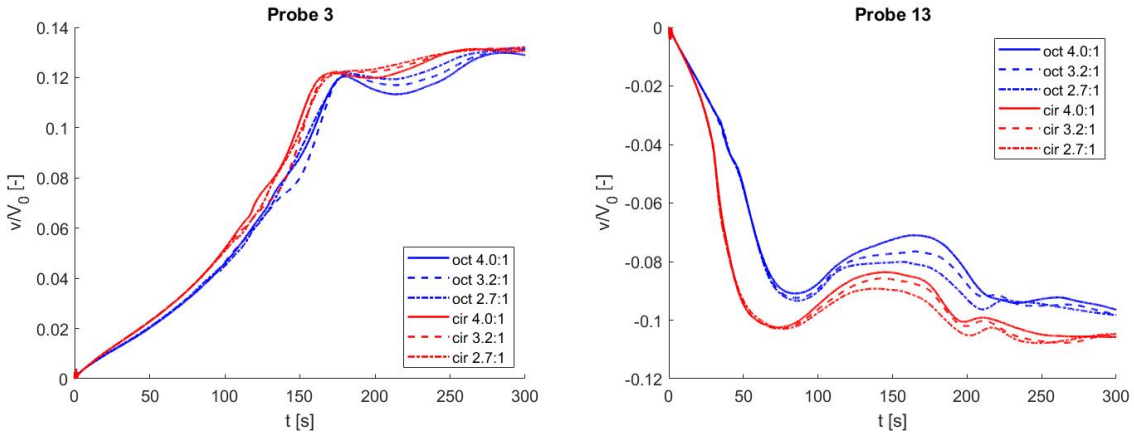

(a) Probe 3 **(b)** Probe 13

Figure 4.2.2: Time series of tangential velocities at probes 1.5 m from the tank walls

Figure 4.2.3 shows the velocity magnitude as percentage of inflow velocity plotted across the tank center at the probes shown in figure 3.3.9. Both the octagonal and circular

tanks achieve high velocities in the wall region closest to the inlet. At x = 7.5 m, the maximum velocities are 20 % and 18 % of the inflow velocity for octagonal and circular tanks respectively, at both water depths. Thus, the maximum velocity observed in the center plane is 10 % higher for octagonal geometries compared to a circular design. The diameter-to-depth ratio did not affect the results. The radial velocity profile towards the center are similar regardless of the geometric design, as they approach zero close to the middle due to the absence of a center drain. A circular tank design do however provide slightly higher velocities in the tank region between x = 7.0 m and the center, which are more prominent at higher water depths. The difference is even higher across the radius further downstream, e.g. 15% difference in favour of the circular design at x = 2.5 m, indicating more uniform conditions across the diameter in circular tanks.

The flow is influenced by wall- and bottom friction in addition to diffusion as it propagates downstream from the inlet. This is observed as a skewness in velocity profile across the tank. By considering figure 4.2.3a, the velocity reduction between the probes closest to each side of the tank, i.e. at x = 7.5 and 0.5 m, is 29 % and 43 % for octagonal and circular geometries respectively. This effect is slightly reduced at higher water depths, where the velocities are reduced by 23 % and 33 % across the diameter in octagonal and circular tanks respectively, as shown in figure 4.2.3b.

The most significant result difference between the designs are seen in near the wall region furthest downstream from the inlet, i.e. for low x-values. The octagonal tanks remain uniformly high velocities of $0.14V_0$ within 1.5 m distance from the wall. In contrast, the circular geometries has a peak at this location before a significant reduction is seen towards the wall where the velocities are reduced by 27 % close to the tank bottom. Higher in the water column however, the velocities remain high in the region for circular tanks, while they increase outward in octagonal tanks.

The primary flow show similar behaviour regardless of the tank water depth, which is indicated by the tangential velocity distribution of both the circular and octagonal tanks. Although high velocities are seen both near the bottom and higher in the water column at the right hand side of the tanks, viscous effects such as friction show greater influence further downstream especially in the circular tanks. The difference between z = 0.25 m and z = 1.5 m at x = 0.5 m is 7 % and 17 % for octagonal and circular tanks respectively. Since the inlet velocity source is defined through the whole water column in all cases, the graphs display almost no discrepancy between the various diameter-to-depth ratios.

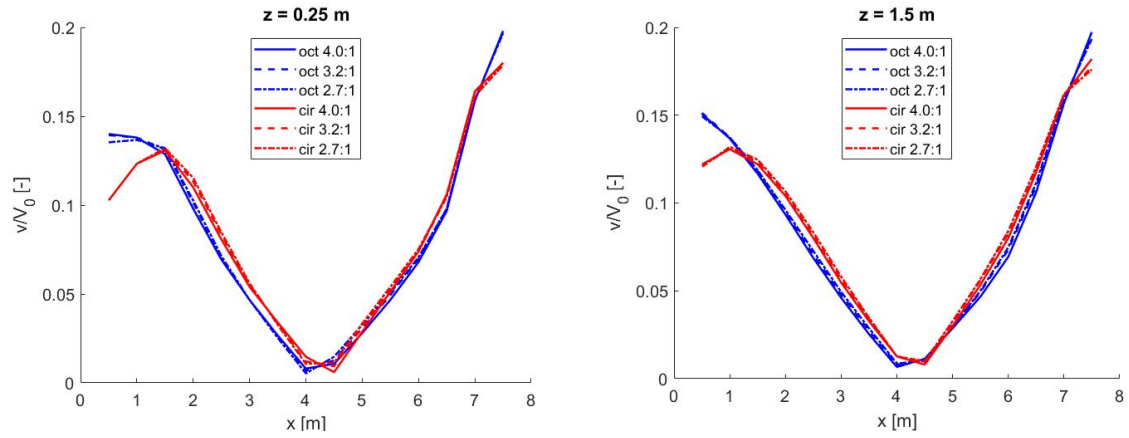

(a) At z = 0.25 m **(b)** At z = 1.5 m

Figure 4.2.3: Dimensionless tangential velocity profile at the x-z-plane across the tank center

Secondary flow

The time series of non-dimensional radial velocities measured across the central x-z-plane at probes 1.5 m from the side respective walls are shown in figure 4.2.4. In contrast to the tangential velocities, which according to figure 4.2.2 displayed a gradual increase in magnitude towards steady state, the radial velocities experience high fluctuations that accumulate to a peak around 150 s and 50 s at probe 3 and 13 respectively. The values are only temporary however, and rapidly decrease in an interval of 50 s. After a simulation time of 200 s, the gradients at both probes are low in all cases which indicates convergence towards steady state.

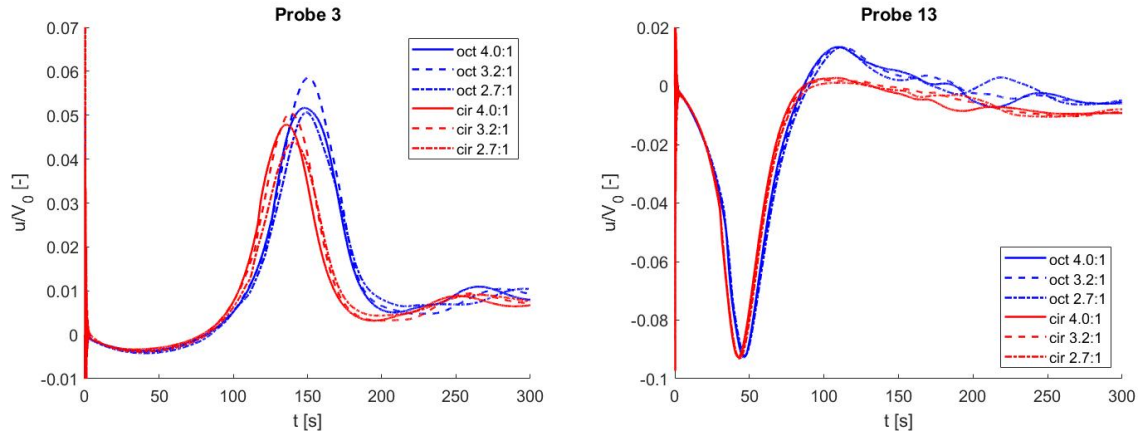

(a) Probe 3 **(b)** Probe 13

Figure 4.2.4: Time series of radial velocities at probes 1.5 m from the tank walls

The radial flow patterns in octagonal tanks with various diameter-to-depth ratios are shown in figure 4.2.5. The presented x-z-planes were measured across the tank center, at y = 4.2 m, and display streamline contours coloured by the velocity u-component, i.e. radial velocity in the x-direction. The tangential inflow in the closed circular shaped tanks

creates a circular motion in the radial plane, known as secondary flow. The streamlines represent the expected movement pattern of which the fluid and and particles are transported in the radial direction. Red colour indicates flow in positive x-direction, blue in negative x-direction, and the color mode indicates the strength. The circular motion of nearly concentric streamlines show the occurrence of turbulence, which promote mixing and affect the flushing rates of solid particles. A strong continuous vortex is preferred over multiple smaller vortices of low strength as it improves mixing and provides better action on particle transport. However, vortex strength beyond a critical value can increase the stress levels of the fish (Gorle et al. 2019).

In all cases displayed in figure 4.2.5, the occurrence of vortices are observed in the near wall region at both sides of the tanks, which imply sufficient mixing in these regions. In the central region however, $x \in [2.0, 6.0]$ m, straight streamlines indicate laminar flow with low degree of mixing. At the right hand side of the tank, closest to the inlet, vortex shedding is observed to a greater extent through the formation of two separate vortices. Vortex shedding near the inlet occurs regardless of tank water depth. Further downstream, at the left hand side, the formation of a single more distinctive vortex can be seen. A darker color mode around the single vortex indicate higher strength and radial velocities compared to the shedded vortices further upstream. The formation of a second vortex downstream near the free surface is however implied, which is more clearly seen for lower D:d-ratios.

The distribution of radial velocities V_r varies more significantly along the height of the water column than that of the tangential velocities, V_{Theata}. Darker colouring in the periphery lower region of the water column show that the secondary flow is more substantial near the bottom, and that the vortices near the wall are the driving forces for radial flow. The streamlines and coloring of the slice indicate that the fluid and particles are transported to a location around x = 6.5 m, and that the most amount of mixing between the inward radial flows occur at $z \in [1.5, 2.0]$ m regardless of tank water depth. Skewed radial flow towards the side at which the inlet is directed can thus be seen. Ideally, the red and blue colored streamlines should meet at the center of the tank, i.e. at x = 4.2 m, to direct feed and faeces toward the central drain. Due to the absence of a center drain in the present study however, the flow in the central region of the tank is erroneous, as the presence of an outlet in the region is expected to significantly affect the hydrodynamics through the bathtub effect (Oca & Masalo 2013).

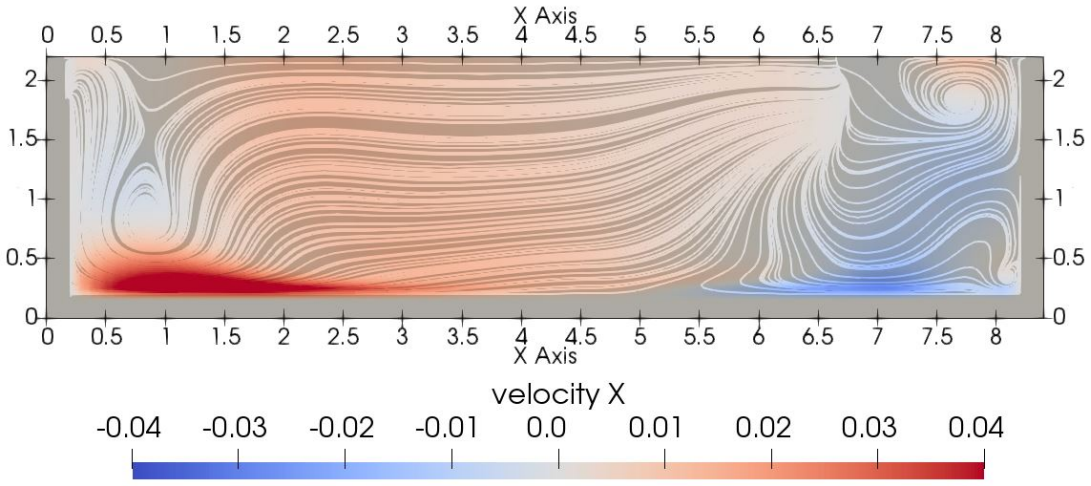

(a) D:d = 4.0:1

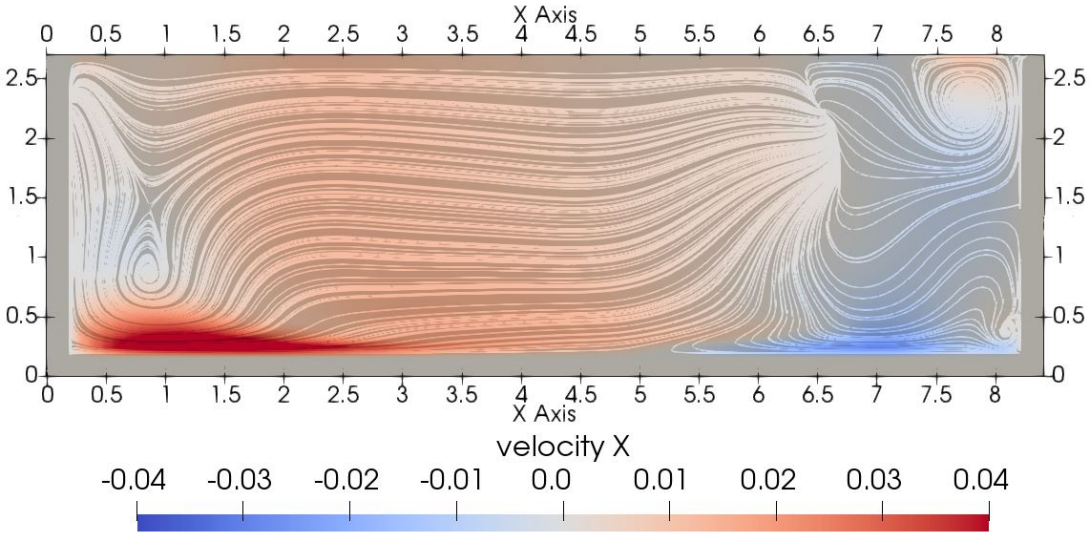

(b) D:d = 3.2:1

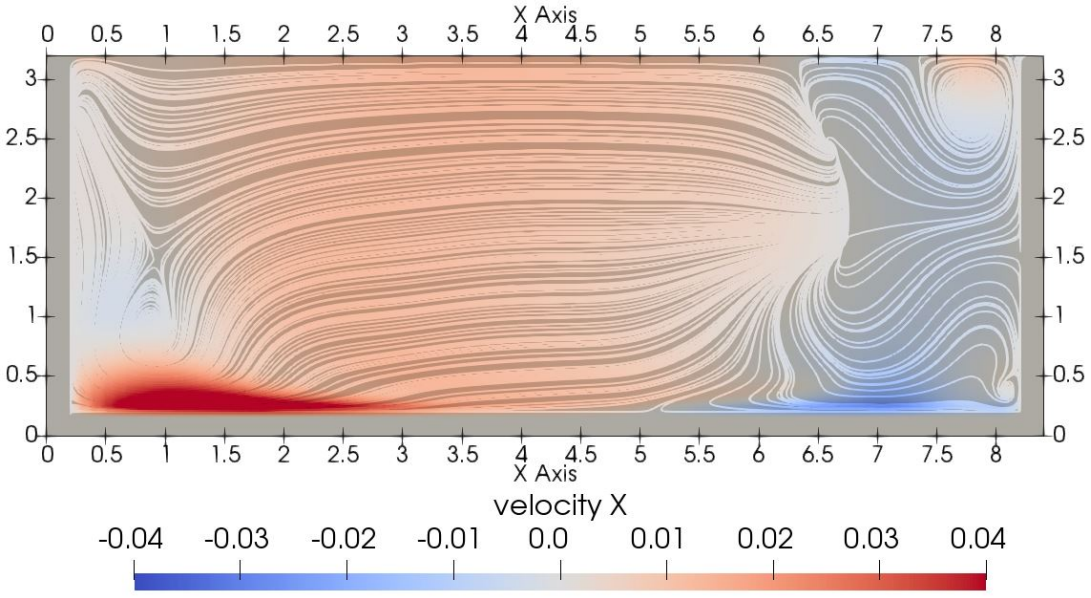

(c) D:d = 2.7:1

Figure 4.2.5: Radial flow pattern across octagonal tanks

Figure 4.2.6 show the radial flow pattern at the same location as described above, however for circular tanks. The streamlines appear similar to those present in the octagonal tanks, as turbulent flow due to the occurrence of vortices is seen in the outer regions near the walls, and less intensive laminar flow is present in the central region. Some distinct differences from the octagonal case can be observed however.

First, considering the right hand side furthest upstream of the flow, the occurrence of two separate vortices is not as obvious as displayed in the octagonal tanks. Instead, a single smaller vortex that is stretched throughout the water columm may be implied. Also, a darker blue color indicate that this vortex is more intense and result in larger radial velocities towards the tank center compared to the octagonal tanks. A more advantageous secondary flow pattern is also implied by the streamline pattern, which indicate the mixing between the inward radial flows happen around x = 5.5 m, one meter closer to the center compared to that in the octagonal tanks.

Second, considering the downstream side of the tanks at low x-locations, a larger vortex occupying the whole water column is seen in the tank with the smallest water depth. This indicates better mixing vertically throughout the water column. As the D:d-ratio is reduced however, the vortex i prone to increased shedding resulting in two separate vortices of lower intensity in the deepest tank. Thus, tanks with higher D:d-ratios are expected to achieve better mixing properties. The vortex intensity is however lower in the left side region compared to tanks with octagonal geometries, as the radial velocities in positive x-direction are lower.

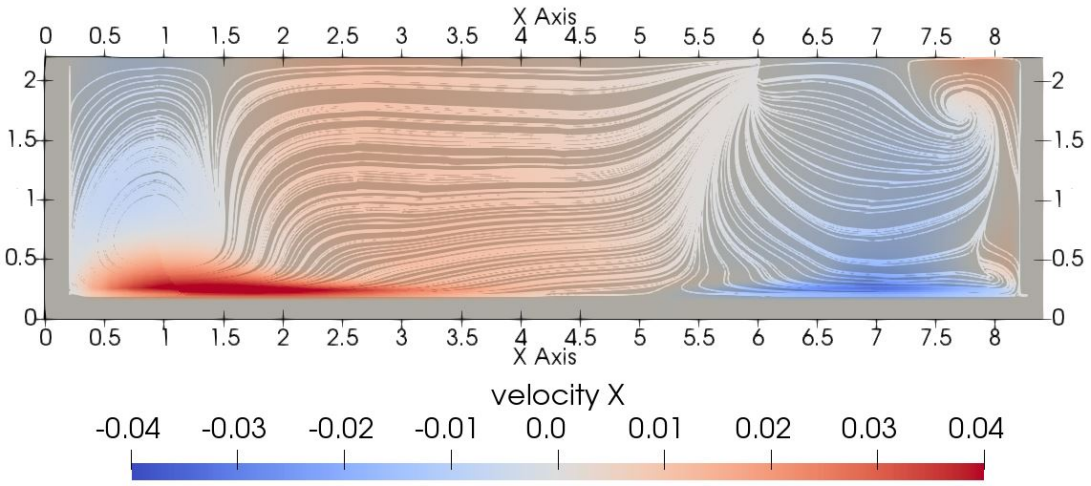

(a) D:d = 4.0:1

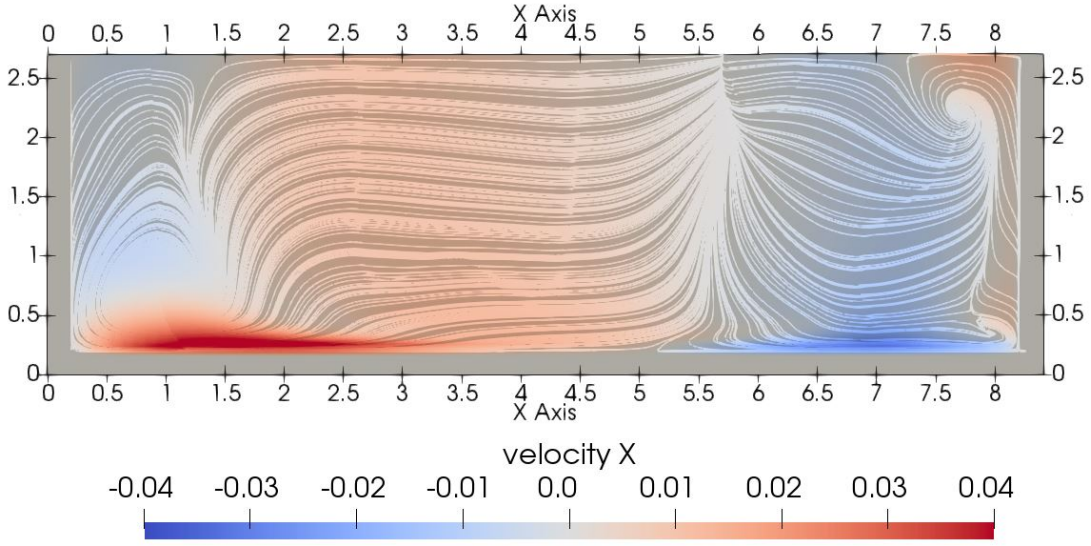

(b) D:d = 3.2:1

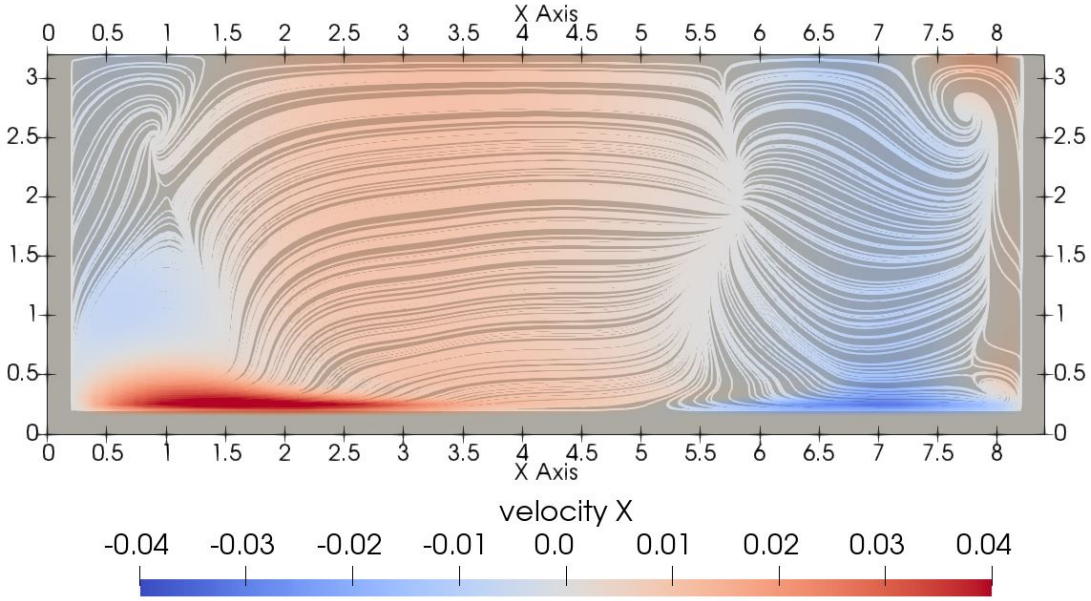

(c) D:d = 2.7:1

Figure 4.2.6: Radial flow pattern across circular tanks

The normalized velocity distribution of the radial velocities is shown in figure 4.2.7. The u-component of the velocities recorded across the central diameter close to the bottom is displayed in the figure, where negative values indicate flow in the negative x-direction. Blue and red lines represent octagonal and circular tanks respectively, where the line type indicate various D:d-ratios. An asymmetric velocity distribution towards the right hand side, at which the inflow is directed, is observed. The skewness towards the right hand side is most prevalent in the octagonal tanks. The point where the radial velocities are zero indicates the location of where the flow is directed and particles transported, which happen approximately at x = 5 and 6 m for circular and octagonal tanks respectively. Hence, a circular geometry impose particle transport further towards a potential central drain. The radial flow strength is however better in octagonal tanks, as higher velocities are measured. Furthermore, slightly higher maximum velocities in the wall region are seen for lower D:d-ratios. Compared to the tangential velocities measured in figure 4.2.3, the scale indicate that $V_\Theta \approx 10V_r$, which correspond with the findings in Grotle et al. (2018).

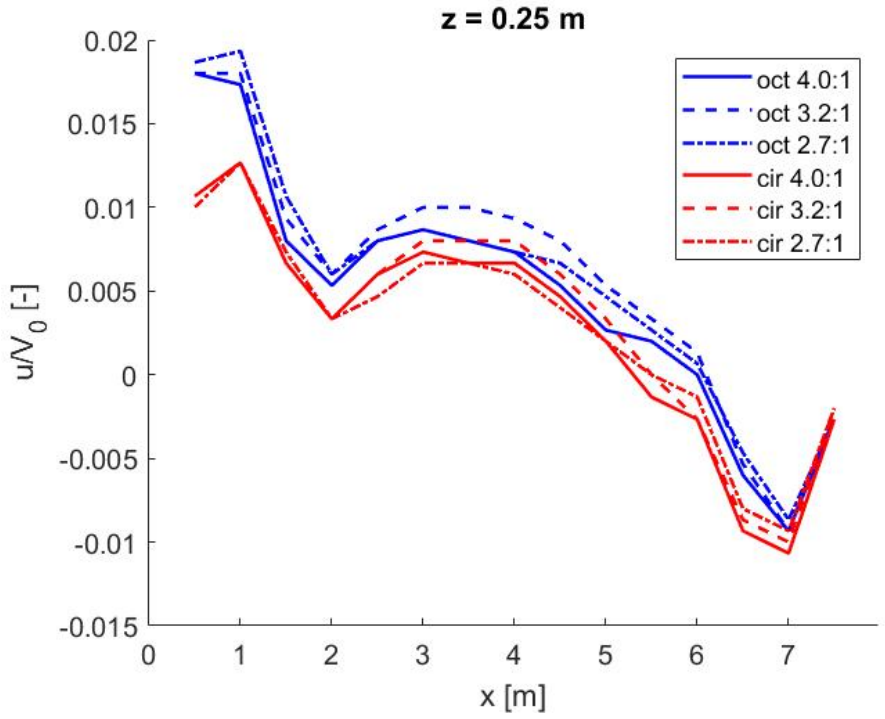

Figure 4.2.7: Radial velocities at z = 0.25 m

4.2.2 Effect of inflow conditions

The parameter study of inlet conditions was performed using octagonal tanks with a diameter-to-depth ratio of 3.2:1. Three different inlet configurations were tested: a single inlet placed symmetric about the y-axis, double inlets symmetric about both the x- and

y-axis, and a single outlet placed close to a chamfered corner, as shown in figure 3.3.6 to 3.3.8. The same total inflow as the cases with single inlet was assumed in the double inlet configuration, hence the the prescribed velocities at each inlet were halved to 0.75 m/s in the case with two inlets. Furthermore, each inlet configuration was tested with three varying nozzle angles: one parallel to the tank wall, one slightly rotated towards the wall and one slightly rotated towards the tank center. ϕ indicates the angle of attack of the inflow relative to the x-axis.

The figures 4.2.8 and 4.2.9 show time series measured 1.5 m from the tank wall of tangential and radial velocity profiles respectively. The velocities are normalized by the inflow velocity, which was 1.5 m/s for the single inlets and 0.75 m/s for the double inlets. The different colors indicate different inlet configurations, where blue show the single center inlet, red show double inlets and pink show the corner inlet, as illustrated by figure 3.3.6 - 3.3.8. Various line types indicate the inflow angles as annotated by the legend. The figures show a gradual increase in velocities up to steady state in most cases. Larger variations are however seen for some cases with inlets directed inward at $\phi = 320.2°$. Overall, 300 s seemed to be adequate for steady state to be reached.

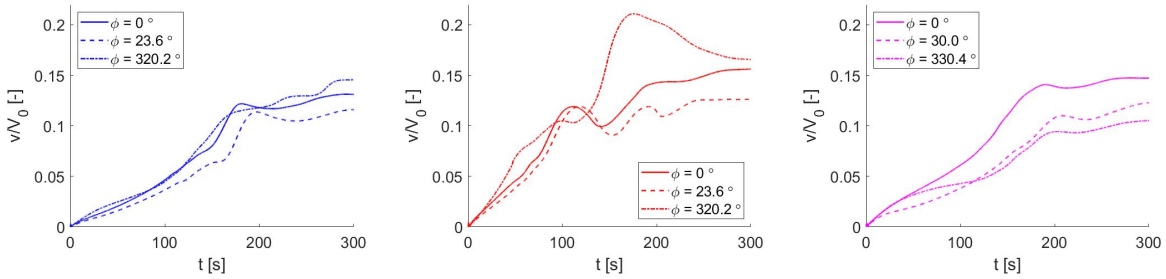

(a) Single symmetric inlet **(b)** Double inlets **(c)** Single corner inlet

Figure 4.2.8: Time series of tangential velocities at probe 3

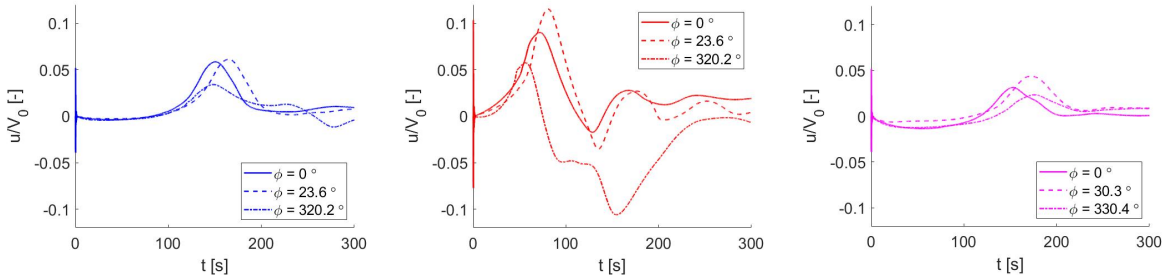

(a) Single symmetric inlet **(b)** Double inlets **(c)** Single corner inlet

Figure 4.2.9: Time series of radial velocities at probe 3

Primary flow

The base case in figure 4.2.10a show the streamline pattern of the primary flow from a single inlet placed symmetric about the y-axis with attack angle parallel to the x-axis. The flow pattern is similar to that presented above in figure 4.2.1, and show the occurrence of turbulent flow near the inlet due to high velocity difference between the injected inflow and the rotating flow already present in the tank. Accelerating flow can be seen parallel to the straight walls, while quiescent zones subject to low velocities are observed in the chamfered corners as well as the central region of the tank.

The curled streamlines near the inlet disappears with the inflow rotated slightly towards the tank wall (figure 4.2.10b), indicating less turbulent flow. Higher velocities in the corner and walls adjacent to the inlet are observed, which implies that the wall shear stresses are increased in the region due to the no slip condition. A favorable consequence of increased wall shear stress is that it provide worse conditions for algae growth on the walls, thus reducing the probability of severe biofouling in the region. Increased wall shear stresses do however also imply that more energy is wasted through fluid-solid interaction, which can be seen in the form of lower velocities further downstream in the tank.

Considering figure 4.2.10c, the formation of a large separate vortex can be seen in the region between the inlet and adjacent corner when the flow is directed more towards the tank center. This might be problematic regarding fish behaviour, as too strong vortices could cause stress or in worst case trap the fish. The streamline pattern also indicate increased turbulent flow, which enhances mixing within the tank. Higher velocities are observed in the central region of the tank, as well as more uniform conditions further downstream. Velocities in the near wall region close to the inlet are low, which makes the growth of biofouling more likely. Increased turbidity in the wall region should however counteract algae growth to some degree.

Figure 4.2.11 display the primary flow pattern in the tanks with a double inlet configuration. The overall velocity distribution is lower compared to the cases with a single inlet since the velocity prescribed at the boundary was halved at each inlet. The double inlet configuration with flow injected in both directions creates a symmetric flow pattern about the x-axis, resulting in a more uniform distribution of the velocity field in the tank. The trends are however similar to those observed in the case with a single inlet. An inlet angle of $\phi = 23.6^{\circ}$ provide higher velocities in the near wall region which is favourable in impeding algae growth and sedimentation. The downside is however reduced velocities towards the tank centre due to increased wall friction loss.

The inflow directed at $\phi = 320.2°$ naturally increase the velocities in the center of the tank. Furthermore, the streamline pattern appears more wide spread from the velocity source, which is a sign of improved mixing of the injected water. Higher velocities across a larger tank diameter can also be seen in figure 4.2.11c, which enhances the growth conditions for the biomass (Nilsen et al. 2019). A drawback with the design is still low velocities in the periphery regions, which is unfortunate regarding algae growth on the walls. Compared to the case displayed in figure 4.2.10c however, the appearing vortex between the inlet and adjacent corner is not as prevalent, thus lowering the probability of fish being trapped outside the primary flow.

The absence of curled streamlines near the inlet in figure 4.2.12 indicate less turbulent flow from the inlet when it is placed near the corner compared to the mid-wall placement. Less energy is then 'wasted' in through turbulent dissipation, resulting in higher velocities in the tangential direction. This is observed by the red coloring being more widespread across the tank diameter. Except for in the center region of the tank, high velocities are observed in all regions in figure 4.2.12a. As mentioned above, an outward rotation of the inflow angle results in higher wall velocities, but generally reduced velocities further downstream. Due to momentum conservation, a large vortex is formed in the upper right corner when the inflow is directed inwards as shown in figure 4.2.12c. The significance of this vortex could cause alterations to the fish shoaling pattern, increase stress by trapping and hence reduce the growth rates through sub-optimal conditions.

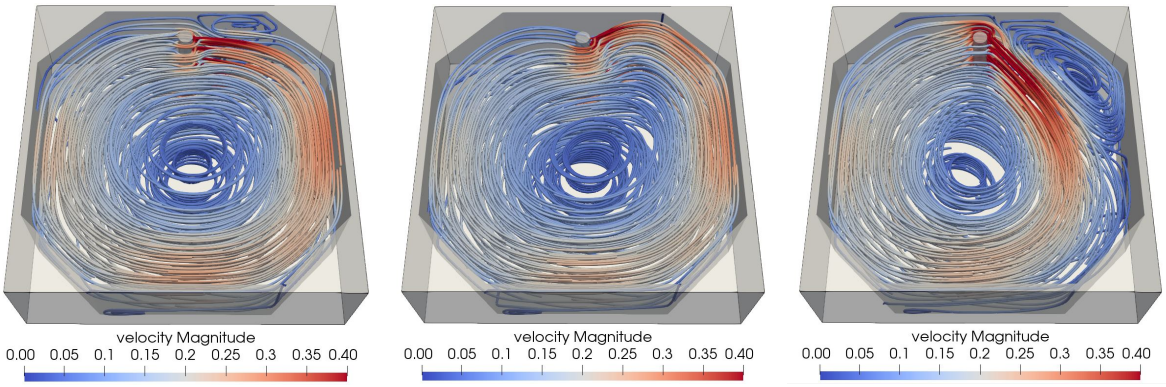

(a) $\phi = 0°$ **(b)** $\phi = 23.6°$ **(c)** $\phi = 320.2°$

Figure 4.2.10: Single inlet symmetric about the y-axis

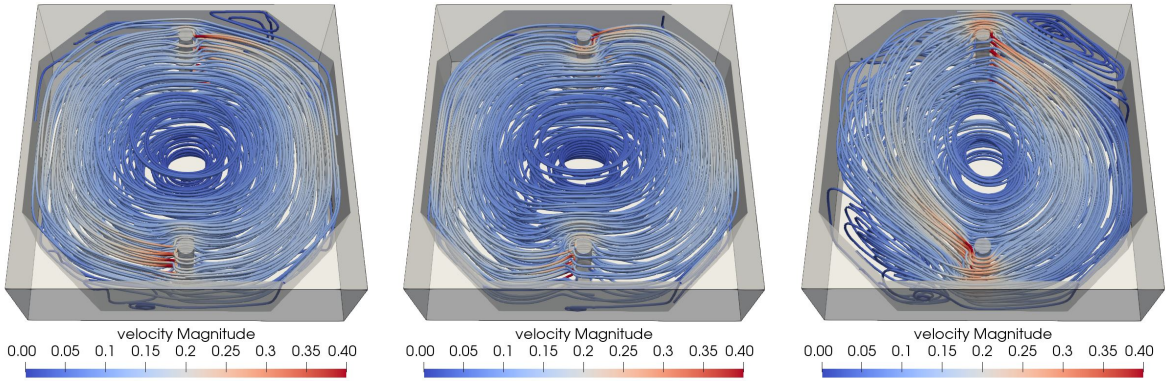

(a) $\phi = 0°$ **(b)** $\phi = 23.6°$ **(c)** $\phi = 320.2°$

Figure 4.2.11: Double inlets

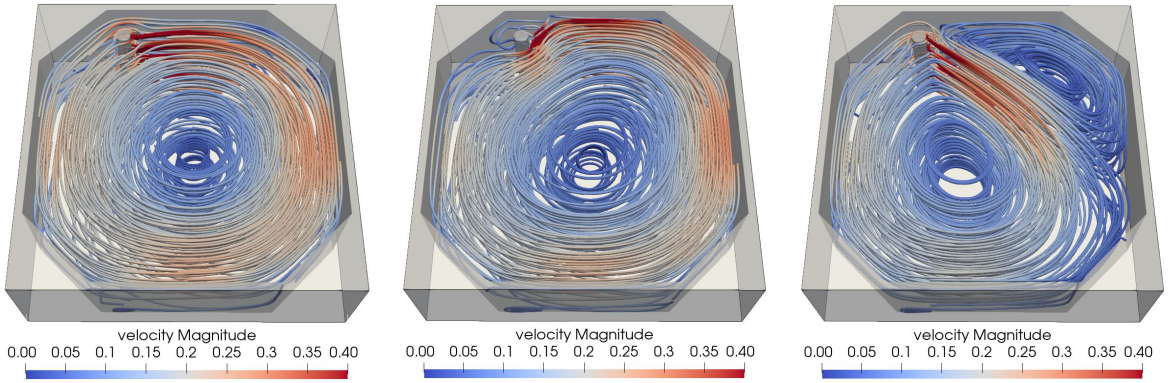

(a) $\phi = 0°$ **(b)** $\phi = 30.3°$ **(c)** $\phi = 330.4°$

Figure 4.2.12: Single corner inlet

Figure 4.2.13 and figure 4.2.14 show the normalized profiles of tangential velocity magnitude across the diameter of the tank, measured 0.25 m and 1.5 m from the tank bottom respectively. Different colors indicate the inlet configuration, while various line types represent the direction of the flow as annotated by the legends. The maximum recorded velocity and its location are summarized for each case in table 4.2.1. Generally for all inlet configurations, the highest velocities are obtained when the the inlet is directed parallel to the side wall, occurring in the near-wall region at the side at which the inflow is pointing. Exceptions can however be seen for the single inlet configurations; a symmetric placement with inward angle off attack achieve as high velocities however 2 m towards the tank center, while the corner inlet achieve slightly higher velocities near the wall when the inflow is directed outwards towards the wall. Of the configurations investigated in the study, double inlets with the inflow directed parallel to the side wall achieve the highest relative velocity of approximately 25 % of the velocity prescribed at the inlet. This condition do however require identical inlet velocities at both inlets, which in practice is unlikely due to unequal flow rates through the pipes of up to 40 % (Gorle et al. 2019).

Table 4.2.1: Maximum velocities and where they occur for the different inlet configurations

Inlet configuration	Inflow direction	$\frac{v_{max}}{V_0}$ [-]	x [m]
Single, y-symmetric	Outward, ϕ23.6°	0.18	7.5
Single, y-symmetric	Parallel, ϕ0°	0.195	7.5
Single, y-symmetric	Inward, ϕ320.2°	0.193	6.0
Double	Outward, ϕ23.6°	0.24	0.5, 7.5
Double	Parallel, ϕ0°	0.247	0.5, 7.5
Double	Inward, ϕ320.2°	0.20	2.0, 6.5
Single, corner	Outward, ϕ30.3°	0.185	7.5
Single, corner	Parallel, ϕ0°	0.182	7.5
Single, corner	Inward, ϕ330.4°	0.137	5.5

The optimal inflow angle depend on the placement of the inlet. Considering figure 4.2.13 and 4.2.14, a rotation inward towards the centre is favourable when a single inlet is placed symmetric about the y-axis, due to higher velocities towards the tank center as well as further downstream at low x-values. An inward angle of attack is also favourable in a double inlet configuration as it obtain significantly higher velocities towards the center. In contrast, an inflow parallel to the wall is favourable when the inlet is placed near a corner, as higher velocities across the whole left-hand radius in addition to increased velocities closer to the inlet are achieved.

A skeewness in the velocity profile can be observed in tanks with a single inlet. Naturally, higher velocities occur across the half-radius side at which the inflow is directed. The flow undergoes gradual diffusion as well as get influenced by friction which results in lower velocities further downstream. Since the double inlet configuration has flow injected in both directions, the skeewness is removed and the velocity profile become symmetric about the tank centre, indicating more uniform flow conditions. The largest variance between the maximum velocities recorded at each side of the tank centre varied with inflow angle, where increased inward directed flow resulted in lower skeewness between velocity peaks. Furthermore, the single corner inlet achieve higher velocities closer to the tank center compared to the y-symmetric single inlet. E.g. for an inflow angle $\phi = 0°$, the velocities at x = 2 were 0.14 V_0 and 0.17 V_0 respectively for the y-symmetric and corner inlet. This implies that placing the single inlet closer to a corner, as well as directing the flow slightly inwards lead to more uniform flow conditions.

The velocity profiles vertical variation increases as the inflow is directed inward towards the centre. E.g. considering the case with double inlets, the discrepancy between the

recorded maximum velocities displayed by figure 4.2.13b and 4.2.14b are 1.1%, 4.3% and 12.7% respectively for inflow angles of $\phi 23.6°, \phi 0°$ and $\phi 320.2°$. This indicate that wall friction is the dominant restriction of the velocities when the inflow is pointed parallel or outwards, whereas bottom friction is more prominent for flow directed inwards towards the centre.

An outward rotation of the inlet flow towards the wall implies reduced velocities across the whole diameter of the tank, regardless of inlet configuration. E.g. the reduction at x = 1.5 m is 11.7%, 18.8% and 16.7% respectively for the single y-symmetric-, double- and single corner inlet configuration. A general trend is that the relative velocity decrease is larger closer to the bottom and in the near wall region, indicating larger friction losses due to higher shear stress at the boundaries. Increased shear stresses are however favourable for cleaning of walls, making a heavy accumulation of biofouling less likely in the respective regions. In the opposite case, inward an inflow direction with single inlets result in low velocities in the near wall region at the side furthest upstream, which indicate occurrence of quiescent zones. Thus, a trade-off has to be made between optimizing velocities towards the tank centre to improve uniformity and biomass growth conditions, or use more energy to increase shear stresses at the wall area to reduce the occurrence of biofouling.

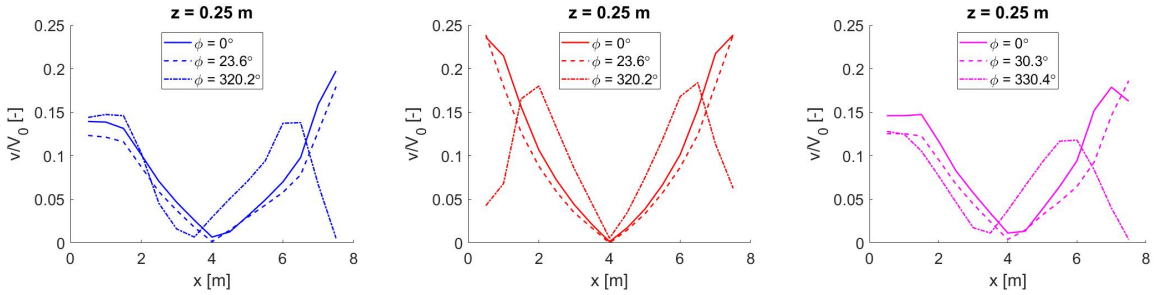

(a) Single symmetric inlet **(b)** Double inlets **(c)** Single corner inlet

Figure 4.2.13: Tangential velocity profile across the tank center, water height 0.25 m

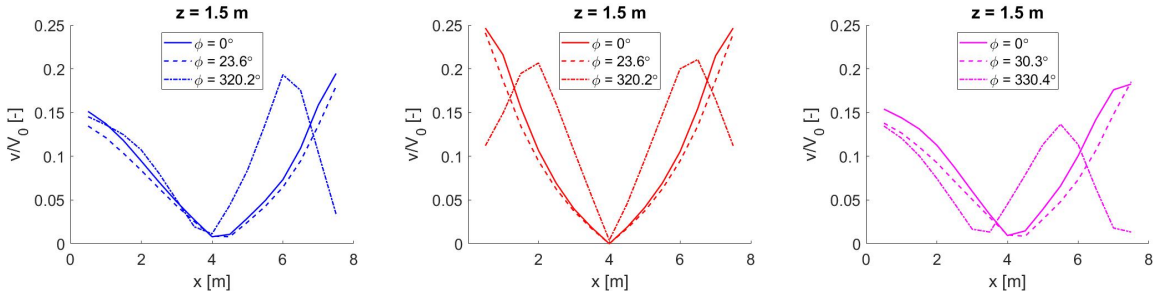

(a) Single symmetric inlet **(b)** Double inlets **(c)** Single corner inlet

Figure 4.2.14: Tangential velocity profile across the tank center, water height 0.25 m

Secondary flow

Figure 4.2.15 shows the radial flow pattern in tanks with various inlet configurations and an inflow angle $\phi = 0°$. The streamlines representing the fluid and particle transport pattern are contoured across the x-z-plane at the tank center, i.e. at y = 4.2 m. The planes are colored by the u-velocity, which indicates the strength and direction of the radial flow. Vortices and concentric streamlines show regions with high turbulence, which influence mixing of the fluid and the flushing rates of solid particles.

Prevalent vortex structures in the whole water column indicate large degree of mixing in the double inlet and single corner inlet designs. Double inlets show large vortices occupying the whole radius at both sides of the tank with strong inwards bottom currents, which promotes the self-cleaning abilities of the tank as well as sufficient mixing of the new oxygen-rich inflow water. A large degree of mixing is also observed in the design with a corner inlet, especially at the side furthest downstream the inlet. The streamline patter near the bottom indicate some transport towards the centre lower in the water column, which is favourable in tanks with central drains. Small vortices indicates that some mixing occur in periphery regions in a single y-symmetric inflow design, however low mixing is expected to occur in the central region.

In all designs, the radial velocities increase in magnitude further towards the bottom. This is an important feature for imposing self-cleaning properties of the tank, avoiding particle settling and sedimentation at the bottom by directing large particles towards the outlet. The largest velocities seems to occur in the single y-symmetric design, however primarily in the positive x-direction which results in a skewed flow pattern where the flow is transported to $x \in [5.5, 6.5]$ m. Ideally the inward flows should meet at the center of the tanks, as drains placed in the centre are the most common outlet configuration in aquaculture tanks (An et al. 2018). The streamline pattern of single corner inlet indicate that the majority of the flow is leaning towards x = 2 m, although flow close to the bottom is transported to the center.

The radial flow pattern for when the inflow is directed towards the side wall is shown in figure 4.2.16. Less degree of mixing seems to be the overall trend when considering the streamline patterns in the tanks. Furthermore, slightly lower radial velocities near the bottom as well as higher velocities higher in the water column are observed, meaning less flow momentum and more uniform conditions across the water depth. The flow pattern occurring from a single inlet placed at the mid-wall span looks similar to that displayed in figure 4.2.15a. Velocities in the positive x-direction have slightly increased, leading the

transport of the fluid to the tank side most upstream. The concentric streamlines at the right hand side of the tank are heavily reduced or disappeared, indicating lower mixing in the region when the tangential inflow is directed outwards. Mixing in the downstream region to the left remains unaffected.

By comparing figure 4.2.16a and 4.2.16b, the large inwards circular motion across both radii observed for wall-parallel inflow is replaced by less rotary flow in multiple directions. Generally, two main patterns can be seen: an inward flow from the wall to a distance of approximately 2.5 m in the bottom region, and a flow from the centre approximately 1.5 m outwards. This is less favourable compared to the steady self-cleaning currents towards the tank centre observed in figure 4.2.16a, as particles are expected to be transported away from the outflow and re-suspended up in the water column. The disappearance of vortices in the tank mid-region also indicate that less mixing occurs when the tangential inlet is rotated outwards.

This assumption is particularly evident when comparing the flow patterns of figure 4.2.17a and 4.2.17b, where significant rotary motion from prominent vortices can be seen in the former, while some small vortex structures are observed in periphery regions in the latter. However, the meeting of streamlines traversing inward at x = 4.2 m indicate advection to the tank centre, which is a better particle removal mechanism compared to the skewed flow pattern observed for the inlet oriented parallel to the wall.

The slices in figure 4.2.17 display the radial flow pattern when the tangential inlet is directed inward towards the centre. The color modes show a large increase in velocities compared to the other inflow configurations. The tanks with a single inlet suffer from strong currents towards the wall at which the inflow is directed, and practically no flow in the negative x-direction. This is unfortunate not only for the particle transport, but it may also affect the fish behaviour and cause stress if the current gets too intense. The single corner inlet provide the worst case of the configurations, where the largest velocities and low degree of mixing occur. The single y-symmetric inlet show improved conditions with a slightly more gentle current in the x-direction and mixing furthest downstream in the tank.

Double inlets show an interesting flow pattern that is significantly improved compared to the cases with single inlets. The strongest current is seen outwards at increased water depths. The velocity magnitude around the periphery vortices indicate that sufficient mixing is obtained in regions close to the wall. The velocity distribution near the tank

bottom show that the self-cleaning properties are to some degree intact by radial flow towards the centre. The velocities are however relatively lower than the outward flow seen at higher depths.

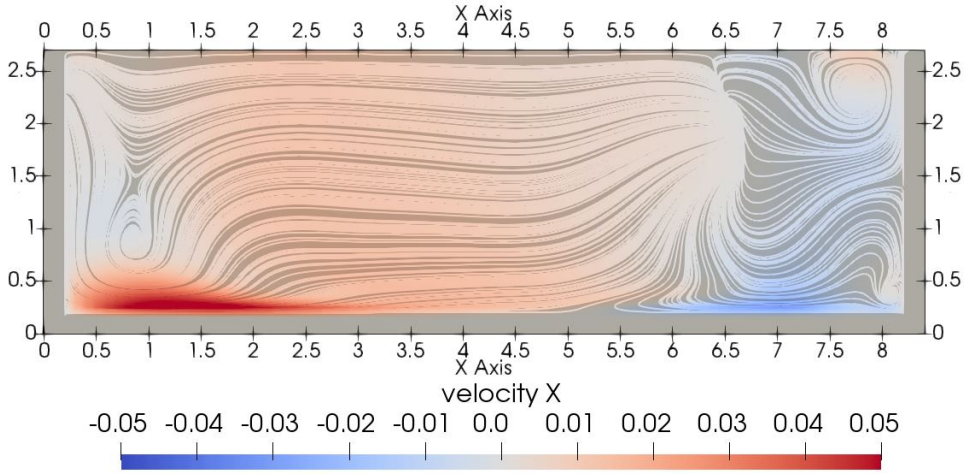

(a) Single y-symmetric inlet

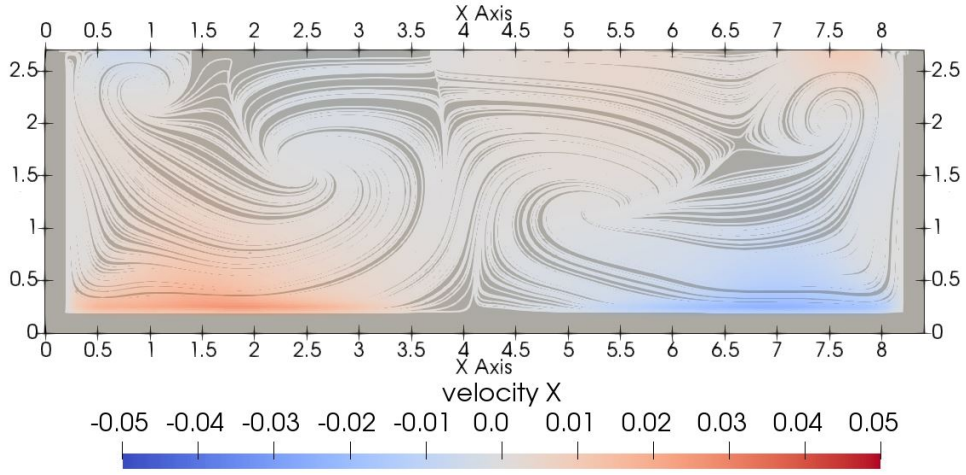

(b) Double inlets

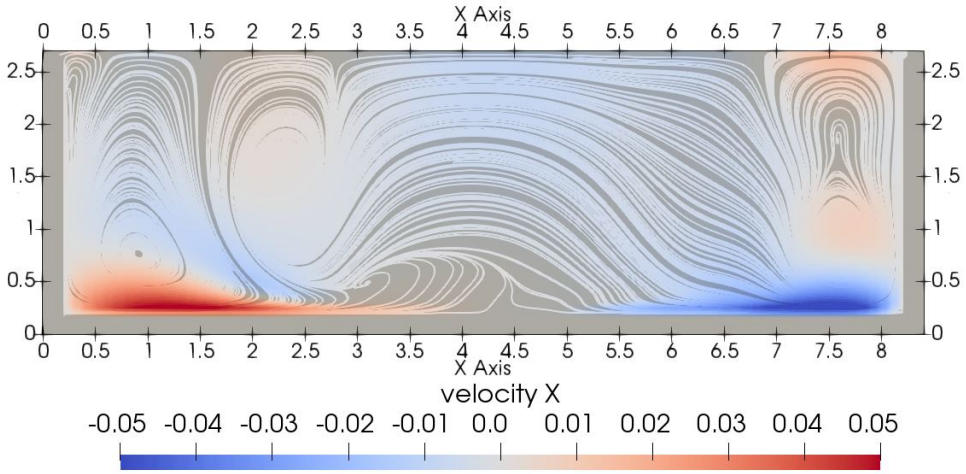

(c) Single corner inlet

Figure 4.2.15: Inflow parallel to the wall, $\phi = 0°$

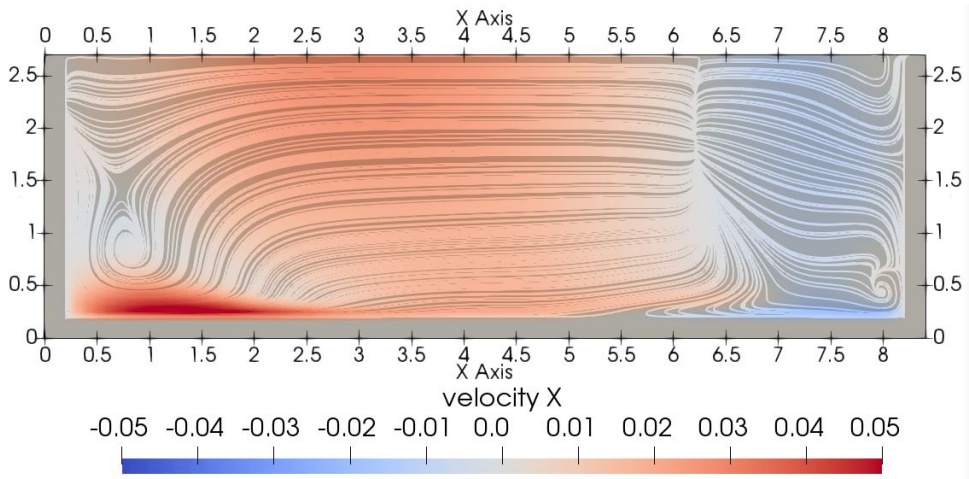

(a) Single y-symmetric inlet

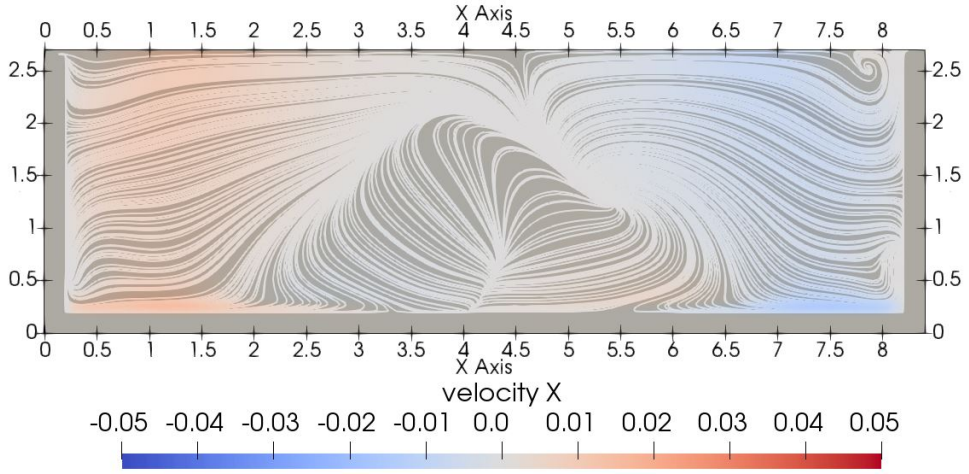

(b) Double inlets

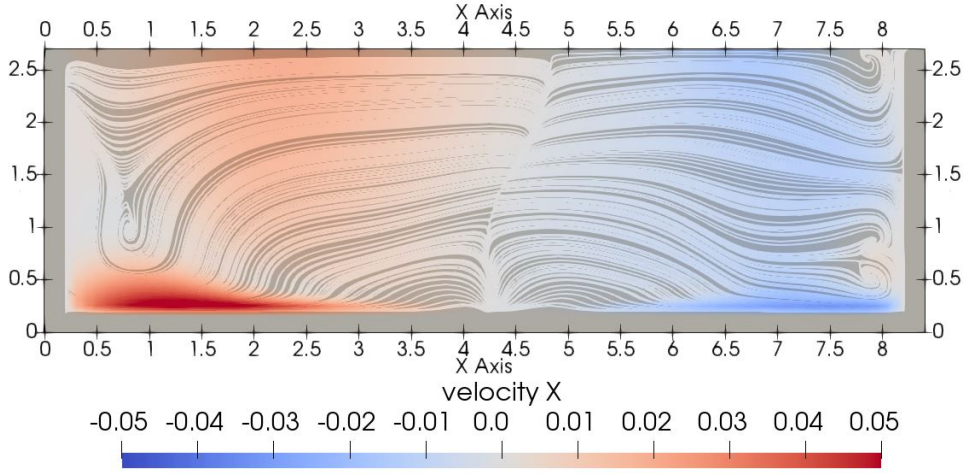

(c) Single corner inlet

Figure 4.2.16: Inflow outward towards the wall, $\phi = 23.6°$ and $\phi = 30.3°$

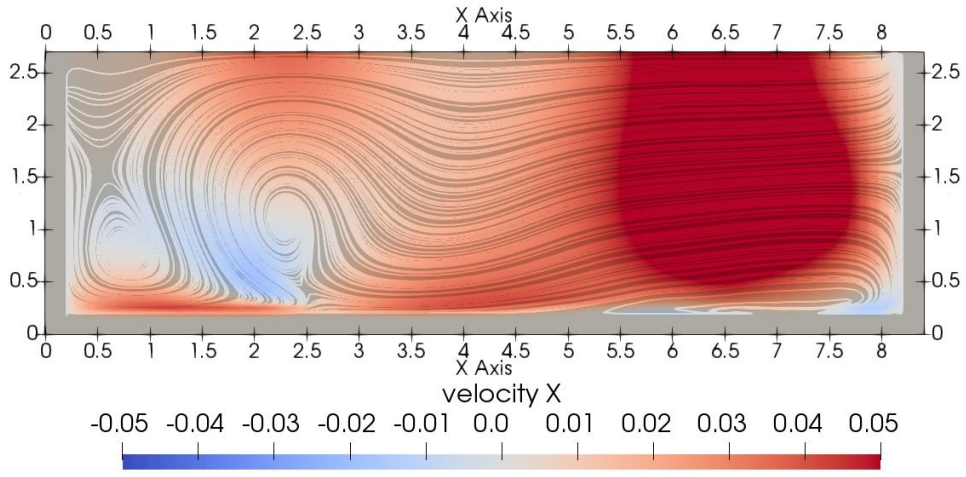

(a) Single y-symmetric inlet

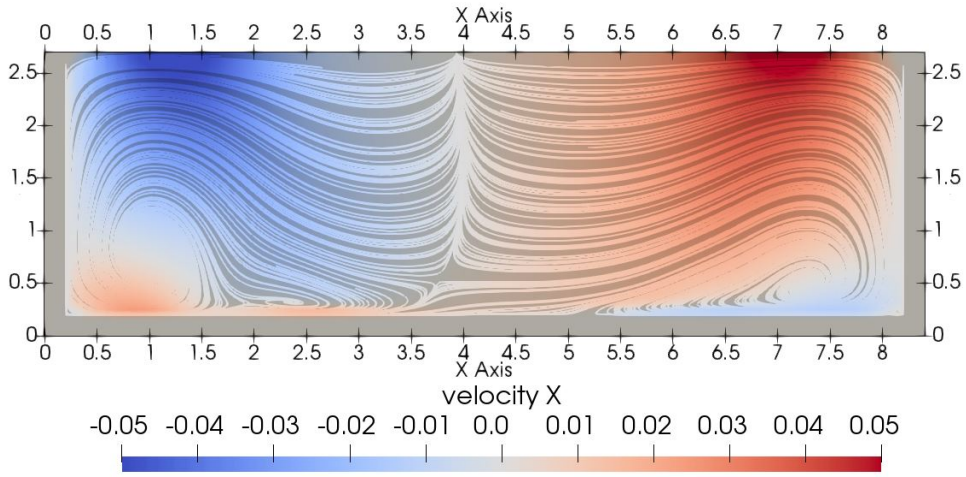

(b) Double inlets

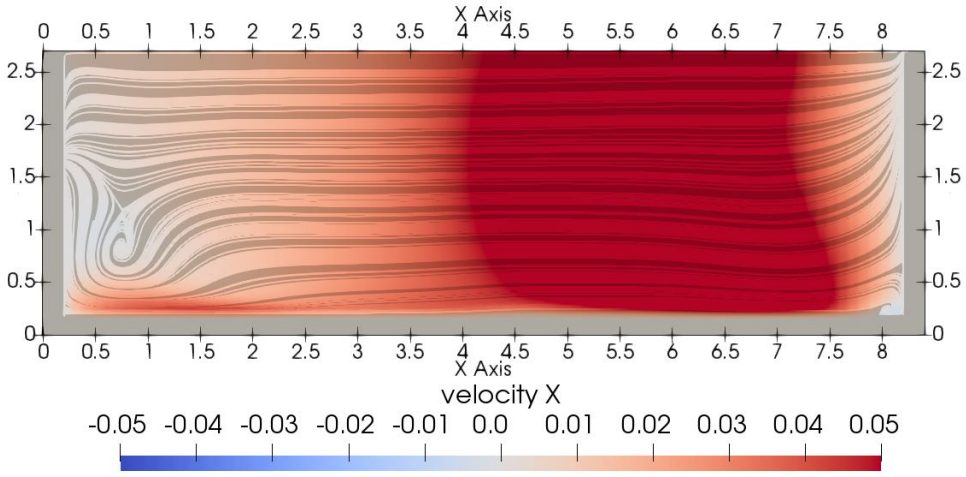

(c) Single corner inlet

Figure 4.2.17: Inflow inward towards the center, $\phi = 320.2°$ and $\phi = 330.4°$

Figure 4.2.18 show the normalized radial velocity distribution across the tank diameter. The velocities were measured at y = 4.2 m and z = 0.25 m, as shown in figure 3.3.9. The u-component of the velocities recorded across the central diameter close to the bottom is displayed in the figure, where negative values indicate flow in the negative x-direction.

Thus, an optimal solution has flow transported to the tank centre, i.e. have velocities reaching zero at x = 4.2 m. The results show that the highest velocities occurs when the tangential inflow is directed inwards, however the flow is transported in the wrong direction regarding optimal transport of particles. Having the inlet directed parallel to the side wall generally provide the most stable secondary flow of high velocities near the tank wall. Applying double inlets improves the secondary flow by providing strong inward bottom currents from both sides of the tank, which is favourable for particle removal in tanks with central outlets. In the cases of single inlets, placement near the corner is more favourable due to increased flushing in the negative x-direction at high x-locations. Compared to the tangential velocities measured in figure 4.2.13, the scale indicate that $V_\Theta \approx 10V_r$, which correspond with the findings in Grotle et al. (2018).

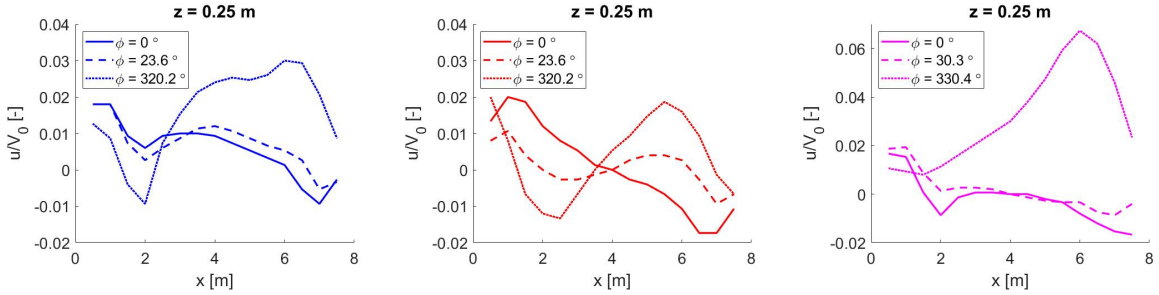

(a) Single y-symmetric inlet **(b)** Double inlets **(c)** Single corner inlet

Figure 4.2.18: Velocity profile across the diameter of the tank

4.3 Hydrodynamics in RAS culture tanks

The following chapter provide the concluding answers to the research questions stipulated in chapter 1.2. The answers are based on the findings of the literature review as well as the results obtained from the validation and numerical investigation of various tank designs. First, the findings by the qualitative study are presented. Next, the quantitative results from the CFD-simulations are summarized. Finally, the qualitative and quantitative findings are assessed and discussed collectively to triangulate the results. Literature supporting the viewpoints provided in the present chapter is listed in appendix B.

4.3.1 Important hydrodynamic features

The purpose of rearing Atlantic salmon in land-based tanks is to provide an environment that efficiently produce a desired biomass of fish. By moving production on shore, the producer's possibilities to take control over the breeding environment increases by enabling manipulation of water quality parameters such as temperature, oxygen, algae growth and current flows. Increased control over the environment do however incur greater re-

sponsibility to safeguard fish welfare by ensuring optimal water quality within the tanks, e.g. supplying adequate amounts of oxygen for respiration, preventing accumulation of pathogens and disease outbreaks and minimizing stress factors that influence the fish.

The basic inputs into an aquaculture tank are feed and dissolved oxygen, which are fundamental for metabolism and respiration. Furthermore, the circulatory system in Atlantic salmon require constant motion and they tend to swim counter current in high velocity flows. The most important excess outputs from metabolic loading and respiration are CO_2, total ammonium nitrogen (TAN) and total suspended solids (TSS), which are the main waste products that must be removed from the environment in order to sustain good water quality. CO_2 and TAN are poisonous gases that are dangerous in high concentrations, which usually are removed by special filters and degassing techniques that are outside the scope of this study. Increased production of these gases can be seen in tanks with severe algae growth that occur due to biofouling of wetted surfaces, which is particularly prominent in quiescent regions where water velocities are low. Hence, the occurrence of quiescent zones should be avoided through optimal design of the tanks. Furthermore, the tank design alters the inherent hydrodynamic flow pattern, which in turn dictate the transport of suspended solids. The most important hydrodynamic features, i.e. properties that occur in the rearing environment which can be manipulated by convective water transport, in aquaculture tanks are:

Mixing: In addition to active removal of hazardous compounds by filtration and degassing, concentrations can be diluted through sufficient mixing of the inlet water and thus avoid zones of high concentrations. I.e. the solution to pollution is dilution, where water with low concentrations of dissolved oxygen gets exchanged with clean, oxygen-rich water. Mixing is improved by turbulent flow, and the occurrence of vortices and concentric streamlines are good indicators of mixing. Furthermore, the presence of fish is expected to increase turbulence and enhance mixing through re-suspension of the fluid.

Uniform conditions: Which is closely related to mixing in the way that increased mixing secure uniform conditions across the water column, by reducing gradients of compound concentrations. The biomass tends to regions where rearing conditions are optimal, thus ensuring uniform flow conditions is important in order to fully utilize the whole production volume. Furthermore, large velocity gradients could cause stressful fish behaviour and quiescent zones of low velocities should be avoided to reduce biofouling and presence of pathogens. Thus, a uniform primary flow that creates prevalent secondary currents is advantageous.

Solids removal: Feeding loads could reach several tonnes per day in large culture tanks, which are required to be transported out of the environment to maintain high water quality. Undigested feed and faeces large sources of nutrients that promote algae growth that depletes DO and increase $CO2$ concentrations, as well as increase the risk of arising pathogens. A large portion of suspended solids can also cause gill irritation which stress the fish. Thus, high velocity radial flows towards drains should be imposed to avoid sedimentation of waste solids and dead fish at the tank bottom, that give rise to pathogens and bacteria.

Fish exercise: Generally, muscle growth and thus total biomass growth rates increases with increasing current velocities. However, it does also entail larger power requirements from pumps, which means that the increased cost of acquiring higher velocities could become larger than the gained benefit of better growth rates. Tank design optimization could thus be beneficial to reduce friction losses and increase current velocities relative to the inflow. Furthermore, the overall rotational velocities are expected to decrease with fish present in the tank.

4.3.2 Influence by tank geometry and inlet conditions

A major drawback in quantitative study in the present work was the exclusion of outlet effects from the numerical model. Although several different outlet designs are in commercial use, almost all circular type tanks include a drain placed in the bottom centre. The suction force from the drain influence the flow pattern and velocities within the tank through what is called the 'bathtub effect', which has greater affection closer to the tank centre. The hydrodynamic pattern in the central region is therefore erroneous in the present work. The primary flow solely caused by the inlet impulse force obtain low velocities in the tank centre, which is shown by the numerical results regardless of geometry or inlet configuration. Realistically however, a centre drain is expected to increase velocities near the centre through the formation of a free vortex, in which the strength will vary depending on the mean hydraulic retention time (HRT) and volume of the tank.

Validation of the numerical model do however show good match between numerical and experimental results in the regions outside of the half radius, where most of the computational results were close to or within the standard deviation of the experimental data. The parameter study found that both geometry and inflow conditions had significant impact the velocity distribution and flow pattern. Changes to the hydrodynamics of the primary flow has a particularly large effect on growth conditions of the biomass through

uniformity and fish exercise features, while the secondary flow is especially important regarding mixing and particle removal features. The most important findings regarding the hydrodynamic influence of tank geometry and inlet conditions are summarized in table 4.3.1

Table 4.3.1: Hydrodynamic influence by tank geometry and inlet conditions

Feature	**Influence**
Fish exercise	Octagonal tanks provide higher tangential velocities in the near wall region.
Uniformity	Circular tanks higher tangential velocities towards the centre.
Uniformity	Quiescent zones of low velocities at the chamfered corners in octagonal tanks.
Uniformity, fish exercise	Gradual velocity decreases further downstream in circular tanks, accelerating flow along the straight walls in octagonal tanks.
Fish exercise	Diameter-to-depth ratio has little influence on the primary flow.
Mixing	More prominent vortices observed in the secondary flow for higher D:d-ratios.
Mixing	Circular tanks show more prominent vortices occurring in the secondary flow compared to octagonal tanks.
Solids removal	Circular tanks show a more symmetric radial flow patter, i.e. particles are transported further towards the centre.
Fish exercise	An outward inlet rotation towards the wall reduces velocities across the primary flow.
Fish exercise, uniformity	An inward rotation towards the tank centre increase velocities in the central region, but significantly reduce velocities near the wall.
Mixing	Larger vortices observed in the primary flow for inlets directed inwards.
Fish exercise, uniformity	Locating inlet pipes near the corners increases rotational velocities compared to inlet pipes along the side wall, especially in the centre region.
Uniformity	Double inlets show symmetric velocity distribution about the tank centre.
Mixing, solids removal	Directing the inflow parallel to the side wall is advantageous for secondary flow, showing more prominent vortices and higher radial velocities near the bottom.
Solids removal	The double inlet configuration provides the most favourable secondary flow pattern regardless of inflow direction.
Solids removal	An inward inlet rotation causes large velocities concurrent with the inflow, and no radial transport in the opposite direction.

4.3.3 Improved hydrodynamics by tank design optimization

The results in the qualitative study show that both geometric design and inflow configuration have large impact on the hydrodynamics in land-based aquaculture tanks. The flow patterns and velocities occurring in the tanks dictate the prevalence of mixing, uniform conditions, particle removal and fish exercise, which are important features that influence growth rates and fish welfare. As the industry trend towards utilizing larger tanks to increase production per investment cost, the complexity of the flow field within the tank environment increases. The challenge of concurrently optimize fish swimming speeds, obtain self-cleaning by rapidly flush settleable solids, as well as creating uniform conditions with minimal gradients of DO, CO_2 and NH_3, gets more severe as the size and complexity of the tanks increase. As the total concentration of biomass or stocking density increase per production unit, maintaining optimal hydrodynamic features that safeguard fish welfare is more important than ever.

Numerical investigation by use of CFD is regarded as a promising tool appropriate for optimization of aquaculture tank design, as it offers the possibility to study the flow filed in detail for relatively cheap investment costs compared to experimental setups. The primary flow can be studied to optimize design with regards to uniformity and growth rates, making sure that the fish is provided proper swimming conditions and that feed is distributed evenly. Also, regions with low velocities can be identified, which indicate where biofouling is expected to occur. Furthermore, the secondary flow can be studied to optimize velocities and flow patterns in the radial direction to enhance mixing and solids removal, thus making sure that input dissolved oxygen is evenly distributed, poisonous gases are diluted and self-cleaning is imposed to avoid sedimentation.

Parameters other than hydrodynamic optimization are often governing in tank design. E.g. if the cost of land area is high, initial incentives for maximizing volume per square meter increase. In this regard, square tanks with low D:d-ratio, often called 'mixed cell raceways' (MCR), are the most efficient as it increases both water height and wetted area, as well as offer the possibility of shared walls between units which make the design even more compact. In contrast, circular tanks with high diameter-to-depth ratio appear as a bad investment. From a hydrodynamic perspective however, the opposite is preferred. Quiescent zones with low velocities appear in the square corners, and lower D:d-ratio results in less prevalent vortices and radial velocities across the water column. Regions of low flow velocities provide fertile ground for algae growth and biofouling, whereas smaller vortices and reduced secondary flow reduce mixing of oxygen, dilution of poisonous gases and transport of particles towards drains. In combination, the factors contribute to poor

water quality and promotion of pathogens that cause disease. In extreme cases, the presence of sulphate reducing bacteria, low concentrations of dissolved oxygen and a substantial amount of sedimented organic matter give rise to production of the lethal gas H_2S, which cause mass mortality of the fish at very low concentrations. Risk assessments regarding the hydrodynamic performance of tanks is therefore necessary. Application of CFD can in this respect contribute to quantification of the hydrodynamic features, which in turn an associate a cost to poor hydrodynamic performance of the rearing tanks.

A major drawback of numerical models is however that they are simplified imitations of the real world, and the results would thus never be perfectly realistic. In the present study, significant simplifications were made to the inlets as well as outlet effects were neglected, making the flow field erroneous in large portions of the tanks. Conditions at the free surface boundary were also simplified, making it stress-free to reduce the computational demand. Furthermore, the hydrodynamic influence by fish biomass cannot be resolved in detail, although its presence has a large impact on the average velocity distribution. To make sure that the acquired numerical results are accurate and trustworthy, measurements from experiments are required for validation of the numerical model. The research institute 'Nofima', which provide developing research for the aquaculture industry, was contacted regarding gaining access to experimental data of velocities in land-based tanks, however without any luck.

Numerical modelling also faces another challenge by the trade-off between accuracy and computational efficiency. Timely completion of accurate simulations gets harder as tank sizes and thus the computational domain increase. The required wall time of the tanks investigated in the presents study was roughly three hours when applying 128 cores on the Notur supercomputer 'Fram', which achieved steady state conditions in a domain of approximately 1.5 M cells. Considering that the investigated tanks held a volume of 100 m^3, and that commercial tanks used in post-smolt production of Atlantic salmon usually operates with volumes $\in 1000m^3$, the challenge regarding computational demand is clearly highlighted. The Cartesian grid in the applied numerical model is regarded inefficient, as a halving in grid size cause and eight-fold increase in total cells. Stretching to locally refine the grid is neither optimal in aquaculture tanks, due to a relatively large number of inherent pipes and regions where turbulent flow occurs. The boundary 'wrapping' property of an unstructured grid would be advantageous in the present flow problem, especially in larger tank domains where the computational demand rapidly increases, yet sufficient refinement close to inlets and drains is critical to achieve a stable and accurate numerical solution.

Furthermore, validation of the numerical model indicated that free surface modelling improved the results by showing a slightly more realistic velocity distribution in the central tank region. However, the computational wall time was increased by roughly 22%. The simplified inflow suffered from significant numerical diffusion, and thus the boundary conditions at inlet(s) need to be described in greater detail, e.g. with a fixed volume and prescribed velocities or by a mass inflow condition. The latter consequently require mass outflow at the boundaries of drains, which further complicate the discretization process leading to increased computational demand. However, modelling of outflow effects is a must for achieving accurate solutions in the central tank area, and it is therefore regarded as the main area of improvement for the model applied in the present study.

5 Conclusion

The main function of aquaculture tanks is to provide a rearing environment that efficiently produce a desired biomass of fish. The basic inputs are feed and dissolved oxygen, which are fundamental for metabolism and respiration. These processes result in excess waste products that must be rapidly transported out of the environment to avoid problems related to fish welfare, mainly suspended solids, carbon dioxide and ammonium nitrogen. The distribution uniformity of the fundamental inputs as well as the efficiency of waste products removal and dilution constitute important measures of the quality of the rearing environment. The most important hydrodynamic features affecting the water quality were identified by the scoping literature review to be mixing, uniform conditions, solids removal and fish exercise. The prevalence and magnitude of these features are dependant of flow patterns and velocities of primary and secondary flow occurring in the rearing tanks, and the findings in the present study indicate that the hydrodynamics to a large extent may be manipulated by engineers and fish farmers through tank design and inflow direction adjustments.

Both tank geometry and inlet conditions significantly influence on tank hydrodynamics. Whereas geometric parameters mainly impacted velocities in the primary flow, major differences were observed in both primary and secondary flow patterns with respect to the inlet conditions investigated in the study. Octagonal tanks achieve higher maximum velocities in the near wall region, whereas circular tanks lower peaks but more uniform conditions overall towards the tank centre. Low velocities at the chamfered corners in octagonal tanks show that occurrence of dead zones and algae growth is expected, even close to the inlet. Circular tanks show more gradual reduction of velocities near the wall, making biofouling probable at the half side opposite to the direction of the inlet. Circular tanks show more advantageous secondary flow pattern, with better mixing properties throughout the water column and particle transport further towards the centre.

The study did not identify a best practice inlet configuration, but rather the different designs optimize different aspects of the hydrodynamics. Inflows directed inward towards the tank centre provide better mixing and generally higher velocity distribution. However, large gradients concurrent with the inflow direction were observed in the radial flow pattern, impeding particle transport towards the tank centre. Inflows directed outwards

provide lower velocities relative to the other configurations due to increased wall friction. However, high velocities near the tank wall indicate high shear stresses which are beneficial to prevent algae growth on walls. Inflows tangential to the tank wall or use of double inlets create more uniform conditions and more stable radial flows advantageous for particle removal. Locating the single inlet near a corner reduces drag forces and increases rotational velocities compared to an inlet pipe placed along the side.

Numerical investigation by use of CFD is regarded as a promising tool appropriate for optimization of aquaculture tank design. With accurate and computationally efficient models, the primary and secondary flows occurring due to tangential inflow in the enclosed tanks can be studied in detail at relatively cheap investment costs. This is particularly important as the industry is trending towards larger post-smolt facilities and tanks with increased biomass, making the hydrodynamics in the rearing environment more complex. Factors other than hydrodynamic concerns might be governing for tank design, e.g. land cost that incentivises rectangular tanks with low D:d-ratios, which could defile the inherent flow patterns and velocities. By quantifying the effects of improved hydrodynamics within the rearing environment, a more holistic assessment of the facility design may be provided, thus guiding design engineers and contractors into making better decisions in the early phase of projects.

Further work

The numerical model applied in the thesis was subject to several simplifications limiting the accuracy of the results. The main drawback of the quantitative study was the exclusion of outlets in the model. In particular, the bathtub effect created by a central drain is expected to have large influence on the velocities and flow patterns near the tank centre, resulting in large discrepancies between the numerical results and experimental measurements in the region. Also, the simplified inflow by a prescribed velocity line near the inlet boundary suffered from severe numerical diffusion, which affected the convergence rate and accuracy of the solutions. Consequently, several suggestions to further work that may be conducted using the existing numerical model, as well as further development of the numerical model are presented.

Work that may be conducted using the existing numerical model:

- **Tanks of larger volume:** the present study investigated tanks with an approximate volume of 100 m^3, however commercial tanks might be 10 – 20 times as large.
- **Other geometries and inflow conditions:** the present study investigated two

commonly applied geometries, circular and octagonal, with three different diameter-to-depth ratios. However, other geometries such as MCR are in commercial use. Furthermore, coarse changes to the inlet design were made, and more cases should be examined to find the major factors influencing the tank hydrodynamics.

- **Various tank materials:** materials such as concrete, HDPE and fiberglass are in commercial use. Different friction coefficients and boundary roughness can be modelled.

- **Sloping bottom:** a flat bottom was assumed in the present study. Commercial tanks do however often apply a sloping bottom.

- **Internal piping:** several structures can be present within the tanks, obstructing the flow and increasing turbulence.

Work that require further development of the numerical model:

- **Outflow modelling:** a central drain is present in all commercial tanks. Furthermore, dual drain designs with additional outflows through the tank wall also exist.

- **Improved inflow:** the prescribed velocity line applied in this thesis suffered from numerical diffusion. A fixed inflow volume with a prescribed velocity, or mass inflow boundary condition is suggested.

- **Biomass modelling:** the presence of fish significantly alters the flow within the tanks by reducing mean velocities and increasing turbulence. The sheer scale and fish behaviour make it impossible to model these effects in full detail. However, a porous media model may be incorporated to simply account for biomass influence.

- **Feed modelling:** the tank environment is subject to large amounts of feed pellets, which are transported around by convective flow. Streamlines were used to visualize the flow in the present study, which represent the advective movement of particles of low mass. Due to drag forces and gravitation however, large and heavy particles is transported slower horizontally and settle faster vertically. In order to investigate the tank self-cleaning properties in detail, particle tracking should be incorporated into the model.

Bibliography

Afzal, M. S. (2013), 3d numerical modeling of sediment transport under current and waves, Master's thesis, Marine Civil Engineering, NTNU, Trondheim.

Aggarwal, A. (2015), Numerical modelling of irregular waves and wave forces with reef3d, Master's thesis, Marine Civil Engineering, NTNU, Trondheim.

Akvakulturdriftsforskriften (2018), 'Forskrift om endring i forskrift om drift av akvakulturanlegg (for-2018-04-19-673)'.
URL: *https://lovdata.no/dokument/LTI/forskrift/2018-04-19-673* *(Cited: 29. Jan. 2020)*

An, C.-H., Sin, M.-G., Kim, M.-J., Jong, I.-B., Song, G.-J. & Choe, C. (2018), 'Effect of bottom drain positions on circular tank hydraulics: Cfd simulations', Aquacultural Engineering **83**, 138–150.

Badiola, M., Basurko, O., Piedrahita, R., Hundley, P. & Mendiola, D. (2018), 'Energy use in recirculating aquaculture systems (ras): A review', Aquacultural engineering **81**, 57–70.

Badiola, M., Mendiola, D. & Bostock, J. (2012), 'Recirculating aquaculture systems (ras) analysis: Main issues on management and future challenges', Aquacultural Engineering **51**, 26–35.

Bergheim, A., Drengstig, A., Ulgenes, Y. & Fivelstad, S. (2009), 'Production of atlantic salmon smolts in europe—current characteristics and future trends', Aquacultural Engineering **41**(2), 46–52.

Berthelsen, P. A. & Faltinsen, O. M. (2008), 'A local directional ghost cell approach for incompressible viscous flow problems with irregular boundaries', Journal of computational physics **227**(9), 4354–4397.

Bihs, H. (2011), Three-Dimensional Numerical Modeling of Local Scouring in Open Channel Flow, PhD thesis, NTNU, Trondheim.

Bihs, H. (2020), 'Reef3d :: User guide'.
URL: *https://reef3d.wordpress.com/user-guide/* *(Cited: 9. Mar. 2020)*

Bihs, H., Kamath, A., Chella, M. A., Aggarwal, A. & Arntsen, Ø. A. (2016), 'A new level set numerical wave tank with improved density interpolation for complex wave hydrodynamics', Computers & Fluids **140**, 191–208.

Bihs, H., Wang, W., Pakozdi, C. & Kamath, A. (2020), 'Reef3d:: Fnpf—a flexible fully nonlinear potential flow solver', Journal of Offshore Mechanics and Arctic Engineering **142**(4).

Blancheton, J., Attramadal, K., Michaud, L., d'Orbcastel, E. R. & Vadstein, O. (2013), 'Insight into bacterial population in aquaculture systems and its implication', Aquacultural engineering **53**, 30–39.

Bredberg, J. (2000), 'On the wall boundary condition for turbulence models', Chalmers University of Technology, Department of Thermo and Fluid Dynamics. Internal Report 00/4. G oteborg .

Bryman, A. (2006), 'Integrating quantitative and qualitative research: how is it done?', Qualitative research **6**(1), 97–113.

Castro, V., Grisdale-Helland, B., Helland, S. J., Kristensen, T., Jørgensen, S. M., Helgerud, J., Claireaux, G., Farrell, A. P., Krasnov, A. & Takle, H. (2011), 'Aerobic training stimulates growth and promotes disease resistance in atlantic salmon (salmo salar)', Comparative Biochemistry and Physiology Part A: Molecular & Integrative Physiology **160**(2), 278–290.

Chella, M. A., Bihs, H., Myrhaug, D. & Muskulus, M. (2015), 'Breaking characteristics and geometric properties of spilling breakers over slopes', Coastal Engineering **95**, 4–19.

Chorin, A. J. (1968), 'Numerical solution of the navier-stokes equations', Mathematics of computation **22**(104), 745–762.

Chung, T. (2010), Computational fluid dynamics, Cambridge university press.

Clarivate, A. (2018), 'Incites journal citation reports', Clarivate Analytics.
URL: *https://jcr.clarivate.com/ (Cited: 18. feb. 2020)*

Clarivate, A. (2020), 'Web of science', Clarivate Analytics.
URL: *https://clarivate.com/webofsciencegroup/solutions/web-of-science/ (Cited: 18. feb. 2020)*

Courant, R., Friedrichs, K. & Lewy, H. (1967), 'On the partial difference equations of mathematical physics', IBM journal of Research and Development **11**(2), 215–234.

Creswell, J. W. & Creswell, J. D. (2017), Research design: Qualitative, quantitative, and mixed methods approaches, Sage publications, chapter 10 Mixed Methods Procedures.

Creswell, J. W. & Miller, D. L. (2000), 'Determining validity in qualitative inquiry', Theory into practice **39**(3), 124–130.

Dahlum, S. (2018), '*In Norwegian:* validitet', Store Norske Leksikon (SNL).
URL: *https://snl.no/validitet (Cited: 7. Feb. 2020)*

Davidson, J. & Summerfelt, S. (2004), 'Solids flushing, mixing, and water velocity profiles within large (10 and 150 m3) circular 'cornell-type'dual-drain tanks', Aquacultural Engineering **32**(1), 245–271.

Duarte, S., Reig, L., Masaló, I., Blanco, M. & Oca, J. (2011), 'Influence of tank geometry and flow pattern in fish distribution', Aquacultural engineering **44**(2), 48–54.

Ebeling, J. M., Michael, B. & Summerfelt, S. T. (2010), Culture units, in 'Recirculating aquaculture', Cayuga Aqua Ventures, chapter 4, pp. 115–165.

Elakel, M. (2018), Investigation of wave transformation and breaking processes in the coastal zone using reef3d, Master's thesis, Marine Civil Engineering, NTNU, Trondheim.

Elsevier (2020), 'About scopus'.
URL: *https://www.elsevier.com/solutions/scopus (Cited: 18. feb. 2020)*

FAO (2005), 'National aquaculture legislation overview', Rome.
URL: *http://www.fao.org/fishery/legalframework/nalo_norway/en (Cited: 28. Jan. 2020)*

FAO (2018), 'The state of world fisheries and aquaculture 2018 - meeting the sustainable development goals', Rome, Italy.
URL: *http://www.fao.org/documents/card/en/c/I9540EN/ (Cited: 22. Jan. 2020)*

Ferziger, J. H., Perić, M. & Street, R. L. (2020), Computational methods for fluid dynamics, Vol. 3, Springer.

Froehlich, H. E., Runge, C. A., Gentry, R. R., Gaines, S. D. & Halpern, B. S. (2018), 'Comparative terrestrial feed and land use of an aquaculture-dominant world', Proceedings of the National Academy of Sciences **115**(20), 5295–5300.

Fry, J. P., Mailloux, N. A., Love, D. C., Milli, M. C. & Cao, L. (2018), 'Feed conversion efficiency in aquaculture: do we measure it correctly?', Environmental Research Letters **13**(2), 024017.

Golafshani, N. (2003), 'Understanding reliability and validity in qualitative research', The qualitative report **8**(4), 597–607.

Good, C., Davidson, J., Terjesen, B. F., Takle, H., Kolarevic, J., Bæverfjord, G. & Summerfelt, S. (2018), 'The effects of long-term 20 mg/l carbon dioxide exposure on the health and performance of atlantic salmon salmo salar post-smolts in water recirculation aquaculture systems', Aquacultural Engineering **81**, 1–9.

Gorle, J., Terjesen, B. F. & Summerfelt, S. (2018a), 'Water velocity in commercial ras culture tanks for atlantic salmon smolt production', Aquacultural Engineering **81**, 89–100.

Gorle, J., Terjesen, B. F. & Summerfelt, S. T. (2018b), 'Hydrodynamics of octagonal culture tanks with cornell-type dual-drain system', Computers and Electronics in Agriculture **151**, 354–364.

Gorle, J., Terjesen, B. & Summerfelt, S. (2019), 'Hydrodynamics of atlantic salmon culture tank: Effect of inlet nozzle angle on the velocity field', Computers and electronics in agriculture **158**, 79–91.

Gottlieb, S. & Shu, C.-W. (1998), 'Total variation diminishing runge-kutta schemes', Mathematics of computation **67**(221), 73–85.

Griebel, Michael, D. T. N. T. (1997), Numerical simulation in fluid dynamics: a practical introduction, Vol. 3, Siam.

Grotle, E. L., Bihs, H., Æsøy, V. & Pedersen, E. (2018), 'Computational fluid dynamics simulations of nonlinear sloshing in a rotating rectangular tank using the level set method', Journal of Offshore Mechanics and Arctic Engineering **140**(6).

Hagspiel, V., Hannevik, J., Lavrutich, M., Naustdal, M. & Struksnæs, H. (2018), 'Real options under technological uncertainty: A case study of investment in a post-smolt facility in norway', Marine Policy **88**, 158–166.

Harten, A., Engquist, B., Osher, S. & Chakravarthy, S. R. (1987), Uniformly high order accurate essentially non-oscillatory schemes, iii, in 'Upwind and high-resolution schemes', Springer, pp. 218–290.

Hilborn, R., Banobi, J., Hall, S. J., Pucylowski, T. & Walsworth, T. E. (2018), 'The environmental cost of animal source foods', Frontiers in Ecology and the Environment **16**(6), 329–335.

Hu, H. H. (2012), Computational fluid dynamics, in 'Fluid mechanics', Elsevier, pp. 421–472.

Huggins, D. L., Piedrahita, R. H. & Rumsey, T. (2005), 'Use of computational fluid dynamics (cfd) for aquaculture raceway design to increase settling effectiveness', Aquacultural Engineering **33**(3), 167–180.

Jiang, G.-S. (1995), Efficient implementation of weighted ENO schemes, Department of Mathematics, University of California, Los Angeles.

Kamath, A. (2012), Wave forces on structures using reef3d, Master's thesis, Marine Civil Engineering, NTNU, Trondheim.

Kimberlin, C. L. & Winterstein, A. G. (2008), 'Validity and reliability of measurement instruments used in research', American journal of health-system pharmacy **65**(23), 2276–2284.

Kirk, J., Miller, M. L. & Miller, M. L. (1986), Reliability and validity in qualitative research, Vol. 1, Sage.

Klebert, P., Volent, Z. & Rosten, T. (2018), 'Measurement and simulation of the three-dimensional flow pattern and particle removal efficiencies in a large floating closed sea cage with multiple inlets and drains', Aquacultural Engineering **80**, 11–21.

Klinger, D. & Naylor, R. (2012), 'Searching for solutions in aquaculture: Charting a sustainable course', Annual Review of Environment and Resources **37**, 247–276.

Kolarevic, J., Baeverfjord, G., Takle, H., Ytteborg, E., Reiten, B. K. M., Nergård, S. & Terjesen, B. F. (2014), 'Performance and welfare of atlantic salmon smolt reared in recirculating or flow through aquaculture systems', Aquaculture **432**, 15–25.

Kristensen, T., Åtland, Å., Rosten, T., Urke, H. & Rosseland, B. (2009), 'Important influent-water quality parameters at freshwater production sites in two salmon producing countries', Aquacultural Engineering **41**(2), 53–59.

Lekang, O.-I. (2007), Tanks, basins and other closed production units, in 'Aquaculture Engineering', Blackwell Pub., chapter 13, pp. 158–173.

Levy, Y. & Ellis, T. J. (2006), 'A systems approach to conduct an effective literature review in support of information systems research.', Informing Science **9**.

Lincoln, Y. S. & Guba, E. G. (1985), Naturalistic Inquiry, SAGE.

Martin, T., Kamath, A. & Bihs, H. (2020a), 'A lagrangian approach for the coupled simulation of fixed net structures in a eulerian fluid model', Journal of Fluids and Structures **94**, 102962.

Martin, T., Kamath, A. & Bihs, H. (2020b), 'Modeling and simulation of moored-floating structures using the tension element method', Journal of Offshore Mechanics and Arctic Engineering **142**(1).

Martins, C., Eding, E. H., Verdegem, M. C., Heinsbroek, L. T., Schneider, O., Blancheton, J.-P., d'Orbcastel, E. R. & Verreth, J. (2010), 'New developments in recirculating aquaculture systems in europe: A perspective on environmental sustainability', Aquacultural Engineering **43**(3), 83–93.

Msangi, S., Kobayashi, M., Batka, M., Vannuccini, S., Dey, M. & Anderson, J. (2013), 'Fish to 2030: prospects for fisheries and aquaculture', World Bank Report **83177**(1), 102.

Naylor, R. L., Hardy, R. W., Bureau, D. P., Chiu, A., Elliott, M., Farrell, A. P., Forster, I., Gatlin, D. M., Goldburg, R. J., Hua, K. et al. (2009), 'Feeding aquaculture in an era of finite resources', Proceedings of the National Academy of Sciences **106**(36), 15103–15110.

Nilsen, A., Hagen, Ø., Johnsen, C. A., Prytz, H., Zhou, B., Nielsen, K. V. & Bjørnevik, M. (2019), 'The importance of exercise: Increased water velocity improves growth of atlantic salmon in closed cages', Aquaculture **501**, 537–546.

NTNU (2018), 'Advanced literature search'.
URL: *https://innsida.ntnu.no/wiki/-/wiki/English/Advanced+literature+search (Cited: 18. feb. 2020)*

Nyhus, O. J. (2020), 'Personal communication', Unstructured interview, 24. March 2020.

Oca, J. & Masaló, I. (2007), 'Design criteria for rotating flow cells in rectangular aquaculture tanks', Aquacultural Engineering **36**(1), 36–44.

Oca, J. & Masalo, I. (2013), 'Flow pattern in aquaculture circular tanks: Influence of flow rate, water depth, and water inlet & outlet features', Aquacultural engineering **52**, 65–72.

Papáček, Š., Petera, K., Masaló, I. & Oca, J. (2018), On the optimization of recirculated aquaculture systems, in 'International Conference on Engineering Optimization', Springer, pp. 1229–1240.

Parker, R. W., Blanchard, J. L., Gardner, C., Green, B. S., Hartmann, K., Tyedmers, P. H. & Watson, R. A. (2018), 'Fuel use and greenhouse gas emissions of world fisheries', Nature Climate Change **8**(4), 333.

Plew, D. R., Klebert, P., Rosten, T. W., Aspaas, S. & Birkevold, J. (2015), 'Changes to flow and turbulence caused by different concentrations of fish in a circular tank', Journal of Hydraulic Research **53**(3), 364–383.

Poore, J. & Nemecek, T. (2018), 'Reducing food's environmental impacts through producers and consumers', Science **360**(6392), 987–992.

Schlichting, H. & Gersten, K. (2016), Boundary-layer theory, Springer.

Scholar, G. (2020), 'About google scholar', Google.
URL: *https://scholar.google.com/intl/en/scholar/about.html* *(Cited: 18. feb. 2020)*

Seale, C. (1999), 'Quality in qualitative research', Qualitative inquiry **5**(4), 465–478.

Shahzad, K. (2019), 'Importance of computer modeling in aquaculture (supported by examples)', CtrlAQUA.
URL: *https://ctrlaqua.no/?publication=fact-sheet-hydro* *(Cited: 29. Jan. 2020)*

Shewchuk, J. R. et al. (1994), 'An introduction to the conjugate gradient method without the agonizing pain'.

Skolbekken, J., Songe-Møller, V., Ruyter, K. & Hovland, B. (2010), 'Veiledning for forskningsetisk og vitenskapelig vurdering av kvalitative forskningsprosjekt innen medisin og helsefag', Oslo: Den nasjonale forskningsetiske komité for medisin og helsefag (NEM) .

Souza, A. C. d., Alexandre, N. M. C. & Guirardello, E. d. B. (2017), 'Psychometric properties in instruments evaluation of reliability and validity', Epidemiologia e Serviços de Saúde **26**, 649–659.

Stenbacka, C. (2001), 'Qualitative research requires quality concepts of its own', Management decision .

Summerfelt, S. T., Mathisen, F., Holan, A. B. & Terjesen, B. F. (2016), 'Survey of large circular and octagonal tanks operated at norwegian commercial smolt and post-smolt sites', Aquacultural Engineering **74**, 105–110.

Sussman, M., Smereka, P., Osher, S. et al. (1994), 'A level set approach for computing solutions to incompressible two-phase flow'.

Svartdal, F. (2018), '*In Norwegian:* relabilitet', Store Norske Leksikon (SNL).
URL: *https://snl.no/reliabilitet (Cited: 7. Feb. 2020)*

Terjesen, B., Rosten, T., Ulgenes, Y., Henriksen, K., Aarhus, I. & Winther, U. (2013), 'Betydning av vannmiljøet ved produksjon av laksefisk i lukkede systemer i sjø. water quality requirements for efficient farming of atlantic salmon in closed systems', Norwegian, english abstract. VANN **48**, 14–27.

Thomas, E. & Magilvy, J. K. (2011), 'Qualitative rigor or research validity in qualitative research', Journal for specialists in pediatric nursing **16**(2), 151–155.

Timmons, M. B., Summerfelt, S. T. & Vinci, B. J. (1998), 'Review of circular tank technology and management', Aquacultural engineering **18**(1), 51–69.

Tseng, Y.-H. & Ferziger, J. H. (2003), 'A ghost-cell immersed boundary method for flow in complex geometry', Journal of computational physics **192**(2), 593–623.

Tvinnereim, K. & Skybakmoen, S. (1989), 'Water exchange and self-cleaning in fish-rearing tanks'.

UN (2015), 'World population prospects: The 2015 revision', United Nations Econ Soc Aff **33**(2), 1–66.

Vadstein, O., Attramadal, K. J., Bakke, I., Forberg, T., Olsen, Y., Verdegem, M., Giatsis, C., Skjermo, J., Aasen, I. M., Gatesoupe, F.-J. et al. (2018), 'Managing the microbial community of marine fish larvae: a holistic perspective for larviculture', Frontiers in microbiology **9**, 1820.

Van der Vorst, H. A. (1992), 'Bi-cgstab: A fast and smoothly converging variant of bi-cg for the solution of nonsymmetric linear systems', SIAM Journal on scientific and Statistical Computing **13**(2), 631–644.

Venkatesh, V., Brown, S. A. & Bala, H. (2013), 'Bridging the qualitative-quantitative divide: Guidelines for conducting mixed methods research in information systems', MIS quarterly pp. 21–54.

Vermeulen, S. J., Campbell, B. M. & Ingram, J. S. (2012), 'Climate change and food systems', Annual review of environment and resources **37**.

Vollset, K. W., Dohoo, I., Karlsen, Ø., Halttunen, E., Kvamme, B. O., Finstad, B., Wennevik, V., Diserud, O. H., Bateman, A., Friedland, K. D. et al. (2018), 'Disentangling the role of sea lice on the marine survival of atlantic salmon', ICES Journal of Marine Science **75**(1), 50–60.

Wang, W., Martin, T., Kamath, A. & Bihs, H. (2020), 'An improved depth-averaged non-hydrostatic shallow water model with quadratic pressure approximation', International Journal for Numerical Methods in Fluids .

Webster, J. & Watson, R. T. (2002), 'Analyzing the past to prepare for the future: Writing a literature review', MIS quarterly pp. xiii–xxiii.

Wilcox, D. C. et al. (1998), Turbulence modeling for CFD, Vol. 2, DCW industries La Canada, CA.

Willett, W., Rockström, J., Loken, B., Springmann, M., Lang, T., Vermeulen, S., Garnett, T., Tilman, D., DeClerck, F., Wood, A. et al. (2019), 'Food in the anthropocene: the eat–lancet commission on healthy diets from sustainable food systems', The Lancet **393**(10170), 447–492.

Wohlin, C. (2014), Guidelines for snowballing in systematic literature studies and a replication in software engineering, in 'Proceedings of the 18th international conference on evaluation and assessment in software engineering', pp. 1–10.

Yilmaz, K. (2013), 'Comparison of quantitative and qualitative research traditions: Epistemological, theoretical, and methodological differences', European journal of education **48**(2), 311–325.

Ytrestøyl, T., Takle, H., Kolarevic, J., Calabrese, S., Rosseland, B., Teien, H., Nilsen, T., Stefansson, S., Handeland, S. & Terjesen, B. (2013), 'Effects of salinity and exercise on performance and physiology of atlantic salmon postsmolts reared in ras', Abstracts Aquaculture Europe p. 465.

Yunus, A. C. (2010), Fluid Mechanics: Fundamentals And Applications (Si Units)., Tata McGraw Hill Education Private Limited.

A Control Scripts

Control-file DiveMESH

```
C 11 21
C 12 21
C 13 21
C 14 21
C 15 21
C 16 3

B 1 0.05
B 10 0.0 8.4 0.0 8.4 0.0 2.7
B 130 1

M 10 128
M 20 2

S 1 1
S 33 4.2 7.325 0.2
```

Ctrl-file REEF3D

```
B 10 1
B 50 0.001

D 10 4
D 11 1
D 20 2
D 30 1

F 30 0
F 40 0

I 10 0

M 10 128

N 40 3
N 41 300.0
N 48 0
N 49 0.02
```

```
P 10 1
P 18 1
P 25 1
P 28 1
P 30 1.0
P 40 1
P 42 30.0
P 75 1
P 78 1

T 10 2
T 36 0

W 1 1000.0
W 22 -9.81
W 41 4.45 7.325 0.2 2.7 1.5 0.0

P 61 0.7 4.2 0.45
P 61 1.2 4.2 0.45
P 61 1.7 4.2 0.45
P 61 2.2 4.2 0.45
P 61 2.7 4.2 0.45
P 61 3.2 4.2 0.45
P 61 3.7 4.2 0.45
P 61 4.2 4.2 0.45
P 61 4.7 4.2 0.45
P 61 5.2 4.2 0.45
P 61 5.7 4.2 0.45
P 61 6.2 4.2 0.45
P 61 6.7 4.2 0.45
P 61 7.2 4.2 0.45
P 61 7.7 4.2 0.45

P 61 0.7 4.2 1.7
P 61 1.2 4.2 1.7
P 61 1.7 4.2 1.7
P 61 2.2 4.2 1.7
P 61 2.7 4.2 1.7
P 61 3.2 4.2 1.7
P 61 3.7 4.2 1.7
P 61 4.2 4.2 1.7
P 61 4.7 4.2 1.7
P 61 5.2 4.2 1.7
P 61 5.7 4.2 1.7
P 61 6.2 4.2 1.7
P 61 6.7 4.2 1.7
P 61 7.2 4.2 1.7
P 61 7.7 4.2 1.7
```

B Detailed Bibliography Matrix

#	Author	Title	Year	Published	Database	Keywords	Relevance
1	Blancheton, J.P., Attramadal, K.J.K., Michaud, L., d'Orbcastel, E.R., Vadstein, O.	Insight into bacterial population in aquaculture systems and its implication	2013	Aquacultural Engineering	Oria	Attramadal, K.	RQ1
	Terjesen, B.F, Summerfelt, S.T, Nerland, S., et. Al	Design, dimensioning and performance of a research facility for studies on the requirements of fish in RAS environments	2013	Aquacultural Engineering	Scopus	RAS tank design, aquaculture	RQ1
2	Timmons, M.B., Summerfelt, S.T., Vinci, B.J.	Review of circular tank technology and management	1998	Aquacultural Engineering	Web of Science	Tank design aquaculture	RQ1, RQ2
3	Lekang, O.I.	Aquacultural Engineering	2007	Wiley-Blackwell	Oria	Aquaculture	RQ1, RQ2
4	Ebeling, J.M, Michael, B.	Recirculating Auaculture	2010	Cayuga Aqua	Snowballed	Lekang (2007)	RQ1, RQ2
5	Tvinnereim, K., Skybakmoen	Water exchange and self-cleaning in fish-rearing tanks	1989	Flanders Marine Institute	Snowballed	Lekang (2007)	RQ1
6	Wheaton, F. W.	Aquacultural Engineering	1993	Krieger Publish.	Snowballed	Ebeling (2010)	RQ1
7	Duarte, S. Reig, L. Masaló, I. Blanco, M., Oca, J	Influence of tank geometry and flow pattern in fish distribution	2011	Aquacultural Engineering	Snowballed	Lekang (2007)	RQ2
8	Oca, J., Masaló, I.	Flow pattern in aquaculture circular tanks: Influence of flow rate, water depth, and water inlet & outlet features	2013	Aquacultural Engineering	Scopus	Tank design aquaculture	RQ1, RQ2
9	Oca, J., Masaló, I., Reig, L.	Comparative analysis of flow patterns in aquaculture rectangular tanks with different water inlet characteristics	2004	Aquacultural Engineering	Snowballed	Oca (2013)	RQ2
10	Andersen, A. Bohr, T. et. Al	The bathtub vortex in a rotating container	2006	J. of Fluid Mech.	Snowballed	Oca (2013)	RQ1
11	Davidson, J., Summerfelt, S.T.	'Solids flushing, mixing, and water velocity profiles within large (10 and 150 m3) circular 'cornell-type' dual-drain tanks'	2004	Aquacultural Engineering	Snowballed	Timmons (1998)	RQ1, RQ2
12	Summerfelt, S.T., Sharrer, M., Marshall, C., Obaldo, L.	Controlling water velocity within large Cornell-type dual-drain culture tanks	2006	6th Recirculating Aquaculture	Snowballed	Summerfelt (2016)	RQ2
13	Plew, D.R., Klebert, P. Rosten, T.W., Aspaas, S. Birkevold, J.	Changes to flow and turbulence caused by different concentrations of fish in a circular tank	2015	Journal of Hydraulic Research	Scopus	Turbulence aquaculture tanks	RQ1

14	Nilsen, A., Hagen, Ø., Johnsen, C.A. et. Al	The importance of exercise: Increased water velocity improves growth of Atlantic salmon in closed cages	2019	Aquaculture	Oria	Fish exercise aquaculture tank	RQ1
15	Hvas, M., Folkedal, O., Solstorm, D.	Assessing swimming capacity and schooling behaviour in farmed Atlantic salmon Salmo salar with experimental push-cages	2017	Aquaculture	Snowballed	Nilsen (2019)	RQ1
16	Castro, V. Grisdale-Helland, B. Helland, S.J., Kristensen, T. et. Al	Aerobic training stimulates growth and promotes disease resistance in Atlantic salmon (Salmo salar)	2011	Comparative Biochemistry Physiology	Snowballed	Oca (2013)	RQ1
17	Masaló, I., Oca, J.	Influence of fish swimming on the flow pattern of circular tanks	2016	Aquacultural Engineering	Snowballed	Oca (2013)	RQ1
18	Summerfelt, S.T., Mathisen, F., Holan, A.B, Terjesen, B.F.	Survey of large circular and octagonal tanks operated at Norwegian commercial smolt and post-smolt sites	2016	Aquacultural Engineering	Oria	Aquaculture tank design	RQ2, RQ3
19	Gorle, J., Terjesen, B.F, Mota, V.C, Summerfelt, S.	Water velocity in commercial RAS culture tanks for Atlantic salmon smolt production	2018	Aquacultural Engineering	Oria	Hydrodynamics, aquaculture	RQ1, RQ3
20	Gorle, J., Terjesen, B.F, Summerfelt, S.	Hydrodynamics of octagonal culture tanks with Cornell-type dual-drain system	2018	Computers and Electronics in Agriculture	Snowballed	Gorle et. Al (2018)	RQ2, RQ3
21	Gorle, J., Terjesen, B.F, Summerfelt, S.	Hydrodynamics of Atlantic salmon culture tanks: Effect of nozzle angle on velocity	2019	Computers and Electronics in Agriculture	Snowballed	Gorle et. Al (2018)	RQ2, RQ3
22	An, C-H., Sin, M-G., Kim, M-J.	Effect of bottom drain positions on circular tank hydraulics: CFD simulations	2018	Aquacultural Engineering	Web of Science	CFD tanks aquaculture	RQ2, RQ3
23	Klebert, P., Volent, Z., Rosten, T.	Measurement and simulation of the 3D flow pattern and particle removal efficiencies in a large floating closed sea cage with multiple inlets and drains	2018	Aquacultural Engineering	Web of Science	Hydrodynamics, aquaculture tanks	RQ2, RQ3
24	Papácek, S., Petera, K., Masaló, I., Oca, J.	On the optimization of recirculated aquaculture systems	2018	Conference on Engineering Optimization	Springer	CFD aquaculture tanks	RQ3